

Universität Heidelberg  
Interdisciplinary Center for Scientific Computing  
Engineering Mathematics and Computing Lab

Bachelor Thesis

# Continuous Modeling of Extracellular Matrix Invasion by Tumor Growth

Name: Maximilian Bing  
Matriculation number: 3606060  
Advisor: Professor Vincent Heuveline  
Date of submission: April 30, 2024

Hiermit versichere ich, dass ich die Arbeit selbst verfasst und keine anderen als die angegebenen Quellen und Hilfsmittel benutzt und wörtlich oder inhaltlich aus fremden Werken Übernommenes als fremd kenntlich gemacht habe. Ferner versichere ich, dass die übermittelte elektronische Version in Inhalt und Wortlaut mit der gedruckten Version meiner Arbeit vollständig übereinstimmt. Ich bin einverstanden, dass diese elektronische Fassung universitätsintern anhand einer Plagiatssoftware auf Plagiate überprüft wird.

---

Abgabedatum:

## Zusammenfassung

Krebszellen können sich vom Primärtumor lösen und das umgebende Gewebe abbauen. Kontinuierliche mathematische Modelle werden verwendet, um diesen Prozess besser zu verstehen.

In diesem Zusammenhang basieren die Modelle in der Regel auf mindestens drei Schlüsselkomponenten: den Tumorzellen, dem umgebenden Gewebe oder der extrazellulären Matrix (ECM) und den matrixabbauenden Enzymen (MDE). Diese Variablen werden in dem hier behandelten Modell in einem System partieller Differentialgleichungen gekoppelt, um den komplexen Prozess der Tumorinvasion zu beschreiben.

Aufgrund der hohen Anzahl der freien Parameter solcher Modelle, hat eine Konfiguration dieser Parameter hohen Einfluss auf die produzierten Ergebnisse. Diese Arbeit untersucht den Einfluss der Wahl dieser Konfigurationen, sowie den, der Dimension auf die Ergebnisse einer Simulation.

Um realitätsnahe biologische Szenarien zu simulieren, verlangen Simulationen mindestens zwei am besten drei räumlichen Dimensionen. Da in der Literatur fast ausschließlich eindimensionale Experimente beschrieben werden, untersuchen wir unser Modell nur in höheren Dimensionen: zwei- oder dreidimensional. Darüber hinaus wurde hauptsächlich die homogene Struktur der extrazellulären Matrix (ECM) behandelt, jedoch für eine heterogene extrazelluläre Matrix Struktur nur solche Fälle analysiert, die wenig biologische Relevanz haben. Die Struktur der epithelialen Schicht und der benachbarten extrazellulären Matrix ist jedoch in biologischem Gewebe deutlich organisierter als in den meisten später gezeigten Simulationen und anderen Beispielen aus der Literatur. Diese Organisiertheit kann zu erheblichen Veränderungen der Ergebnisse führen, selbst wenn die Parameter des Systems konstant gehalten werden.

Diese Arbeit soll einen Einstiegspunkt geben, um das zu grundliegende Modell für realistische Experimente zu nutzen. Die Parameteranalyse soll hierbei auch helfen eine angebrachte Wahl der Parameter zu erleichtern.

## Abstract

Cancer cells can detach from the primary tumor and degrade the surrounding tissue. Continuous mathematical models are been utilized for a better understanding of the process.

In this context the models typically rely on at least three key components: tumor cells, the surrounding tissue or extracellular matrix (ECM) and matrix-degrading enzymes (MDE). These variables are coupled in the investigated model in a system of partial differential equations to describe the complex process of tumor invasion.

Due to such a model's high degree of freedom, the configuration of the model parameters significantly influences the resulting outcomes. This study examines the influence of choosing these configurations, as well as the dimensionality, on the results of a simulation.

To simulate realistic biological scenarios, simulations require at least two, preferably three, spatial dimensions. Since the literature predominantly describes one-dimensional experiments, we only investigate our model in higher dimensions: two or three dimensions. Furthermore, primarily, the homogeneous structure of the extracellular matrix (ECM) has been addressed, but for a heterogeneous extracellular matrix structure, only cases with little biological relevance have been analyzed. However, the structure of the epithelial layer and the adjacent extracellular matrix is significantly more organized in biological tissue than in most simulations shown later and other examples from the literature. This organization can lead to significant changes in the results, even when the parameters of the system are kept constant.

This work aims to provide a starting point for using the fundamental model for realistic experiments. The parameter analysis should also help facilitate an appropriate choice of parameters.

## Contents

<b>1</b>	<b>Introduction</b>	<b>5</b>
<b>2</b>	<b>Theoretical Basics</b>	<b>6</b>
2.1	Basics of Tumor Biology . . . . .	6
2.2	Mathematical Methods in Oncology . . . . .	8
<b>3</b>	<b>Modeling</b>	<b>10</b>
3.1	Mathematical Formulation . . . . .	10
3.2	Numerical Formulation and Parameters . . . . .	12
<b>4</b>	<b>Experiments and Results</b>	<b>14</b>
4.1	Dimension Variation . . . . .	17
4.2	Parameter Analysis without Proliferation and Renewal - Homogenous ECM	25
4.3	Parameter Analysis with Proliferation and Renewal - Homogenous ECM .	42
4.4	2D Results with Proliferation and Renewal - Heterogenous ECM . . . . .	57
<b>5</b>	<b>Conclusion and Discussion</b>	<b>61</b>

## 1 Introduction

Modeling tumor growth plays a crucial role in understanding the complex mechanisms governing the development and progression of cancer diseases. Since cancer is one of the leading death causes worldwide and many of its forms are incurable, challenges in the area of Oncology require researchers to have a deep understanding in the biological foundation. This Bachelor thesis is dedicated to analyzing Anderson et al.'s [1, 2] model for modeling tumor invasion.

The dynamics of tumorous growth are an intricate system influenced by numerous biological and chemical factors, genetic pre-dispositions, the surrounding tissue of cancer cells, angiogenic processes and interactions with the immune system. Integrating these factors in mathematical models allows us to decode these complex interactions with quantification and helps us understand the fundamental mechanisms surrounding cancerous diseases.

Mathematical models are an essential part of Oncology; they are used to quantify biological phenomena and help to predict and understand tumor development and treatment response. In Mathematical Oncology, we differentiate between continuous, discrete and hybrid models [3].

For the continuous type, cells and tissue are described over time with partial differential equations modeling continuous quantities like, in our case, tumor cell density, extracellular matrix concentration or matrix-degrading enzyme concentration.

In the discrete case, an entity-based model is used, pursued with the goal of better understanding the phenomena on the cell level. This approach allows the researcher to better implement a cell's biological effects with its outer circumstances, like interaction with other cells, nutrients or other microorganisms. As the name implies, use these models discrete values to describe the temporal course of events.

Hybrid models try to combine both approaches to offer efficient systems capturing cell level events and continuous changes in outer circumstances.

This work investigates how a continuous model proposed by Anderson et al. [1, 2] to analyze tumor development performs in the case of different dimensions and free parameter values. The model examines the third and fourth stages of a cancer disease: tumor progression, where the tumor cells grow more extensive and take on more aggressive behavior due to further genetic instabilities and tumor invasion, with the tumor cells gaining the ability to penetrate and invade the surrounding tissue [4].

From examples of the original paper, we can already see that the model's results vary with the dimensionality of the space, we are modeling the partial differential equations in.

Our primary focus is investigating how the model's free parameters influence tumor dynamics growth. Another point of interest is comparing simulations of two dimensions with those of three dimensions of extracellular matrix invasion by tumor growth. Additionally to the variation of dimensions, we will briefly examine how the geometry of the extracellular matrix will influence tumor development.

## 2 Theoretical Basics

### 2.1 Basics of Tumor Biology

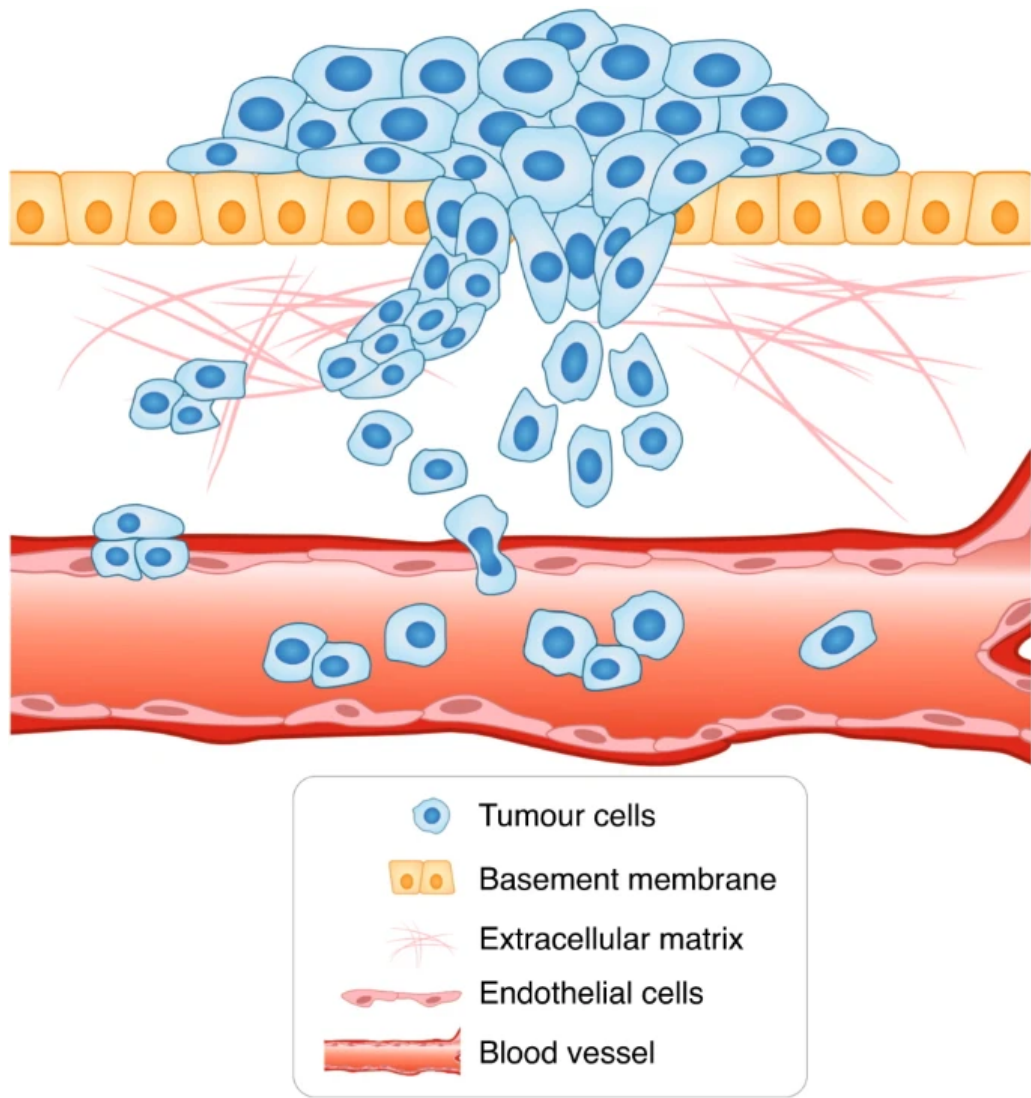


FIGURE 1. Tumor Invasion Stage

The body of a living human being is made up of more than 200 different types of cells; the coordination between the cells and their surroundings keeps the body running. Each of these cells is built from the genetic information encoded in the DNA in the cells' nuclei. Though the nucleotide sequence of DNA is well-checked and maintained throughout the cell's life, mutations still occur that cause changes in a cell's DNA. These mutations may be of a positive, negative or neutral nature. In the case of a harmful mutation, this alteration of the DNA may cause diseases, with cancer being one of them. The failure of the complex system managing cell birth, proliferation and cell death (apoptosis) causes cancer, resulting in uncontrolled cell proliferation in a local area. Abnormal growth of

body tissue is called a tumor, yet these can be malignant or benign.

Cancer diseases can be categorized medically into five stages. First is the tumor initiation phase, where it comes to the above explained genetic mutations of normal cells. The next stage is the tumor promotion stage, in which the mutated cells of phase one may experience further genetic alterations resulting from uncontrolled growth and proliferation of the cancerous cells. The third stage is the tumor progression stage, where the cancerous cells progress in growing and proliferating, reaching a critical mass and forming a tumor at a local site of the body. Fourth comes the invasion stage, shown in figure 1. Here, the tumor can invade surrounding tissue by breaking through the basement membrane, invading the extracellular matrix inside and entering the blood circulation or lymphatic systems. Next, the tumor cells that have invaded the blood circulation of the lymphatic system spread throughout the body and form new tumors. This stage is called Metastization. To grow tumors further, they need access to more nutrients and oxygen. During angiogenesis, a tumor develops its own blood vessels, securing its nutritional provision.

In our model, the focus lies on the third and fourth stages: tumor progression and tumor invasion. The tumor progression stage is characterized by the tumor growing more extensive and the cancerous cells taking on more aggressive behavior by starting to invade the surrounding area. While they keep growing uncontrolled, they are also affected by further genetic instabilities, which lead to more mutations, possibly developing resistance mechanisms against, for example, degrading factors. Already in this stage, the affected area is exposed to heavy tissue damage and functional disabilities. In the next stage, tumor invasion stage, the malignant cells gain the ability to penetrate and invade the surrounding tissue furhter. The tumor cells break through the normal tissue barrier and infiltrate neighboring structures. In order to do so, the cancer cells produce so-called matrix-degrading enzymes which break down the extracellular matrix. The degradation of the extracellular matrix helps local spreading and destroys otherwise healthy tissue and cells in the affected area

The most important factors influencing those two phases are the genetic dispositions of the tumor cells towards proliferation and the evasion of apoptosis, programmed cell death, which increase the invasive potential. Another critical factor is the geometry of the extracellular matrix, as well as the exact macromolecules that make it up. A solid immune biological defense reaction also helps the body defend against spreading cancer cells. Hence, evasion of detection and destruction of the tumor cells plays a vital role in the first stages. To invade the affected area, the malignant cells need to be able to move freely and quickly. In order to do so, cancer cells can gain the ability to lose adhesion properties, which healthy cells usually have, to allow migrating into the surrounding tissue.

Another organization principle for cancerous diseases is found in the Hallmarks of Cancer of Douglas Hanahan and Robert Weinberg [4], shown in figure 2. They describe a set of functional capabilities, eight hallmark capabilities and two enabling characteristics commonly acquired by cancer cells. They contribute to their ability to grow uncontrollably, evade the immune system and metastasize. These hallmarks are sustaining proliferative signaling, evading growth suppressors, avoiding immune destruction, enabling replicative immortality, tumor-promoting inflammation, activating invasion and Metastization, in-



FIGURE 2. Hallmarks of Cancer by Hanahan and Weinberg [4]

ducing or accessing vasculature, genome instability and mutation, resisting cell death, deregulating cellular metabolism. These Hallmarks of Cancer together contribute to the development and progression of cancer and provide targets for therapeutic intervention and research efforts aimed at understanding and treating the disease.

In our model, we see many of the capabilities incorporated. Proliferative signaling only relies on the tumor cells themselves and not on typically other hormones or molecules, allowing them to proliferate rapidly without external growth signals. Immune destruction and induced cell death are avoided, optimizing them to survive and accumulate genetic mutations that promote tumor growth. The tumor cells invade the surrounding tissue, modeled by the extracellular matrix.

## 2.2 Mathematical Methods in Oncology

Mathematical methods and models in Oncology play a crucial role in analyzing, understanding and predicting cancer development. Since the objective of this research underlies complex and intricate biochemical systems and mechanisms, many models exist that find their respective applications in distinct areas of this research field. These methods can be coarsely divided into three sections: continuous, discrete and hybrid models [3].

For describing tumor growth, exponential and logistic growth models are often used,

the latter allowing limiting factors, such as space or nutritional supply to play a role during modeling. These methods are a subclass of the differential equations approach, which bases their functionality on an ordinary or partial differential equation, studying the continuous approach. Like our model, they are not limited to only one equation but can include many, incorporating systematic dependencies on other factors. These models generally deal with continuous quantities like densities or concentrations, for example, spatial and temporal nutritional supply or drug concentration, as well as their effects on the affected area over time.

Discrete models use discrete entities to describe the behavior of tumor cells and their interactions with surrounding tissue. They allow us to model a wide range of biological and chemical processes which are hard to describe continuously. Commonly used types in Mathematical Oncology are, for example, Cellular Automata or Agent-Based Models. Cellular Automata represents cells as entities with states on a grid, with each cell being allowed to change states according to a set of rules based on its own current state and the states of the neighbors. In contrast, Agent-Based Models enable the differentiation of cell types and allow movement that is not restricted to a grid, implementing complex mechanics at cell-cell or cell-environment levels. Using these discrete models allows researchers to focus on biological effects during modeling, which are hard to describe in continuous models. With these approaches, we can simulate genetic and evolutionary events, for example, they are studying the genetic alternations of tumor cells on cell level or the interaction between healthy and cancerous cells.

Hybrid models combine both methods above, using continuous and discrete approaches. Like in the model proposed by Franssen et al. [5] or Anderson et al. [1], these approaches allow to incorporate the exactness of continuous models with a wide range of biological effects described by discrete models. They for example allow to model the motility and proliferation of tumor cells to be modeled by continuous variables, while enabling effects such as the formation of blood vessels, angiogenesis.

However, not all models try to model tumor growth; others are concerned with optimality regarding drug dosages or radiation exposition, offering personalized treatment. Machine Learning and Data Mining methods are used analyzing large datasets to identify patterns and predict outcomes to optimize treatment for individual patients. Though these methods are used in all kinds of applications, also for, spacial and temporal cancer development. Putting all these methods together gives us a powerful toolbox to simulate and understand cancer biology. As the last years have shown, they are applied in a wide range of areas, offering insight into all areas of cancer research [6]. Therefore, it is essential to come up with methods and evaluate their usefulness and meaningfulness in different research areas.

## 3 Modeling

### 3.1 Mathematical Formulation

The model proposed by Anderson et al. [1, 2] and Chaplain et al. [1, 5, 7], extended with terms for modeling cell proliferation and extracellular matrix renewal consists of a system of coupled partial differential equations:

$$\frac{\partial c}{\partial t} = D_c \Delta c - \chi \nabla \cdot (c \nabla e) + \mu_1 c \left(1 - \frac{c}{c_0} - \frac{e}{e_0}\right) \quad (1)$$

$$\frac{\partial e}{\partial t} = -\delta m e + \mu_2 c \left(1 - \frac{c}{c_0} - \frac{e}{e_0}\right) \quad (2)$$

$$\frac{\partial m}{\partial t} = D_m \Delta m + \mu_3 c - \lambda m \quad (3)$$

with zero-flux boundary conditions:

$$\zeta \cdot (-D_c \nabla c + c \chi \nabla e) = 0 \quad (4)$$

$$\zeta \cdot (-D_m \nabla m) = 0 \quad (5)$$

where the free parameters are  $D_c$ ,  $D_m$ ,  $\chi$ ,  $\delta$ ,  $\mu_1$ ,  $\mu_2$ ,  $\mu_3$ ,  $\lambda$  and  $\zeta$  is an appropriate outward unit vector. These free parameters as well as their non-dimensionalized versions are all assumed to be positive real numbers.

The variable  $c$  describes the tumor cell density,  $e$  the concentration of the extracellular matrix and  $m$  the matrix-degrading enzyme concentration. All of those functions are mathematically defined to be mapping a one-, two- or three-dimensional spacial value  $x$  and a temporal value  $t$  to a scalar value describing the respective quantity at a specific point in space and time  $(x, t)$ :

$$\{c, e, m\} : \mathbb{R}^i \times \mathbb{R} \rightarrow \mathbb{R}, i \in \{1, 2, 3\}$$

To derive the expression of the tumor cell density  $c$ , we are going to assume that the tumor cell's motility is subject to two influences: haptotaxis and random movement. Haptotaxis is a directed migratory response of cells to gradients of fixed or bound chemicals [1] and random movement is influenced by, for example, mechanical stress, electric charge or other physical effects [8]. Haptotaxis is responsible for pulling the cancerous cells away from the primary tumor site into the surrounding tissue, towards the extracellular matrix molecules. This enables the tumor invasion process. We must define flux to get an expression of how much or how fast the tumor cells move. Flux is defined to be the amount of a substance that crosses a unit area in a unit time. Incorporating the two assumed influencing factors into our mathematical model; we define the haptotactic flux  $J_{hapt}$  and random flux  $J_{random}$ :

$$\begin{aligned} J_{hapt} &= \chi c \nabla e \\ J_{random} &= -D_c \nabla c \end{aligned}$$

$\chi$  is the haptotactic flux coefficient and  $D_c$  is a random mobility coefficient. These parameters could also be a function of, for example, extracellular matrix and or matrix-degrading enzyme concentration. Knowing that cells grow over time and proliferate, we want to respect this in our model with a term for tumor cell proliferation:

$$\mu_1 c \left(1 - \frac{c}{c_0} - \frac{e}{e_0}\right)$$

The idea is that this term describes the cell proliferation with a logistic growth model respecting spacial limiting factors of already present extracellular matrix molecules and tumor cells,  $\mu_1$  describes the rate at which tumor cell proliferation and growth happens. In the initial model proposed by Anderson et al. [1, 2] and Chaplain et al. [1, 5, 7], they did not respect proliferation of tumor cells and extracellular matrix renewal. They applied a conservation equation for the tumor cells, which yields:

$$\begin{aligned}\frac{\partial c}{\partial t} &= -\nabla \cdot (J_{hapt} + J_{rand}) \\ \frac{\partial c}{\partial t} &= -\nabla \cdot (\chi c \nabla e - D_c \nabla c) \\ \frac{\partial c}{\partial t} &= D_c \Delta c - \chi \nabla \cdot (c \nabla e)\end{aligned}$$

The extended model incorporates proliferation and renewal into this conservation formula, resulting in equation 1:

$$\begin{aligned}\frac{\partial c}{\partial t} &= -\nabla \cdot (J_{hapt} + J_{rand}) + \mu_1 c \left(1 - \frac{c}{c_0} - \frac{e}{e_0}\right) \\ \frac{\partial c}{\partial t} &= D_c \Delta c - \chi \nabla \cdot (c \nabla e) + \mu_1 c \left(1 - \frac{c}{c_0} - \frac{e}{e_0}\right)\end{aligned}$$

To model the extracellular-matrix concentration  $e$ , we assume that the enzymes degrade the extracellular matrix upon contact in an exponential way. The equation models this assumption:

$$\frac{\partial e}{\partial t} = -\delta m e$$

where  $\delta$  is the constant describing this degradation process. For the extended model we add a term describing the renewal process of the extracellular matrix, which is also being modeled by logistic growth incorporating limiting factors of present tumor cells and extracellular matrix molecules:

$$\frac{\partial e}{\partial t} = -\delta m e + \mu_2 c \left(1 - \frac{c}{c_0} - \frac{e}{e_0}\right)$$

with  $\mu_2$  being the coefficient describing the rate of the renewal process.

Modeling the matrix-degrading enzyme concentration  $m$ , we combine a diffusion term with production and decay terms. The diffusion term is described like for the tumor cells:

$$J_{rand} = -D_m \nabla c$$

The production term depends on the tumor cell density  $c$  and the decay term on the extracellular matrix concentration  $m$ . In both cases production and decay we are assuming exponential growth. Incorporating this gives us equation 3:

$$\begin{aligned}\frac{\partial m}{\partial t} &= \nabla \cdot J_{random} + \mu c - \lambda e \\ \frac{\partial m}{\partial t} &= D_m \Delta c + \mu_3 c - \lambda m\end{aligned}$$

$\mu_3$  and  $\delta$  describing production and decay coefficients.

### 3.2 Numerical Formulation and Parameters

To make solving the model easier, we will first non-dimensionalize all the equations 1 to 5 in a standard way to rescale the space domain to a unit size domain  $\Omega$ . For one space dimension this results in the unit interval  $[0, 1]$ , for two the unit square  $[0, 1] \times [0, 1]$  and for three spacial dimensions the unit cube  $[0, 1] \times [0, 1] \times [0, 1]$ .

We start with non-dimensionalizing the three continuous variables  $c, e, m$ :

$$\begin{aligned}\tilde{c} &= \frac{c}{c_0} \\ \tilde{e} &= \frac{e}{e_0} \\ \tilde{m} &= \frac{m}{m_0}\end{aligned}$$

Next we rescale distance with an appropriate length scale  $L$  and time with  $\tau = \frac{L^2}{D}$  [2], which will be described more detailed in section 4.

Modifying the system's free parameters  $D_c, \chi, \delta, D_m, \mu_3, \lambda$  gives us:

$$d_c = \frac{D_c}{D}, \quad \gamma = \chi \frac{e_0}{D}, \quad \eta = \tau m_0 \delta, \quad d_m = \frac{D_m}{D}, \quad \alpha = \tau \mu_3 \frac{c_0}{m_0}, \quad \beta = \tau \lambda.$$

with  $D$  being a reference chemical diffusion coefficient.

These modifications make the new system of coupled partial differential equations, where henceforth the tildes are dropped and we assume  $t$  as  $\tau$  for simplicities' sake:

$$\frac{\partial c}{\partial t} = d_c \Delta c - \gamma \nabla \cdot (c \nabla e) + \mu_1 c (1 - c - e) \quad (6)$$

$$\frac{\partial e}{\partial t} = -\eta m e + \mu_2 e (1 - c - e) \quad (7)$$

$$\frac{\partial m}{\partial t} = d_m \Delta c + \alpha c - \beta m \quad (8)$$

with also updated zero-flux boundary conditions:

$$\zeta \cdot (-d_c \nabla c + c \gamma \nabla e) = 0 \quad (9)$$

$$\zeta \cdot (-d_m \nabla m) = 0 \quad (10)$$

where the free parameters are as described above and  $\zeta$  stays an appropriate outward unit normal vector.

In order to use the Finite Element Method, we will change to the variational formulation. If we assume each species to be in the Hilbert space  $H^1(\Omega)$ , the variational formulation can be derived by multiplying with a test function  $\varphi_j, j \in \{c, e, m\}$ , integrating over the domain  $\Omega$  and using integration by parts and the Gauss theorem. Using the variational formulation will give us a broader solution space and reduce the solution's requirements regarding differentiability. With  $(\cdot, \cdot)$  denoting the  $L^2$ -scalar product on  $\Omega$  the following equation system results:

$$\left( \frac{\partial c}{\partial t}, \varphi_c \right) = -d_c (\nabla c, \nabla \varphi_c) + \gamma (c \nabla e, \nabla \varphi_c) + \mu_1 \left( c \left( 1 - \frac{c}{c_0} - \frac{e}{e_0} \right), \varphi_c \right) \quad (11)$$

$$\left( \frac{\partial e}{\partial t}, \varphi_e \right) = -\eta (m e, \varphi_e) + \mu_2 \left( e \left( 1 - \frac{c}{c_0} - \frac{e}{e_0} \right), \varphi_e \right) \quad (12)$$

$$\left( \frac{\partial m}{\partial t}, \varphi_m \right) = -d_m (\nabla m, \nabla \varphi_m) + \alpha (c, \varphi_m) - \beta (m, \varphi_m) \quad (13)$$

## 4 Experiments and Results

Solving the numerical model HiFlow<sup>3</sup>[9] will be used with the weak form given by equations 11 - 13. ParaView [10] is used to evaluate the numerical simulation results, producing informative plots to compare the evolution of the simulation over time. In particular the tool Plot Over Line is used to produce quantitative results, comparing the three variables  $c, e, m$ . This tool also allows to compare all three variables in one plot, as opposed to using 2D plots, for each variable one plot at one point in time would be needed. Using it makes the results better readable and allows a clearer quantitative insight into the experiments, as shown all the figures below.

This work starts with replicating numerical simulations done by other papers in higher dimensions. Since there were only 1D simulations done previously, the model will be adjusted so that the Plot Over Line graphs mimic the plots given by the previous experiments. This will serve two purposes: first, it will verify the correct implementation of the model and second, it will give a starting point by which to vary the parameters, investigating the phenomena this model exhibits. By replicating previous results, it will also be discussed how changing the dimension of the simulations affects the outcomes and how to adjust the parameters to make simulations across dimensions match approximately. After this there a Parameter Analysis is conducted, examining the model without proliferation of tumor cells and renewal of the extracellular matrix molecules. As the next step proliferation and renewal are introduced into the model with incorporating  $\mu_2$  and  $\mu_2$  in a second Parameter Analysis. Both Parameter Analyses assume the extracellular matrix structure as homogenous, as described below. In the last part of this work, a case is studied that considers the ECM structure as heterogenous. Aside from the discussion regarding change of dimensionality, all of the experiments here are conducted in two spacial dimensions.

For all the plots of the experiments, the red curve indicates the tumor cell density, the blue one the extracellular matrix concentration and the green curve the matrix-degrading enzyme concentration.

Looking at the parameter estimates from [2] to non-dimensionalise the time, we see that  $L \in [0.1cm, 1cm]$  and  $D \approx 10^{-6} \frac{cm^2}{s}$ ,  $t = \frac{L^2}{D}$  gives a big temporal range between,  $t_{min} = 1000s$  and  $t_{max} = 1000000s$ , in which the simulations take place. However, using estimates taken from [11] and [5] for the length scale  $L$ , with  $L = 0.2cm$  gives a concrete value for the non-dimensional time,  $t = 40000s$ .

In the experiments below a timestep of  $dt = 0.01$  was chosen, corresponding to  $400s$ . The simulations are run for a dimensionless time of  $t = 8$  corresponding to  $320000s = 88$  days. The experiments during replicating showed that a relationship between Anderson et al.'s and this work's temporal scale of one unit of time in Anderson et al.'s to 0.4 units of time in this work's timescale make the simulations well comparable.

Another challenge is the diffusion and Haptotaxis coefficients. Since they depend on the dimension the simulation is performed in, the first step is to find appropriate estimates as baseline values. They will be used as a foundation for the Parameter Analysis, where one or more parameters at a time are varied, to get an overview of their effects.

Before starting with the experiments the system's initial conditions are to be discussed. They are stated for three dimensions, but for two or one dimension the additional  $y$ - or

$z$ -terms need to be left out.

It is assumed that at dimensionless time  $t = 0$ , there is already a nodule of cancerous cells located at the center of the unit domain  $\Omega$  that has produced a concentration of matrix-degrading enzymes. The MDEs there have already degraded the extracellular matrix at the center. The initial conditions of the tumor cell density are defined as:

$$c(x, y, z, 0) = \exp\left(-\frac{(x - 0.5)^2 + (y - 0.5)^2 + (z - 0.5)^2}{0.01}\right)$$

and the initial conditions of the matrix-degrading enzymes are described by:

$$m(x, y, z, 0) = 0.5 \exp\left(-\frac{(x - 0.5)^2 + (y - 0.5)^2 + (z - 0.5)^2}{0.01}\right)$$

As mentioned above regarding the structure of the extracellular matrix two cases are discussed; first a homogenous ECM structure and second a heterogenous ECM structure. The strucutre of the homogenous extracellular matrix is defined by:

$$e(x, y, z, 0) = 1 - 0.5 \exp\left(-\frac{(x - 0.5)^2 + (y - 0.5)^2 + (z - 0.5)^2}{0.01}\right)$$

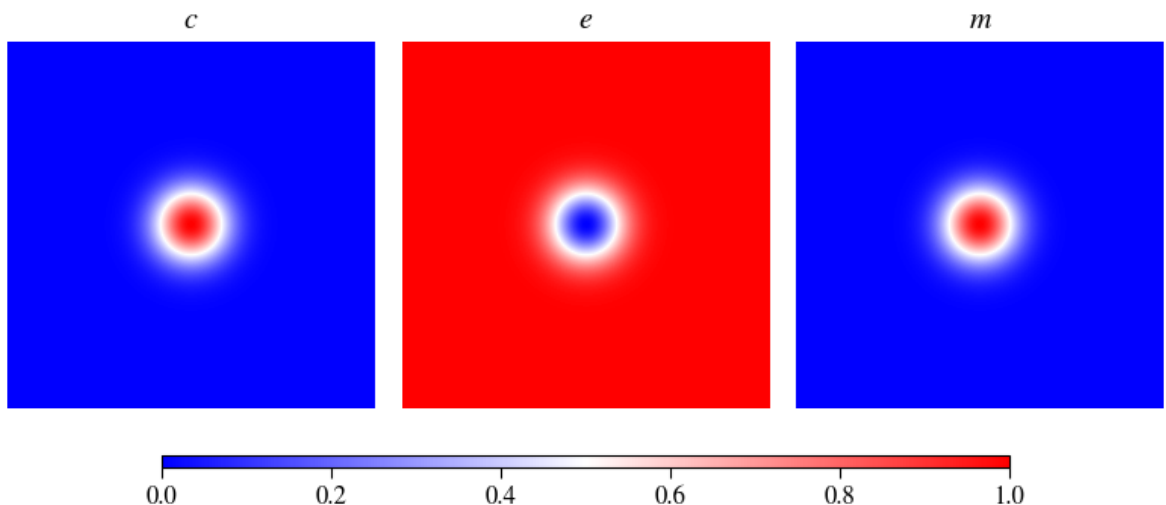


FIGURE 3. Visualization of the initial value distribution for an experiment in two space dimensions with a homogenous extracellular matrix

Figure 3 shows a 2D plot of the initial conditions using the homogenous extracellular matrix structure.

The other case investigated is using a heterogenous structure on the extracellular matrix. In section 4.4 it is studied how a more realistic structure of the ECM will affect the results for a 2D simulation. The initial conditions and assumptions regarding tumor

cell density and matrix-degrading enzyme concentration are the same as above. However, in this section it is assumed that the tumor cells are located at a basement membrane that they already have invaded and are now pushing into the extracellular matrix behind it. These assumptions meet the biological scenario depicted in figure 1. The experiment on the heterogenous ECM structure is conducted in two spacial dimensions, hence we formulate the initial conditions also in two spacial dimensions:

$$e(x, y, 0) = (1 - 0.5 \exp(-\frac{(x - 0.5)^2 + (y - 0.5)^2 + (z - 0.5)^2}{0.01})) \frac{1}{1 + \exp(-\frac{2}{0.1(x-0.5)})}$$

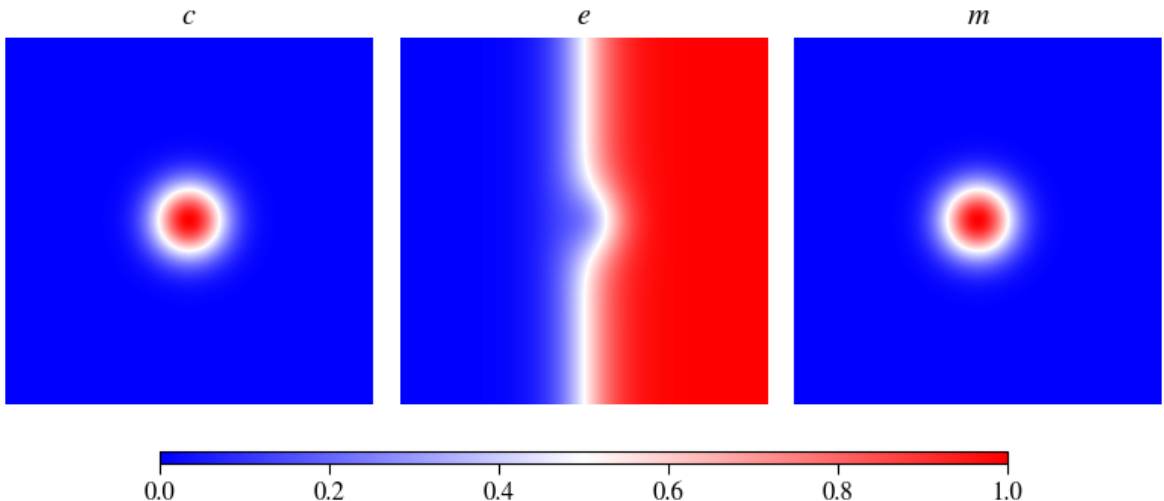


FIGURE 4. Visualization of the initial value distribution for an experiment in two space dimensions with a heterogeneous extracellular matrix

Figure 4 describes these modifications on  $e$  and shows the initial conditions for our system using a heterogeneous ECM structure.

It is worth discussing the mathematical intuition concerning the system of partial differential equations briefly, before starting with the main part of this work.

The equation governing the tumor cell density incorporates two coefficients regarding motility, diffusion and Haptotaxis and one for tumor cell growth and proliferation. As mentioned later in replicating Anderson et al.'s experimental results, the relation between those two factors determines if a secondary lump of tumor cells detaches from the main lump, invading the surrounding tissue faster and how large this lump will be. We see this behaviour in figure 8, varying  $d_c$  whilst keeping  $\gamma$  constant. Diffusive motility depends on the laplacian of the tumor cells themselves,  $\Delta c = \frac{\partial c}{\partial x} + \frac{\partial c}{\partial y} + \frac{\partial c}{\partial z}$  (for three spatial dimensions), which is a fundamental tool in sciences of all sorts to describe the effects of spatial rate of change of a scalar field quantity, in our case tumor cell density, at a specific point in space. Typically, this operator has high values where the respective quantity changes rapidly. The term describing Haptotaxis incorporates a laplacian of the extracellular

matrix with the dot product the gradients for both  $c$  and  $e$ :  $\nabla \cdot (c\nabla e) = \nabla c \cdot \nabla e + \Delta e$ . This means that haptotactic effects are strong not only where the concentration of the extracellular matrix changes rapidly but also where both gradients for tumor cell density and extracellular matrix assimilate in direction. However, the effects of  $\nabla c \cdot \nabla e$  can also annihilate each other. Tumor growth and proliferation is described by a logistic growth term:  $\mu_1 c(1 - c - e)$ , which are commonly used to model population growth or the growth of quantities that are limited by available resources, like space in our case. The logistic growth function has a sigmoidal shape, characterized by an initial exponential growth phase followed by a gradual saturation as resources become limited. As the quantities  $c$  and  $e$  approaches the maximum capacity the growth rate slows down and approaches zero. Overall, the logistic growth function captures the idea of limited growth due to finite resources, providing a more realistic model compared to exponential growth models, especially when dealing with populations or quantities that cannot grow indefinitely, like cells being limited by their spacial resources.

The equation describing the concentration of the extracellular matrix models its exponential decay, taking also the concentration of the matrix-degrading enzymes into account. In spatial and temporal positions where both ECM and MDE concentrations are high, a fast degradation of the extracellular matrix is to be observed. Like for the tumor cells is extracellular matrix renewal modeled with logistic growth. As described above, the quantities  $c$  and  $e$  compete for the limited resource, space.

The equation modeling the matrix-degrading enzyme concentration also combines motility with production and decay terms. The motility of the MDEs is modeled by the same diffusion as the tumor cells, mimicking their behavior in this regard. The tumor cells are responsible for producing the MDEs; the decay is modeled with natural decay and only depends on the MDE concentration itself. Both production and decay are modeled using exponential approaches.

## 4.1 Dimension Variation

Before starting with the Parameter Analysis, the changes on the results varying the dimensions need to be discussed and what adjustments need to be taken, to make higher dimension models mimic the one given by Anderson et al. As a starting point the parameters given by Anderson et al.'s first experiment [2] are used. Figure 5 shows a screenshot of this experiment, unfortunately in low image resolution, since the original paper had not included any digital data containing the diagrams of their results.

In the figure, after  $t = 1$  in their timescale, the tumor cells start develop a division, which is being pulled stronger into the tissue by Haptotaxis. This division propagates to a sharp peak at a later point in time. The concentration of the matrix-degrading enzymes increases and the concentration of the extracellular matrix decreases continuously over time. Their  $x$ -axis is stretched or rescaled to show an interval from 0 to 1, this is not stated in the original paper. In our case, the interval on the plots is between  $x \in [0, 0.5]$ , hence comparing both results can not be exact.

Replicating this experiment in two and three dimensions, we start with the same parameters as Anderson et al., which can be seen in table 2. Resulting 2D and 3D

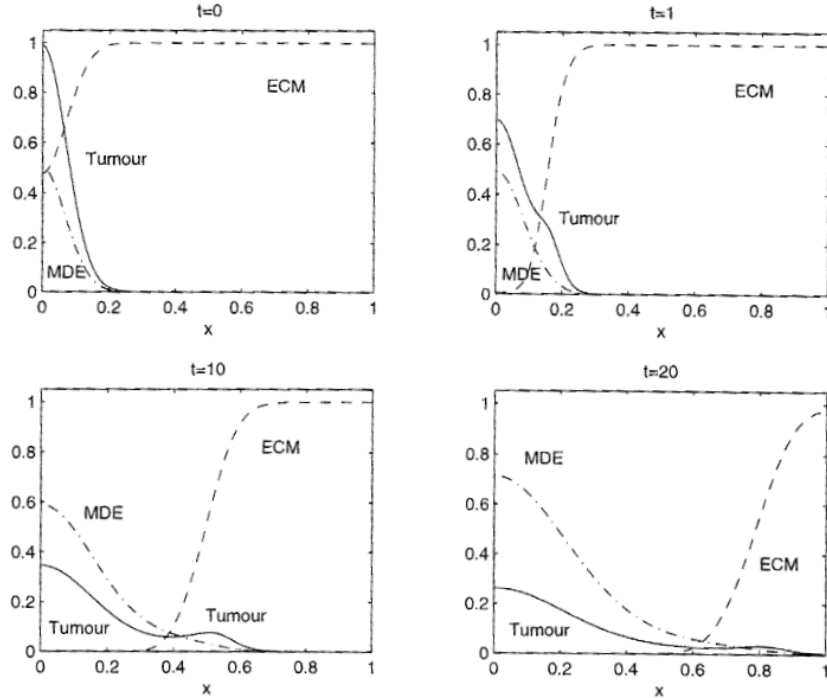


FIGURE 5. Plot of Anderson's first one dimensional experiment

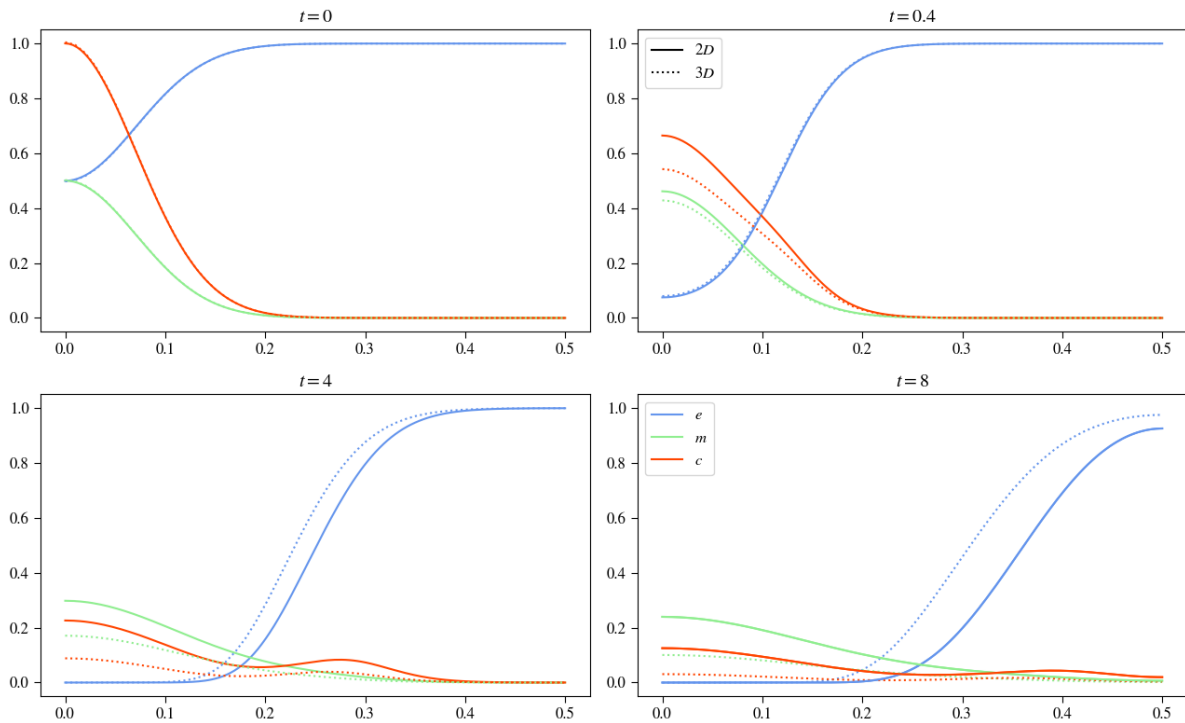


FIGURE 6. Plots using Anderson et al.'s parameters in 2D and 3D

plots are shown in figure 6. Starting from the initial values, after  $t = 0.4$ , a very small division of the tumor cells is starting to form for both dimensions. This division increases strongly for the experiment done in two dimensions and minimal for the experiment done in three dimensions at  $t = 4$ . At  $t = 8$ , both curves visibly flatten, the divisions of tumor cells detaching from the primary lump of cancer cells are not as pregnant as in the one-dimensional experiment of Anderson et al. The interplay of the diffusive and haptotactic factors determines how considerable this division will be. It will also decide how sharp the curve of the secondary lump of tumor cells will be.

Looking at the concentration of matrix-degrading enzymes, it is visibly lower for both dimensions than in Anderson et al.'s experiment. Little increase over time is observed. However this can be changed by adjusting their production factor  $\alpha$  or the motility coefficients of the tumor cells producing them. The factor  $\alpha$  determines how fast the tumor cells produce the matrix-degrading enzymes, degrading the extracellular matrix and allowing the tumor cells to invade the tissue further.

Only the extracellular matrix concentration seems to mimic the behavior of Anderson et al.'s experiment. It decreases continuously and as the last image shows, there is still a considerable amount left.

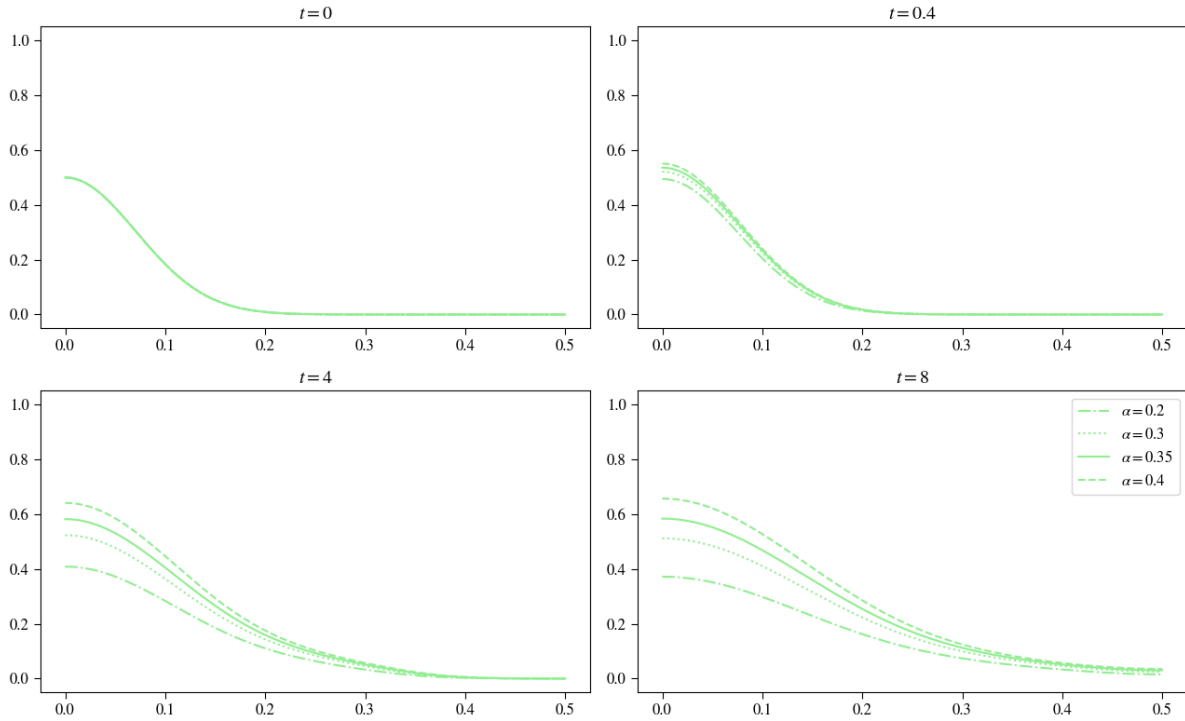
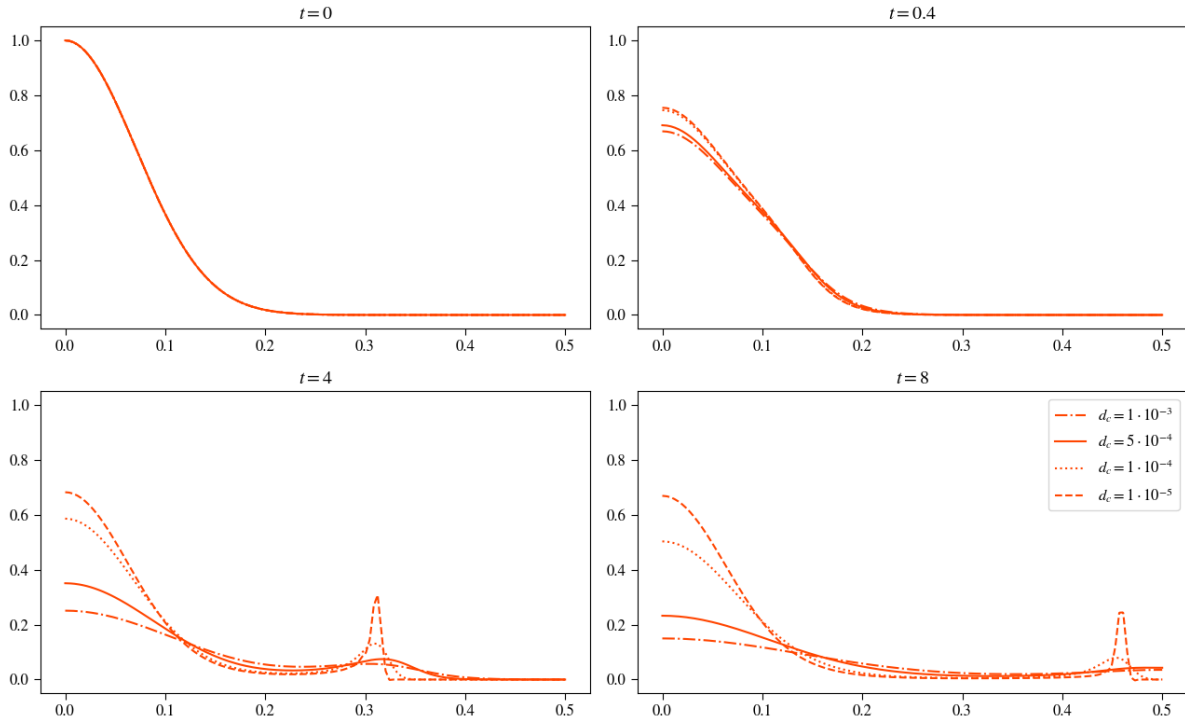
To replicate Anderson et al.'s results, the following parameters will be adjusted exemplary in two spacial dimension: tumor cells' diffusion and haptotaxis coefficients and production rate of the matrix-degrading enzymes. This is performed in two dimensions only due to the immense computational effort a 3D simulation requires.

The focus lies on the values of variables at the origin  $x = 0$  and the same model without proliferation and renewal, as Anderson et al. used, is examined in this section using a homogenous ECM strucutre.

Starting with comparing different values for  $\alpha$ , the figure 7 shows a comparison of how this affects the curve for the matrix-degrading enzyme concentration. A maximum difference between the compared values of 0.2 already causes drastic changes. In Anderson et al.'s experiment, a value of approximately  $m(0, 1) = 0.5$  is observed after, in their timescale,  $t = 1$  at the origin. This value is mimicked best for a value of  $\alpha = 0.2$  in the comparison experiments. However, in the later points in time, this value for  $\alpha$  is insufficient, though choosing  $\alpha$  higher than  $\alpha = 0.4$  results in an accelerated ECM degradation that is too fast. Taking a value between those two allowed our simulations to exhibit the observed behavior. Choosing a value of  $\alpha = 0.35645$  to use in the later experiments as a basecase, proves to be the best choice.

Looking at the diffusion coefficient for the tumor cells, in figure 8 experiments varying the  $d_c$  value are shown depciting the tumor cell density curve. It is clear to see that with decreasing  $d_c$ , the sharpness of the secondary lump of cells, that detaches from the lump at the origin, drastically increases. However, it is also observed, that the remaining lump of tumor cells at the origin increases due to the reduced diffusion. Over time, we experimentally found that  $dc = 5 \cdot 10^{-4}$  describes Anderson et al.'s experimental results best for simulations in two spacial dimensions. Bewlow, this is also confirmed using a algebraic hyptothesis on the tumor cells.

At last, the haptotatic pull needs to be adjusted slightly. Figure 9 shows the curve of the tumor cell density using different values for  $\gamma$ . Comparing these results with Anderson

FIGURE 7. Comparison of  $\alpha$  values to replicate Anderson et al.'s experimentFIGURE 8. Comparison of  $d_c$  values to replicate Anderson et al.'s experiment

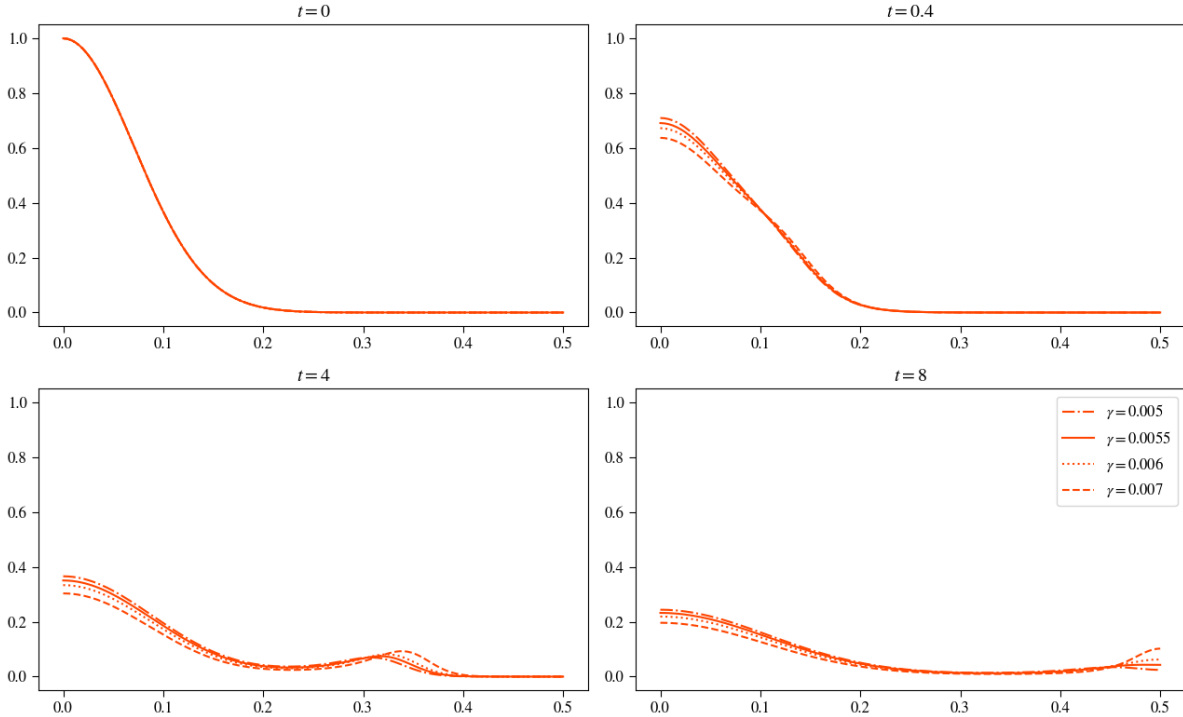


FIGURE 9. Comparison of  $\gamma$  values to replicate Anderson et al.’s experiment

et al.’s, a slightly bigger secondary lump that invades the tumor cells faster is needed. Hence a value of  $\gamma = 0.0055$  is used as the basecase values for further experiments.

These comparisons already underline the interplay between diffusion and Haptotaxis. Decreasing diffusion results in a detaching lump of cells with a sharp curve, increasing diffusion smoothes this out. On the other hand increasing  $\gamma$ , reinforces the haptotactic pull on the tumor cells pulling, though less of them at a faster pace outward to invade the tissue.

The adjustments on  $d_c, \gamma$  and  $\alpha$  generate the final configuration for replicating the system in two spacial dimensions. The primary effects of Anderson et al.’s experiment are met. The production of the matrix-degrading enzymes fits the original experiment and the motility of the tumor cells also matches, with balanced effects of Haptotaxis and diffusion. However comparing the three-dimensional experiment to the original, using these new parameter values, there are still major differences. This again confirms the assumption that with varying the dimensions the parameters need to be adjusted too.

In figure 11, the same scheme is used, as when transforming the values going from one dimension to two, changing  $d_c, \gamma$  and  $\alpha$  to make the 3D simulations mimic the results produced in 2D or 1D. Challenging in this process was, as mentioned previously, that the reduced tumor cell density causes drastic changes in both MDE production and ECM degradation. Settling on the values:  $d_c = 3 \cdot 10^{-4}$ ,  $\gamma = 0.0058$  for the tumor cell motility yields a curve the mimics in shape the curves for lower dimensions, though  $\alpha$  could still be increased a little above  $\alpha = 0.6$ .

Now the question arises why exactly those parameters need to be changed to replicate

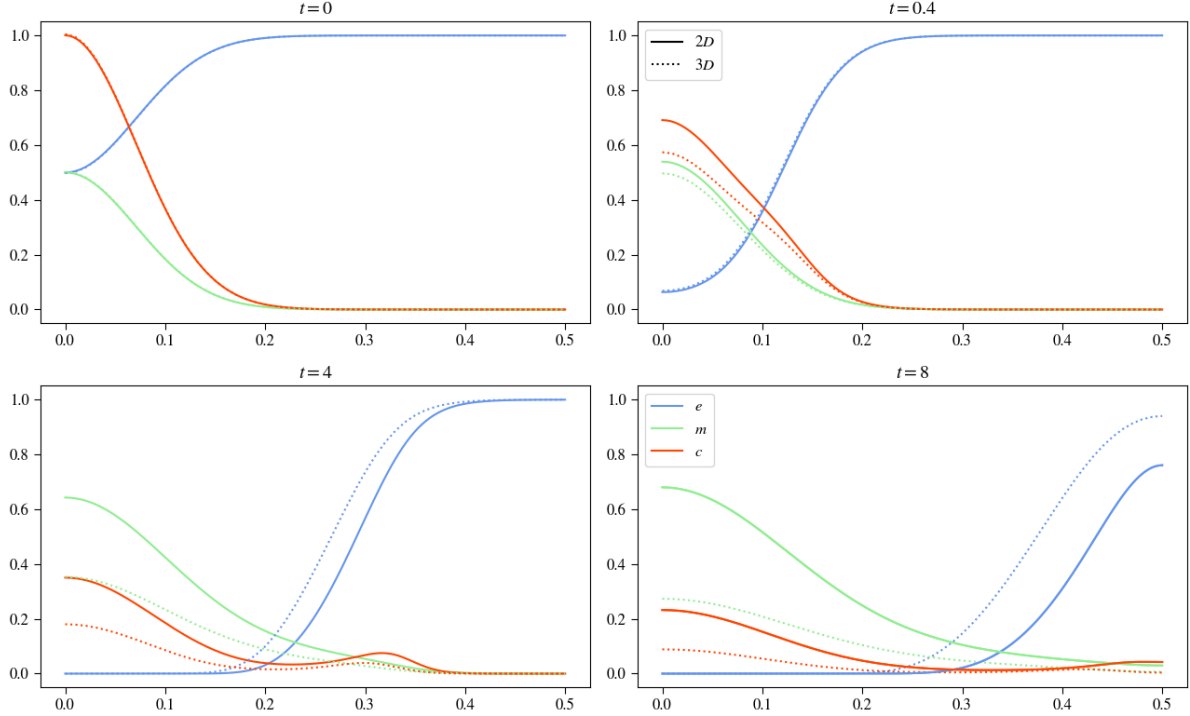


FIGURE 10. 3D Replication of using the 2D basecases values

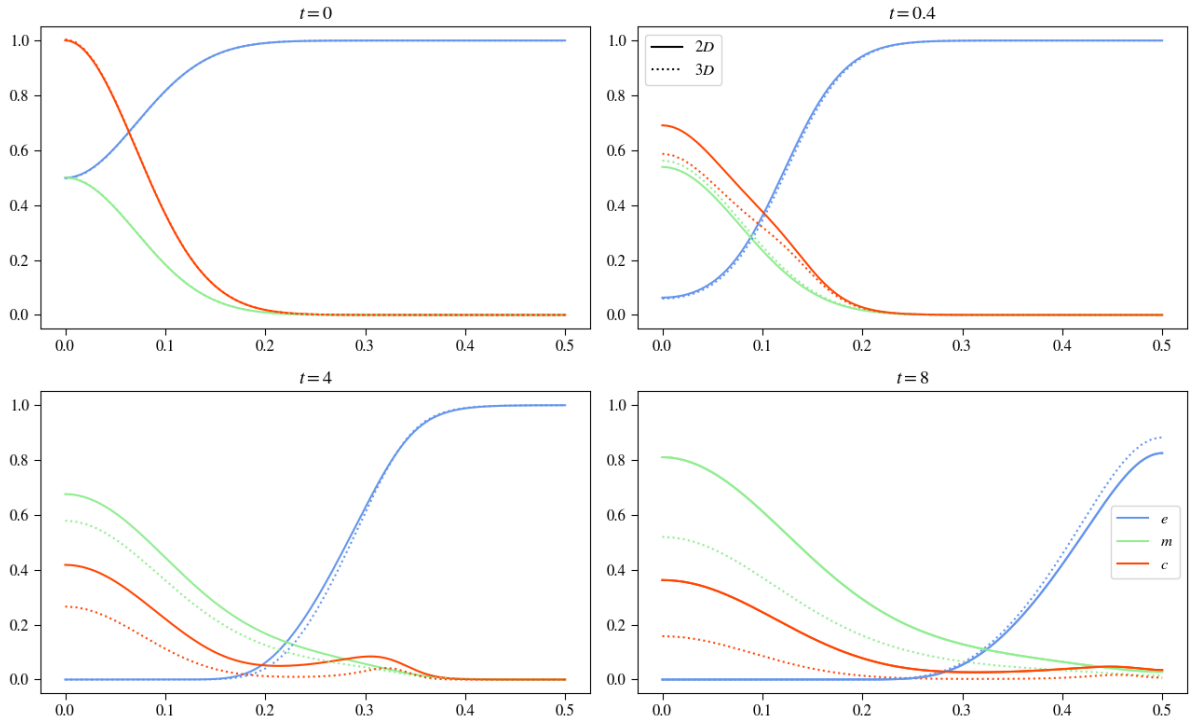


FIGURE 11. Comparing 2D basecase without proliferation and 3D basecase

results. For this we can argue with the following Parameter Analyses, but also with algebraic hypotheses.

Looking at  $\beta$  is assumed for most experiments to be zero, also in Anderson et al.'s one-dimensional result, therefore it was also set to zero for the experiments of this section.

Looking at the Parameter Analysis results for  $d_m$  below, it is found that this parameter has little influence compared to the others of the system. Regarding the spacial occupation and distribution of the matrix-degrading enzymes this parameter should control, the more important factors are motility of the tumor cells, described by  $d_c$  and  $\gamma$ , and the factor  $\alpha$  by which they are produced.

Inspecting the term concerning  $\eta$ ; it depends on local values for the ECM and MDE concentrations;

$$\frac{\partial e}{\partial t}(x, y, z, t) = -\eta m(x, y, z, t)e(x, y, z, t)$$

In the experiments regarding replicating, shows that influencing the MDE concentration works well with adjusting the motility of the tumor cells and their production of the MDEs. The aim is therefore on adjusting the concentration of the MDE concentration to get similar local quantitative values for  $m$  and  $e$  to match the degradation rate of the extracellular matrix.

As mentioned above the tumor cell motility plays a crucial role during temporal development of the system. It is therefore a key component to match these curves. The equation modelling the tumor cell density is for the model without proliferation only governed only by the motility of diffusion and Haptotaxis:

$$\frac{\partial c}{\partial t} = d_c \Delta c - \gamma \nabla \cdot (c \nabla e) = d_c \Delta c - \gamma (\nabla c \cdot \nabla e + \Delta e)$$

	1D	2D	3D
Diffusion	$\frac{\partial^2 c}{\partial x^2}$	$\frac{\partial^2 c}{\partial x^2} + \frac{\partial^2 c}{\partial y^2}$	$\frac{\partial^2 c}{\partial x^2} + \frac{\partial^2 c}{\partial y^2} + \frac{\partial^2 c}{\partial z^2}$
Haptotaxis	$\frac{\partial c}{\partial x} \frac{\partial e}{\partial x} + \frac{\partial^2 e}{\partial x^2}$	$\frac{\partial c}{\partial x} \frac{\partial e}{\partial x} + \frac{\partial c}{\partial y} \frac{\partial e}{\partial y} + \frac{\partial^2 e}{\partial x^2} + \frac{\partial^2 e}{\partial y^2}$	$\frac{\partial c}{\partial x} \frac{\partial e}{\partial x} + \frac{\partial c}{\partial y} \frac{\partial e}{\partial y} + \frac{\partial c}{\partial z} \frac{\partial e}{\partial z} + \frac{\partial^2 e}{\partial x^2} + \frac{\partial^2 e}{\partial y^2} + \frac{\partial^2 e}{\partial z^2}$

TABLE 1. Overview of Diffusion and Haptotaxis terms across dimensions

Comparing the terms for diffusion and haptotaxis with varying the dimension in figure 1, explains why those values need to be adjusted in different dimensions. For the diffusion an additional term is added for each increased dimension. Assuming that  $\frac{\partial^2 c}{\partial x^2} = \frac{\partial^2 c}{\partial y^2} = \frac{\partial^2 c}{\partial z^2} = \kappa(t)$  and also assuming a constant factor  $M$  for diffusion through varying the dimensions, this yields for the different dimensions:

$$\begin{aligned} M &= d_{c,1} \kappa(t) \leftrightarrow d_{c,1} = \frac{M}{\kappa(t)} = 1 \cdot 10^{-3} \\ d_{c,2} &= \frac{M}{2\kappa(t)} = \frac{1}{2} d_{c,1} = \frac{1}{2} 10^{-3} = 5 \cdot 10^{-4} \\ d_{c,3} &= \frac{M}{3\kappa(t)} = \frac{1}{3} d_{c,1} = \frac{1}{3} 10^{-3} = 3.33 \cdot 10^{-4} \end{aligned}$$

The index  $i$  on  $d_{c,i}$  indicates the dimension. These values, as was shown in figure 11, are experimentally confirmed and give researchers a formula by which to calculate the non-dimensionalised version of their respective diffusion coefficient estimates.

Applying the same hypothesis for  $\gamma$ ; assuming a constant factor  $H$  for it and assuming  $\frac{\partial c}{\partial x} \frac{\partial e}{\partial x} = \frac{\partial c}{\partial y} \frac{\partial e}{\partial y} = \frac{\partial c}{\partial z} \frac{\partial e}{\partial z} = \iota(t)$ ,  $\frac{\partial^2 e}{\partial x^2} = \frac{\partial^2 e}{\partial y^2} = \frac{\partial^2 e}{\partial z^2} = \theta(t)$ , yields for the different dimensions:

$$H = \gamma_1(\iota(t) + \theta(t)) \leftrightarrow \gamma_1 = \frac{H}{\iota(t) + \theta(t)} = 0.005$$

$$\gamma_2 = \frac{H}{2\iota(t) + 2\theta(t)} = \frac{1}{2}\gamma_1 = 0.0025$$

$$\gamma_3 = \frac{H}{3\iota(t) + 3\theta(t)} = \frac{1}{3}\gamma_1 = 0.00166$$

Here the index  $i$  on  $\gamma_i$  also indicates the dimension

Experimental results verify in the Parameter Analysis that using  $\gamma = 0.002$  and  $d_c = 5 \cdot 10^{-4}$  yields a curve for the tumor cells that develops no secondary lump of cells detaching from the primary tumor. Adjusting  $\gamma$  the same hypothesis cannot be employed, since the equation describing Haptotaxis also incorporates a term regarding the gradients of both curves:

$$\nabla c(x, y, z, t) \cdot \nabla e(x, y, z, t)$$

Depending on the point in space and time, this term can yield dampening increasing or no additional value at all. Therefore this value needs to be determined experimentally.

The conclusion drawn from adjusting the parameters with varying the dimensions is, that the most important factor is the tumor cell density. The motility is crucial for the shape of the MDE curve as well as the overall concentration of it, which is due to the tumor cells producing them exponentially, though this we can also adjust with the production coefficient  $\alpha$ . The diffusion coefficient  $d_c$  can be calculated algebraically, as seen above, but for Haptotaxis the coefficient must be determined experimentally. It is to say that, though it is possible to make the simulations across dimensions match approximately at one point in time, it is due to the many different parameters and terms impossible to make them fit perfectly over time.

Figure	Linestyle	$d_c$	$\gamma$	$\eta$	$d_m$	$\alpha$	$\beta$
6	—	$1 \cdot 10^{-3}$	0.005	10	$1 \cdot 10^{-3}$	0.1	0
7	- - -	$1 \cdot 10^{-3}$	0.005	10	$1 \cdot 10^{-3}$	0.2	0
7	.....	$1 \cdot 10^{-3}$	0.005	10	$1 \cdot 10^{-3}$	0.3	0
7	—	$1 \cdot 10^{-3}$	0.005	10	$1 \cdot 10^{-3}$	0.35	0
7	- - -	$1 \cdot 10^{-3}$	0.005	10	$1 \cdot 10^{-3}$	0.4	0
8	- - -	$1 \cdot 10^{-3}$	0.005	10	$1 \cdot 10^{-3}$	0.3546	0
8	.....	$1 \cdot 10^{-4}$	0.005	10	$1 \cdot 10^{-3}$	0.3546	0
8	—	$5 \cdot 10^{-4}$	0.005	10	$1 \cdot 10^{-3}$	0.3546	0

Figure	Linestyle	$d_c$	$\gamma$	$\eta$	$d_m$	$\alpha$	$\beta$
8	----	$1 \cdot 10^{-5}$	0.005	10	$1 \cdot 10^{-3}$	0.3546	0
9	---	$5 \cdot 10^{-5}$	0.005	10	$1 \cdot 10^{-3}$	0.3546	0
9	.....	$5 \cdot 10^{-4}$	0.0055	10	$1 \cdot 10^{-3}$	0.3546	0
9	—	$5 \cdot 10^{-4}$	0.006	10	$1 \cdot 10^{-3}$	0.3546	0
9	----	$5 \cdot 10^{-4}$	0.007	10	$1 \cdot 10^{-3}$	0.3546	0
10	—	$5 \cdot 10^{-4}$	0.0055	10	$1 \cdot 10^{-3}$	0.3546	0
10	.....	$5 \cdot 10^{-4}$	0.0055	10	$1 \cdot 10^{-3}$	0.3546	0
11	—	$5 \cdot 10^{-4}$	0.0055	10	$1 \cdot 10^{-3}$	0.3546	0
11	—	$3.3 \cdot 10^{-4}$	0.0058	10	$1 \cdot 10^{-3}$	0.6	0

TABLE 2. Overview of all experiments conducted for the model without proliferation and renewal producing 2D output

In table 2 all experiments with their corresponding parameter configurations and linestyles in the respective figures are listed for this section.

## 4.2 Parameter Analysis without Proliferation and Renewal - Homogenous ECM

The replicated results shown in figure 11, confirm that the results can also vary strongly, varying only one parameter. This section describes a Parameter Analysis done in two spacial dimensions on a homogenous extracellular matrix structure. A basecase, which was established during varying the dimensions, with the parameters as used in 10 for two dimensions is used as a foundation. First every parameter is varied separately keeping the others constant, next in Cross-Variation multiple parameters, at most three, are varied simultaneously.

Figure	Linestyle	$d_c$	$\gamma$	$\eta$	$d_m$	$\alpha$	$\beta$
12	----	$5 \cdot 10^{-5}$	0.0055	10	$1 \cdot 10^{-3}$	0.3546	0
12	—	$1 \cdot 10^{-4}$	0.0055	10	$1 \cdot 10^{-3}$	0.3546	0
12	.....	$1 \cdot 10^{-3}$	0.0055	10	$1 \cdot 10^{-3}$	0.3546	0
13	.....	$5 \cdot 10^{-4}$	0.002	10	$1 \cdot 10^{-3}$	0.3546	0
13	—	$5 \cdot 10^{-4}$	0.008	10	$1 \cdot 10^{-3}$	0.3546	0
13	----	$5 \cdot 10^{-4}$	0.01	10	$1 \cdot 10^{-3}$	0.3546	0
14	—	$5 \cdot 10^{-4}$	0.1	10	$1 \cdot 10^{-3}$	0.3546	0
15	.....	$5 \cdot 10^{-4}$	0.0055	2	$1 \cdot 10^{-3}$	0.3546	0
15	—	$5 \cdot 10^{-4}$	0.0055	12	$1 \cdot 10^{-3}$	0.3546	0
15	.....	$5 \cdot 10^{-4}$	0.0055	20	$1 \cdot 10^{-3}$	0.3546	0
16	.....	$1 \cdot 10^{-3}$	0.0055	10	0.00001	0.3546	0
16	—	$1 \cdot 10^{-4}$	0.0055	10	0.001	0.3546	0
16	----	$1 \cdot 10^{-5}$	0.0055	10	0.1	0.3546	0

continued on next page

Figure	Linestyle	$d_c$	$\gamma$	$\eta$	$d_m$	$\alpha$	$\beta$
17	.....	$5 \cdot 10^{-4}$	0.0055	10	$1 \cdot 10^{-3}$	0	0
17	—	$5 \cdot 10^{-4}$	0.0055	10	$1 \cdot 10^{-3}$	0.6	0
17	.....	$5 \cdot 10^{-4}$	0.0055	10	$1 \cdot 10^{-3}$	1.0	0
18	.....	$5 \cdot 10^{-4}$	0.0055	10	$1 \cdot 10^{-3}$	0.3546	0.1
18	—	$5 \cdot 10^{-4}$	0.0055	10	$1 \cdot 10^{-3}$	0.3546	0.01
18	.....	$5 \cdot 10^{-4}$	0.0055	10	$1 \cdot 10^{-3}$	0.3546	0.005
19 - left	.....	$5 \cdot 10^{-5}$	0.001	10	$1 \cdot 10^{-3}$	0.3546	0
19 - left	—	$5 \cdot 10^{-5}$	0.01	10	$1 \cdot 10^{-3}$	0.3546	0
19 - right	.....	$1 \cdot 10^{-3}$	0.001	10	$1 \cdot 10^{-3}$	0.3546	0
19 - right	—	$1 \cdot 10^{-3}$	0.01	10	$1 \cdot 10^{-3}$	0.3546	0
20 - left	.....	$5 \cdot 10^{-4}$	0.0055	2	$1 \cdot 10^{-5}$	0.3546	0
20 - left	—	$5 \cdot 10^{-4}$	0.0055	20	$1 \cdot 10^{-5}$	0.3546	0
20 - right	.....	$5 \cdot 10^{-4}$	0.0055	2	$1 \cdot 10^{-3}$	0.3546	0
20 - right	—	$5 \cdot 10^{-4}$	0.0055	20	$1 \cdot 10^{-3}$	0.3546	0
21 - left	.....	$5 \cdot 10^{-4}$	0.0055	10	$1 \cdot 10^{-3}$	0.1	0.005
21 - left	—	$5 \cdot 10^{-4}$	0.0055	10	$1 \cdot 10^{-3}$	0.1	0.1
21 - right	.....	$5 \cdot 10^{-4}$	0.0055	10	$1 \cdot 10^{-3}$	1.0	0.005
21 - right	—	$5 \cdot 10^{-4}$	0.0055	10	$1 \cdot 10^{-3}$	1.0	0.1
22 - left	.....	$5 \cdot 10^{-4}$	0.0055	10	$1 \cdot 10^{-5}$	0.1	0.005
22 - left	—	$5 \cdot 10^{-4}$	0.0055	10	$1 \cdot 10^{-5}$	0.1	0.1
22 - right	.....	$5 \cdot 10^{-4}$	0.0055	10	$1 \cdot 10^{-5}$	1.0	0.005
22 - right	—	$5 \cdot 10^{-4}$	0.0055	10	$1 \cdot 10^{-5}$	1.0	0.1
23 - left	.....	$5 \cdot 10^{-4}$	0.0055	10	$1 \cdot 10^{-3}$	0.1	0.005
23 - left	—	$5 \cdot 10^{-4}$	0.0055	10	$1 \cdot 10^{-3}$	0.1	0.1
23 - right	.....	$5 \cdot 10^{-4}$	0.0055	10	$1 \cdot 10^{-3}$	1.0	0.005
23 - right	—	$5 \cdot 10^{-4}$	0.0055	10	$1 \cdot 10^{-3}$	1.0	0.1

TABLE 3. Overview of all experiments conducted for the model without proliferation and renewal producing 2D output

Table 3 gives a detailed overview of all the experiments done in this section and the parameters used to produce the results. We are considering the model without the proliferation of the tumor cells or renewal of the extracellular matrix. In every figure, more than one experiment will be described; the linestyle in table 3 determines exactly which experiment by the set of parameters.

### $d_c$ Variation

This parameter describes the diffusive properties of the tumor cells. As Chaplain et al. assumed in [11], her also an even distribution of this parameter with  $d_c \sim U[1 \cdot 10^{-5}, 1 \cdot 10^{-3}]$  is assumed. However, the experiments here encountered numerical instabilities reducing the parameter below  $5 \cdot 10^{-5}$ .

As described, the intuition is that decreasing  $d_c$  will increase the effects of Haptotaxis

and make  $\gamma$  more influential. This means the tumor cells will drift faster outward with a bigger secondary lump, forming a pointier leading edge. On the other hand, if  $d_c$  is increased, the effects of Haptotaxis will diminish and the tumor cells will be subject to higher diffusion, distributing them more evenly in the accessible area. Additionally, there will be less division from the primary lump of cells. Looking at the experiments

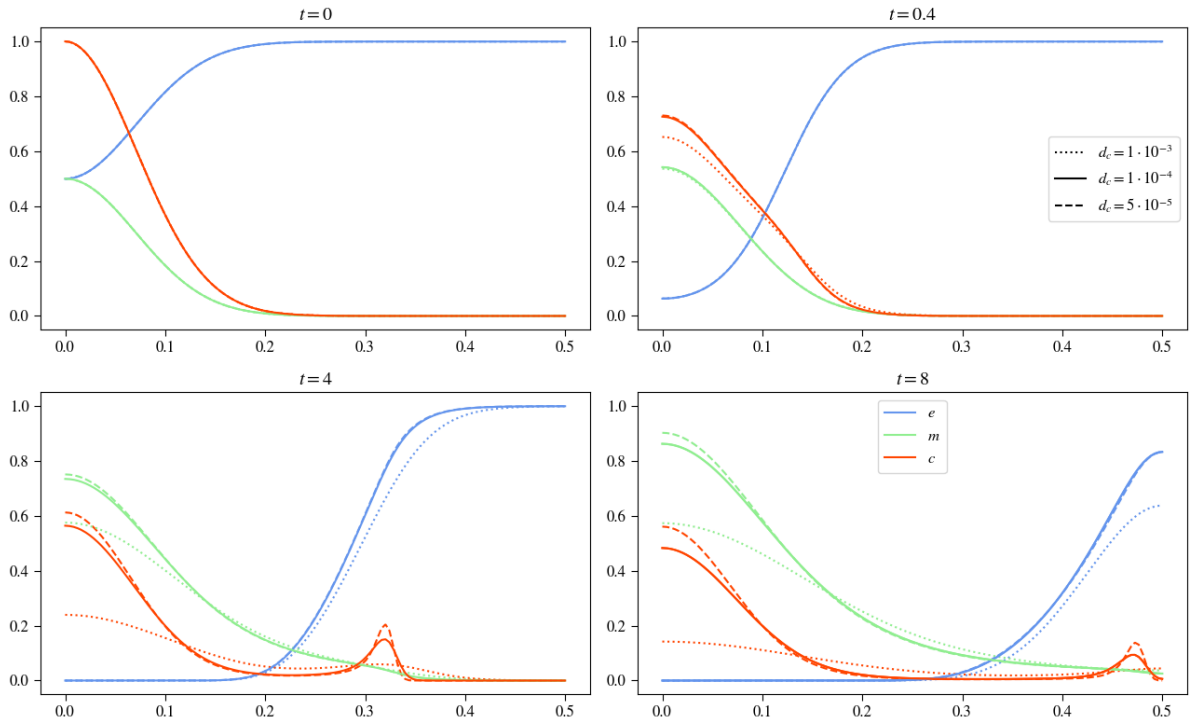


FIGURE 12. Plot results for varying  $d_m$ , keeping the other parameters constant

in figure 12, these assumptions are met. The smaller  $d_c$  gets, the higher the influence of Haptotaxis and vice versa.

Considering the tumor cell density curves shown in red, minor differences are visible after already  $t = 0.4$ . For the two lower values of  $d_c$ , the solid and dashed curves, the tumor cells have a higher concentration at the origin than for the biggest value of  $d_c$ , with nearly overlaying each other. Though the red dashed curve for the highest  $d_c$  value is considerably lower at the origin, it is stretched out more than the other two, indicating a faster invasion. The other curves describing ECM and MDE concentrations do not show any deviations from each other at this point in time.

Looking at the plot results, at time  $t = 4$ , the previously observed effects increase. The curves of the tumor cells confirm that with increasing  $d_c$ , the remaining lump of cells at the origin decreases, distributing the tumor cells more evenly in space and reducing the effect of Haptotaxis, making the secondary lump, which is still visible for the highest diffusion term, less sharp. At this point, the other two curves also show differing behavior. The ECM is degraded faster with increasing  $d_c$  and the slope the ECM curve describes is less steep. Looking at the extracellular matrix, minor differences are depictable between the lower two values of  $d_c$ . Due to the tumor cells' exponential production of MDEs

and the more even spread of the tumor cells, they take on a lower concentration at the origin. However, they have spread farther out than the MDE concentrations describing the experiments with lower  $d_c$  values.

Studying the last plot at  $t = 8$ , no new effects are observable. Increasing  $d_c$ , results in a more even spread of the tumor cells and a reduction of the secondary lump, detaching from the primary tumor. This causes a reduced MDE concentration in total due to the exponential growth rate, especially well observable at the origin. However, they have a more even distribution in space and faster invasion pace. This causes the extracellular matrix degradation process to work faster.

Regarding the sensitivity of this parameter, the higher the value is, the more sensitive the system reacts. Though the lower two values for  $d_c$  are only separated by  $5 \cdot 10^{-5}$  and we can unfortunately not experiment with  $d_c = 1 \cdot 10^{-5}$  due to numerical instabilities, the differences between those two were minimal compared to the difference between the higher two values of  $d_c$ .

From a biological point of view, this increase in diffusion might be caused by a change in temperature, electric potential or mechanical pressure differences. The higher diffusion results in a more even spread of the two actively moving quantities, tumor cells and matrix-degrading enzymes, which degrade their surrounding tissue faster.

### $\gamma$ Variation

$\gamma$  describes the effects of Haptotaxis; it is assumed that it is evenly distributed in  $\gamma \sim U[0.001, 0.01]$ , like Anderson et al. [2] did. Values exceeding this interval are also studied in this section, though this experiments has no biological meaning, it's interesting to study it from a numerical point of view. Inspecting the effects of  $\gamma$ , countering effects on the tumor cells as for varying  $d_c$  can be assumed; selecting higher values for  $\gamma$  will increase the effects of Haptotaxis, creating a larger secondary lump with a sharper maximum that is being pulled faster into the tissue by the extracellular matrix molecules. The experiments described in figure 13 verify the expected behavior.

After  $t = 0.4$ , changes for varying  $\gamma$  are already apparent; the higher  $\gamma$  is, the greater the division for the tumor cells is. The lowest value for  $\gamma$ , undercutting the one for the base case, shows no signs of developing a division at its' leading edge invades the tissue faster. The two higher values for  $\gamma$  show little deviation. Considering extracellular matrix and matrix-degrading enzyme concentration, no change is visible, still overlaying each other at this point in time.

The following plot shows the simulation after  $t = 4$  timesteps; here we can see changes in all three variables. While the tumor cell density for the values of 0.008 and 0.01 differ slightly by the amount of cells that are left at the origin and the distance they have already invaded the surrounding tissue, the curve for the lowest  $\gamma$  value does not show a detaching of the tumor cells from the primary lump, which causes the tumor cells to stay centered around  $x = 0$ , resulting in a higher density of cells there compared to the results of the other experiments. With increasing  $\gamma$ , the invasion speed also increases, as the dashed line for the tumor cell density indicates. For the MDE curve, we observe that the lower  $\gamma$  is, the more concentration is at the origin due to the higher remaining density of tumor cells at the origin producing them. The ECM concentration shows behavior similar to

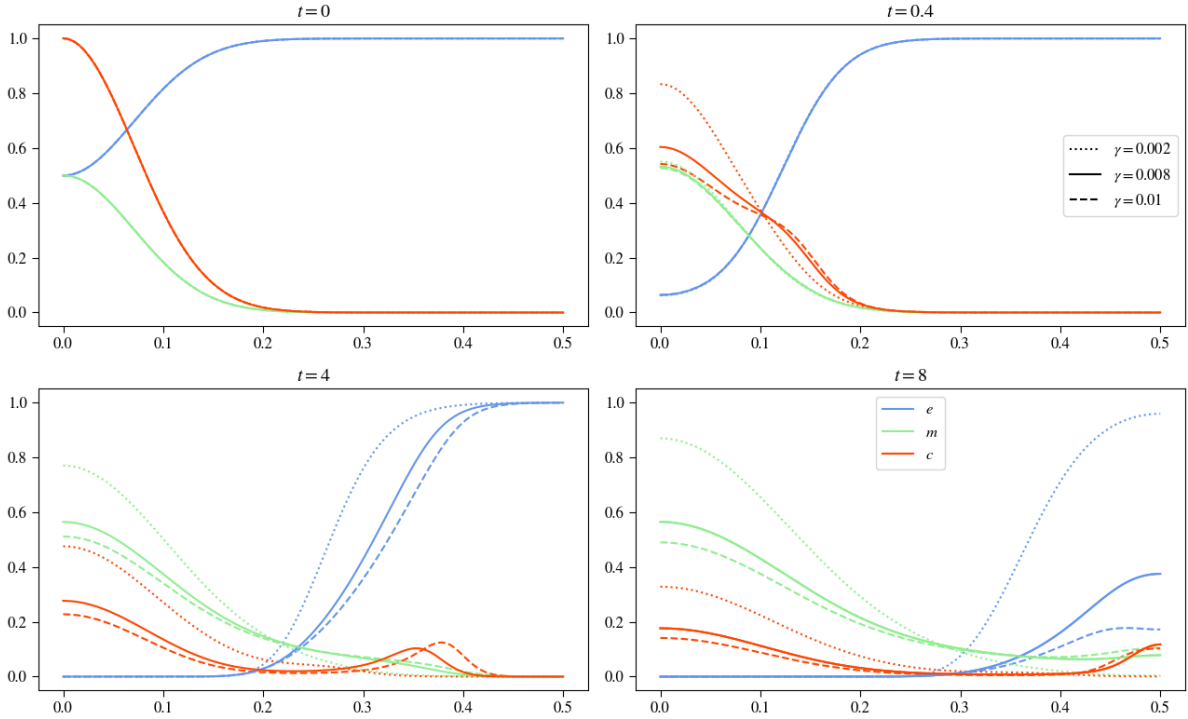


FIGURE 13. Plot results for varying  $\gamma$ , keeping the other parameters constant

the MDE concentration; with increasing  $\gamma$ , the extracellular matrix molecules are faster and more evenly degraded; due to the faster invasion of the tissue, the production of matrix-degrading enzymes also happens in regions farther away from the center. As for varying  $d_c$ , only a little MDE concentration is needed to degrade the extracellular matrix efficiently due to their exponential production, accelerating the ECM degradation process.

In the last plot at  $t = 8$ , the observations from the previous points in time are confirmed; the higher  $\gamma$ , the faster the invasion pace of the tumor cells and the more of a division forms with fewer tumor cells remaining at the origin. The behavior of the tumor cells causes a higher concentration of MDEs at the origin due to exponential growth and a steeper decline moving outwards. With rising  $\gamma$ , the ECM is getting degraded faster.

Out of curiosity, a step furhter is taken increasing  $\gamma$  by one power to  $\gamma = 0.1$ . As previously observed, Haptotaxis pulling the cells into surrounding tissue increase towards high ECM concentrations, causes an even faster invasion process. However, in this case, the invasion pace of the tumor cells is so high that no cells remain at the origin; everything is being pulled into the surrounding tissue. Before finishing the simulation after  $t = 8$ , the tumor cells have reached the domain  $\Omega$ 's border. Upon hitting the border the cells are being reflected back inward due to the boundary conditions of the investigated model, equations 9 and 10. In figure 14, this process is observable. Shortly after  $t = 2$  the tumor cells reach border, the next plot at  $t = 3$  shows them being reflected and moving into the corners of the domain  $\Omega$ , where the ECM concentration is highest. At this point, the pace of the ECM degradation has not been able to keep up with the invasion pace of the tumor cells. After being pulled into the corners at  $t = 3$  and degrading the ECM there,

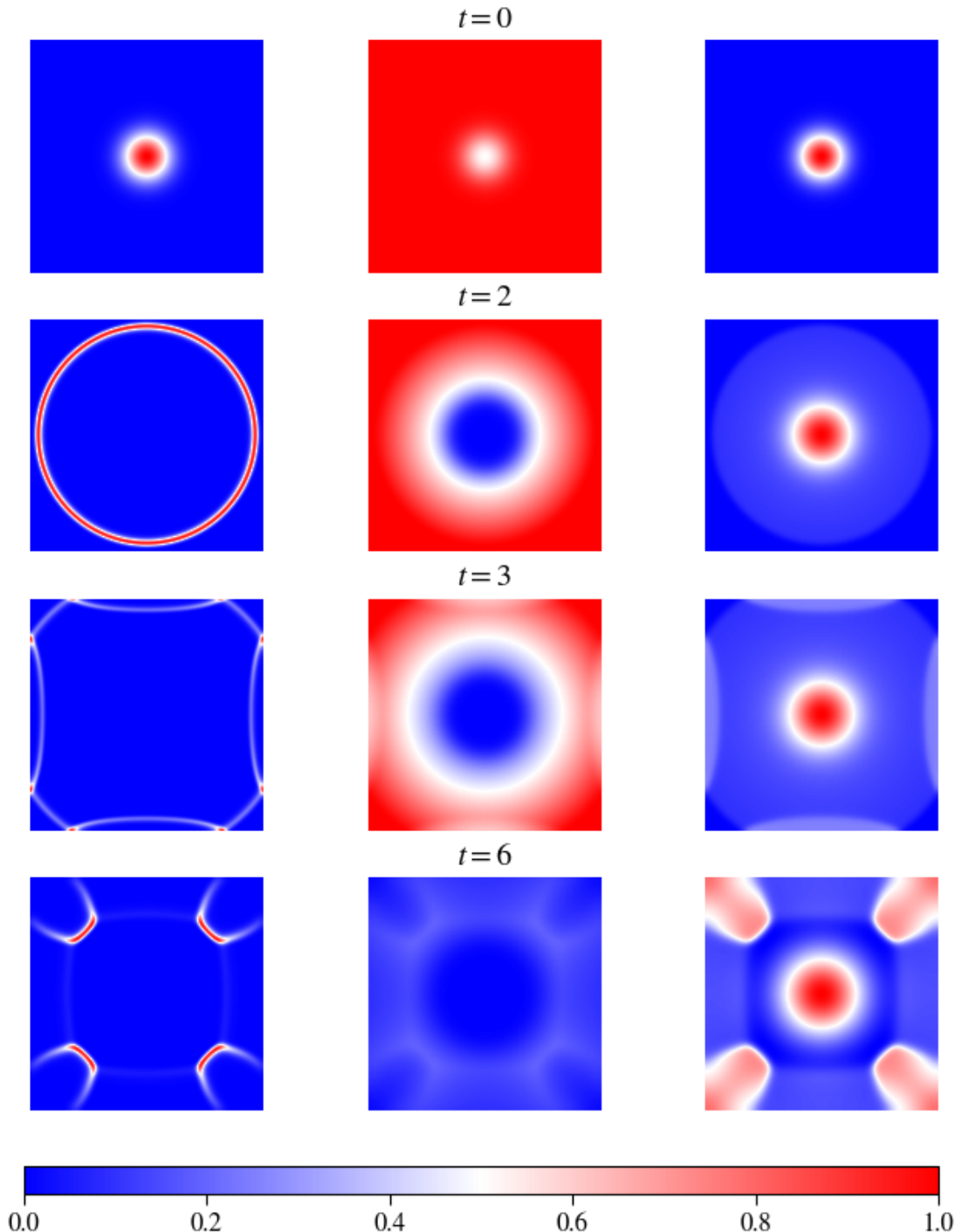


FIGURE 14. 2D Plot results for increasing  $\gamma$  above the definition area, keeping the other parameters constant

at  $t = 6$ , the tumor cells are being pulled back toward the center of the simulation, where

extracellular matrix molecules are still left.

The intuition is met, with increasing  $\gamma$ , the invasion pace of the tumor cells and matrix-degrading enzymes also rises, however getting unexpected behavior in the last experiment, with  $\gamma = 0.1$ . There the ECM degradation has, compared to the experiment with  $\gamma = 0.01$ , been slowed down, due to too high motility of the tumor cells.

Studying those experiments biologically and keeping in mind that the term extracellular matrix describes a whole class of organic and inorganic compounds, the different properties of these elements cause varying effects with respect to Haptotaxis. For example, were the haptotactic effects measured on laminin considerably lower than then ones measured on fibronectin, according to Aznavoorian et al. [12]. Different constellations of extracellular matrix composition will be encountered in different human body sites, which will cause the tumor cells, as seen in the numerical experiments, to behave differently.

### $\eta$ Variation

The parameter  $\eta$  controls the degradation process of the extracellular matrix molecules. Since Anderson et al. [2] used a value of  $\eta = 10$  on all their experiments, an even distribution in  $\eta \sim U[0, 20]$  is assumed in this work. The degradation process of the extracellular matrix is modeled using an exponential decay hypothesis, so with increasing  $\eta$  also an increases in the system's sensitivity concerning the parameter  $\eta$  itself is expected. With its role in controlling the degradation, it will also heavily influence the motility of the tumor cells and with this the motility and production rate of the matrix-degrading enzymes. Slower degradation will result in a stronger haptotactic pull on the tumor cells at the origin. On the other hand increasing  $\eta$ , the ECM will be faster degraded and might provoke a faster invasion of the surrounding tissue by the tumor cells. The higher  $\eta$  is, the fewer MDEs are needed to degrade the ECM efficiently.

Inspecting the results in figure 15 confirms these assumptions.

Significant differences for both curves, tumor cell density and ECM concentration after  $t = 0.4$  are observable. Inspecting the experiment with  $\eta = 2$ , the ECM has only degraded a little, exposing the tumor cells to stronger haptotactic pull of the extracellular matrix molecules in regions closer to the origin, compared to the other experiments. Though it may look like no secondary lump of cells develops, the contrary is the case; even more cells are being pulled into the tissue, with the ECM slowly receding. This smoothes out the bump the other two curves show for the tumor cell density. This results in only one lump of tumor cells that invades the tissue without another remaining at the origin. The same effect is observable when comparing the tumor cell density curves for the higher  $\eta$  values. With fewer tumor cells being pulled outward by the ECM, the higher  $\eta$  gets. Only the curve for the matrix-degrading enzymes has not been affected by the variation of  $\eta$  until now.

The next plot at  $t = 4$  propagates the effects on the tumor cells and the ECM. The slower the degradation process of the extracellular matrix molecules, the more tumor cells invade the tissue and the less of a division is observable. The movement now also affects the concentration of the matrix-degrading enzymes. With the fewer remaining tumor cells at the origin producing the MDEs, also a reduced concentration of MDEs at the origin is observable. However, the distribution of the tumor cells for the lowest case of

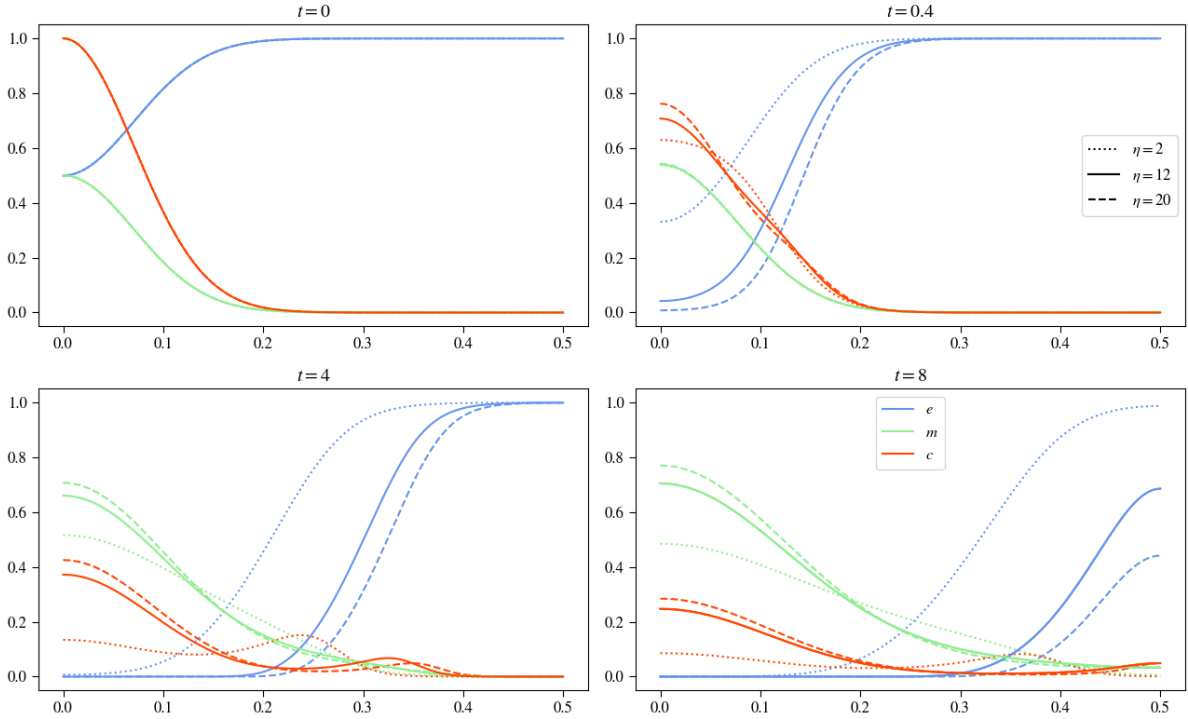


FIGURE 15. Plot results for varying  $\eta$ , keeping the other parameters constant

varying  $\eta$  has a more even distribution of matrix degrading enzymes, compared to the other experiments.

The same goes for the last plot, showing the experiments at  $t = 8$ . The more even the distribution of tumor cells and matrix-degrading enzymes across space, the slower the ECM is degraded.

As mentioned varying  $\gamma$ , the term extracellular matrix include various organic or inorganic compounds. Therefore, the build-up and properties of these compounds vary strongly and motivate this comparison of degradation rates. Some compounds may be degraded faster, while others are complex and need more time to degrade.

### $d_m$ Variation

$d_m$  describes the diffusion coefficient for the matrix-degrading enzymes. As estimates the same values as Anderson et al. and Franssen et al. used in their experiments are used here, assuming an even distribution of  $d_m$  in  $\sim U[1 \cdot 10^{-5}, 1 \cdot 10^{-3}]$ . Having set  $\beta = 0$ , equation 8 modeling the temporal development of the matrix-degrading enzyme concentration solely depends on  $c$  concerning motility and production. Like in the experiments before, an increase of  $\alpha$  causes a higher concentration of MDEs in regions with a high density of tumor cells and increased motility can be expected where the density of the tumor cells rapidly changes. Increasing  $d_m$  will cause a faster, more even spread of the MDEs in the accessible area and results in a faster degradation process of the extracellular matrix molecules. Inspecting the results in figure 16, in the second plot after  $t = 0.4$  it can

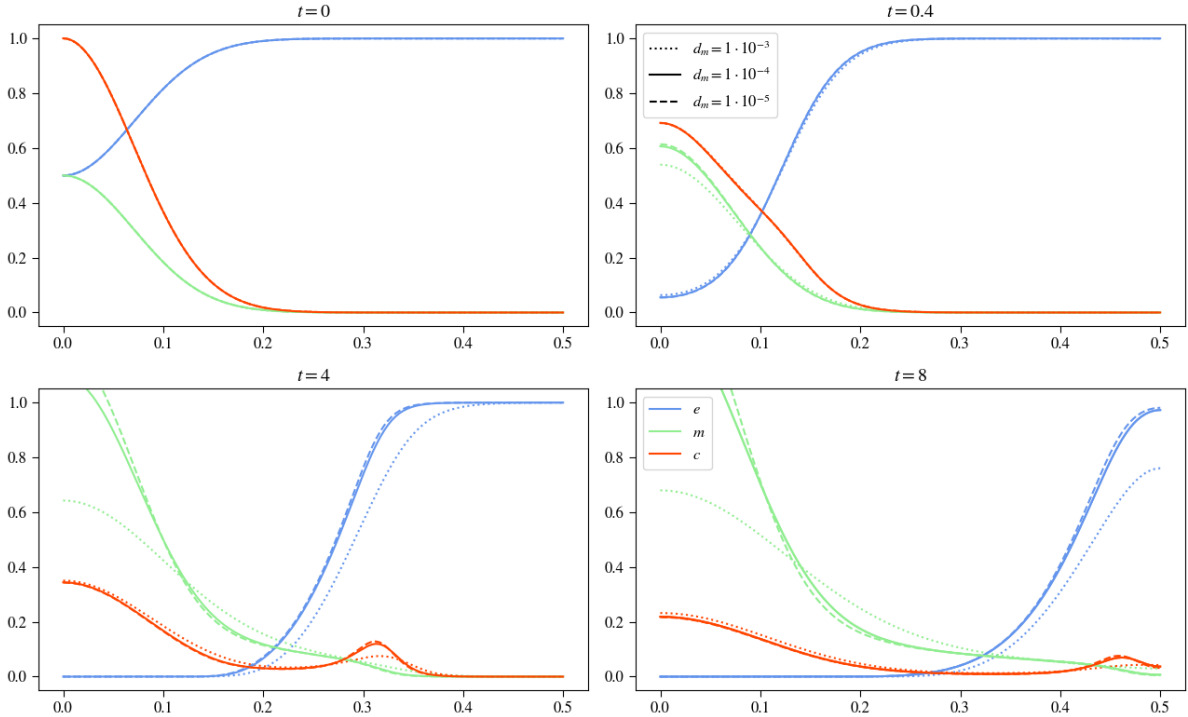


FIGURE 16. Plot results for varying  $d_m$ , keeping the other parameters constant

be observed, that the curves describing the tumor cell density and the ECM are mostly untouched, though looking closely, for the highest  $d_m$  value, the dotted lines, the ECM has at the origin higher and farther out lower concentrations of extracellular matrix molecules. This is caused by the more even distribution of the matrix-degrading enzymes, which reduces the concentration at the origin and causes a faster invasion of the surrounding area of the MDEs, better observable in the plots of later points in time.

The following plot shows the experiments after  $t = 4$  and the differences between the highest  $d_m$  value experiment with the other two are more distinctive. The MDE concentration for this experiment has strongly decreased at the origin, yet having invaded the tissue faster. The ECM has also been degraded faster and like varying  $\eta$ , the faster ECM degradation reduces the effects of Haptotaxis, pulling less tumor cells into the tissue. The other two experiments differ only visibly regarding the MDE concentration, though both exceeding the limits of the plot. The concentration at the origin for the lowest diffusion value is higher than for the experiment with  $d_m = 1 \cdot 10^{-4}$ .

The last plot confirms the above mentioned effects, with the most substantial deviations between the highest  $d_m$  experiment and the other two. A more even spread of the MDEs with a lower concentration at the origin, faster ECM degradation and a tumor cell density curve that has less of a division at its leading edge for the experiment with  $d_m = 1 \cdot 10^{-3}$ . The two experiments with lower  $d_m$  values still have nearly overlaying tumor cell density and ECM curves. Only the MDE concentration differs, showing a more even spread for the higher diffusion value with a lower value at the origin.

Seeing those effects, the intuition is met, however it is to say that looking at the lower

two values for  $d_m$ , the differences are modest. This concludes that the higher the values for  $d_m$  are, the more sensitive the system reacts to changes.

These changes in diffusion, like in the section varying the diffusion coefficient for the tumor cells, might be caused by a multitude of physical influences, such as temperature, electric voltage, pressure, etc. The results show that this change causes a faster degradation of the extracellular matrix molecules but a slightly less aggressive invasive behavior of the tumor cells.

### $\alpha$ Variation

The parameter  $\alpha$  influences how fast the tumor cells produce matrix-degrading enzymes. It is assumed to be evenly distributed with  $\alpha \sim U[0, 1.0]$ , since Anderson et al. assumed the same range in the original paper. Trying to replicate Anderson et al.'s experiment, it was already shown how varying  $\alpha$  affects the simulation results. A higher MDE concentration will cause a faster degradation process of the extracellular matrix molecules. Faster ECM degrading, as seen above, influences the invasion pace of the tumor cells. The previous experiments varying  $d_c$  show that the MDE concentration can take on values higher than one, which we can also expect here for sufficiently high values for  $\alpha$ .

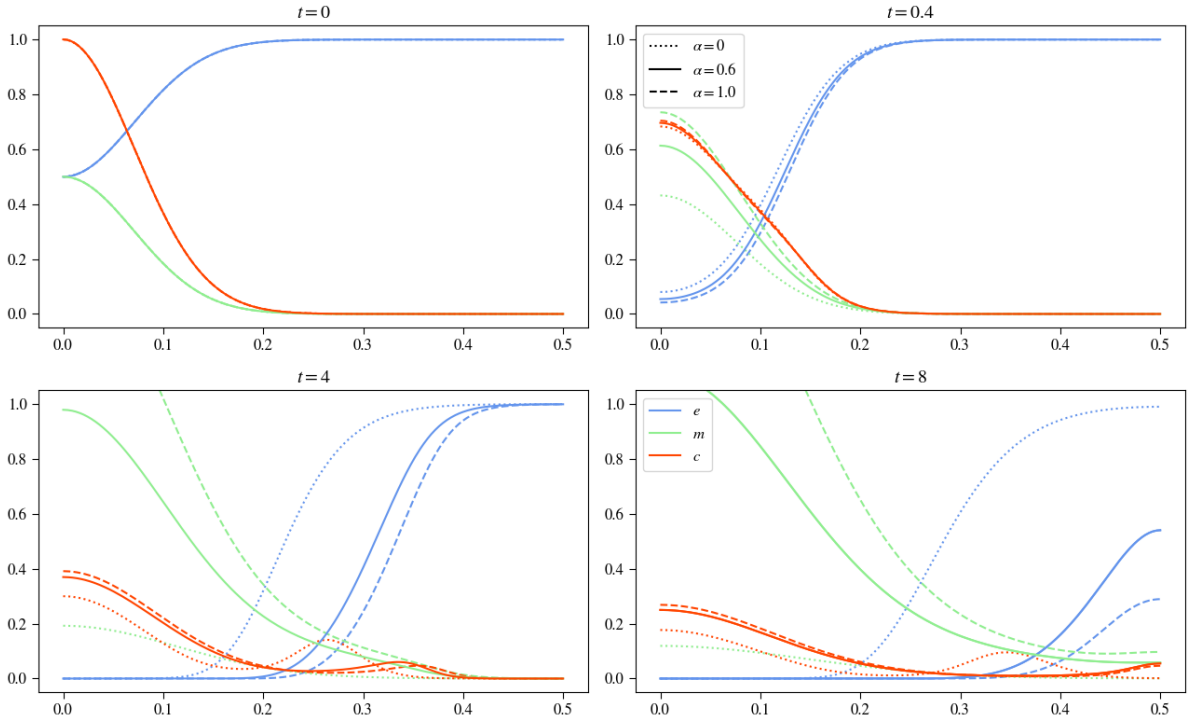


FIGURE 17. Plot results for varying  $\alpha$ , keeping the other parameters constant

The second plot of figure 17 describes the experiments after  $t = 0.4$ . The differences in the MDE curves for the different values of  $\alpha$  are clearly seen. The other curves also show slight deviations. The higher  $\alpha$  is, the faster the ECM degradation. Looking closely, we can observe for the tumor cell densities that the increased rate of ECM degradation

results, as previously already seen, in a curve with less of a bump that will later form the division invading the surrounding tissue due to minor haptotactic influences at the origin.

The next point in time, at  $t = 4$ , shows the previously mentioned effects in a reinforced way. For  $\alpha = 0$ , the MDEs have no producing factor and the curve flattens due to diffusion, though the extracellular matrix has degraded visibly, yet at a considerably slower rate. This experiment has the lowest density of tumor cells at the origin, though the most significant secondary lump of cells detaching from the primary tumor. This behavior is due to the extended exposition of strong haptotactic influences near the origin region, which pulls more cells outward to invade. The solid curves describing  $\alpha = 0.6$  show that at this point, the MDE concentration has almost reached a concentration of one at the center, which will be exceeded later. Compared to the lowest  $\alpha$  experiment, the faster ECM degradation has pulled less of the tumor cells outward, though at a faster invasion pace. Looking at the experiment with the highest  $\alpha$  value, the MDE concentration already exceeds one, the ECM degradation is happening faster and the invasion of the tumor cells is happening faster, though with a lower tumor cell density.

In the last timestep, the MDE curve of  $\alpha = 0.6$  and  $\alpha = 1.0$  exceed one, as was the case varying  $d_m$ . The dotted curve of the MDE concentrations gives a good example of diffusion distributing the concentration throughout space without a producing factor. At the border region the dotted curve is the only one that has not yet degraded any ECM, while the other two experiments show that there is only a little ECM concentration left to degrade in this area. The tumor cells confirm the, in the previous timestep mentioned, effects of faster invasion pace with rising  $\alpha$  though with at a lower density.

The initial assumptions are correct with a faster degradation pace due to higher MDE concentration and faster invasion of the space by both the tumor cells and matrix-degrading enzymes. However, it is interesting to see that the lower  $\alpha$ , the more tumor cells are pulled into the tissue.

While it makes sense from a numerical perspective that the concentration of matrix-degrading enzymes can exceed one, it might make sense to introduce a finer grid or adapt the model in other ways since, judging from a real-world perspective, it does not make sense that at a certain point in space, there is more than one entity occupying this space.

The production of matrix-degrading enzymes can have many biological causes. During many natural processes like tissue repair or remodeling, the extracellular matrix must be degraded, controlled by cells producing enzymes that are responsible for producing matrix-degrading enzymes. This control flow can be interrupted by malignant cells stimulating the production of MDEs without any repair or remodeling tasks to perform. Considering the absence of, or reduced MDE production, we can regard this case as the consequence of a drug treatment. On the other hand, since there are plenty of different types of matrix-degrading enzymes the production rate also varies.

### $\beta$ Variation

The factor  $\beta$  controls the decay of the matrix-degrading enzymes. The results of its variation are shown in figure 18. Using Kolev et al.'s estimate for  $\beta$  in [13], an even distribution of  $\beta$  in  $\beta \sim U[0.005, 0.1]$  is assumed. Interestingly, the ranges for  $\alpha$  and  $\beta$  differ, as the experiments confirm. While the MDEs are produced by the tumor cells,

their decay is controlled by the themselves. This model assumes that the tumor cells do not proliferate, which makes their total amount constant. In contrast, the MDEs are produced by the tumor cells and are expected to change in amount over time due to production or decay. This makes the decay rate of the MDEs more variable because of the changing amount of total MDEs, explaining the change of their differing distributions.

With introducing  $\beta$ , the MDE curve will be lower or at least increase slower. This influences the ECM degrading process and as well the invasion pace as the haptotactic effects on the tumor cells.

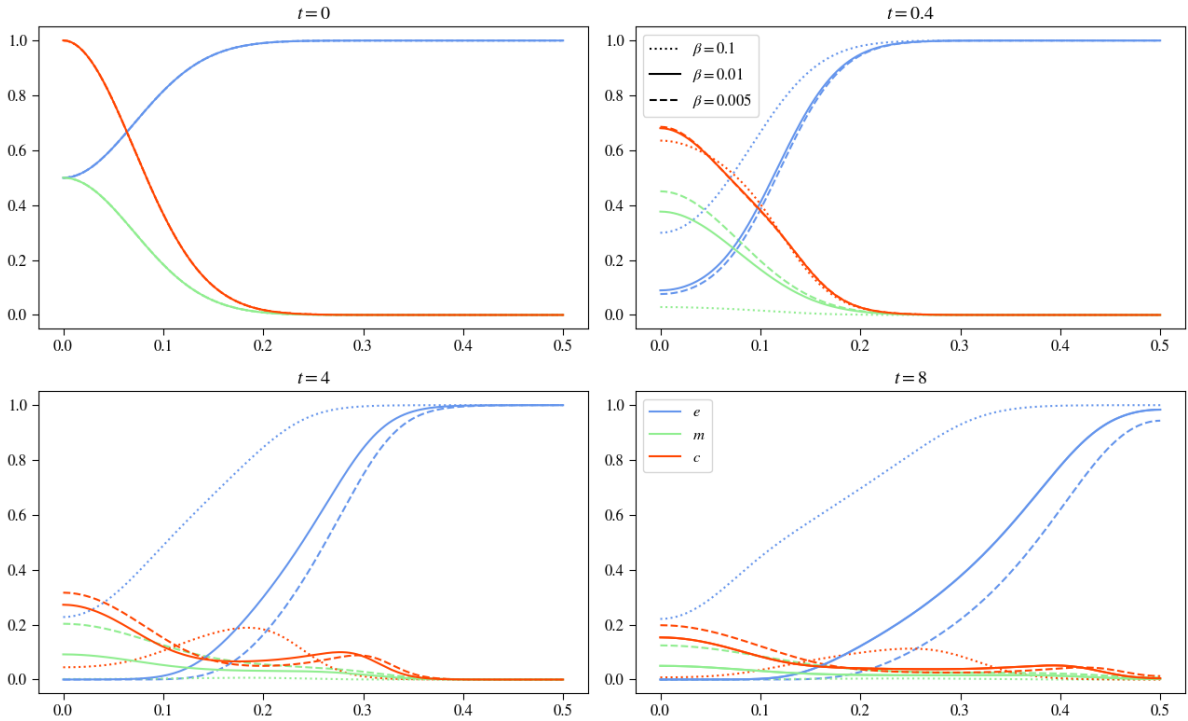


FIGURE 18. Plot results for varying  $\beta$ , keeping the other parameters constant

As seen in the results of figure 18, a value of  $\beta = 0.1$  is sufficient to after already  $t = 0.4$  reduce the MDE concentration to nearly zero. In this case, the decay rate turned out to be too high, outpacing production entirely, with matrix-degrading enzyme concentration vanishing spacially and temporarily. The immediate decay of the MDEs causes a drastically slower ECM degradation, yet it has not stopped entirely since the tumor cells still produce matrix-degrading enzymes. This slow degradation of the extracellular matrix, creates a haptotactic pull, as already described, that lasts a lot longer temporarily in regions around the origin, which pulls all of the cancer cells outward to invade the tissue, leaving no primary lump of tumor cells at the origin. Since more MDEs are produced in regions with high tumor cell density, this also causes a, yet considerably slower, but more even degradation of the extracellular matrix, causing a more substantial stretch of the tumor cells.

In the other experiments, it is observed that with decreasing  $\beta$  and slowing down the decay of the matrix-degrading enzymes, first, the ECM degradation accelerates and this

causes the effects of Haptotaxis to develop the two lumps of tumor cells, one staying at the center the other detaching and invading the tissue at a faster rate.

Since the extracellular matrix can comprise many different organic and inorganic compounds, the matrix-degrading enzymes are also very diverse. This diversity results in different decay rates, so choosing the right one for a specific experiment can be crucial. While this variation describes the effects of different enzymes, it can also describe, like for the production of the MDEs, the influence of a drug to accelerate the decay of the matrix-degrading enzymes.

### Cross-Variation

Having varied every parameter of the model given by equations 6, 7 and 8, neglecting proliferation and renewal, both accelerating and slowing effects on the invasion of the tumor cells were observed. In this section it is examined how supporting and annihilating factors interplay and influence the simulation outcomes, for example, how increasing both  $\alpha$  and  $\beta$  affects the MDe concentration. Another interesting experiment is how diffusion and Haptotaxis behave when increasing or decreasing both factors.

#### $d_c - \gamma$ Variation

Started with varying  $d_c$  and  $\gamma$  and studying these results in figure 19, gives a clearer understanding of the interplay between diffusion and Haptotaxis.

Having set  $d_c = 5 \cdot 10^{-5}$  and  $\gamma = 0.001$ , no division of tumor cells is depictable; the effects of Haptotaxis being too small leaves the tumor cells only subject to diffusion, which results in an even distribution process over time, also causing a slower invasion pace. Because the tumor cells stay in a lump at the origin  $x = 0$ , their curve decreasing monotonely outward, the MDEs also take on their maximum at the origin. The slower invasion pace of both tumor cells and matrix-degrading enzymes causes a slower ECM degradation process.

Setting  $\gamma = 0.01$ , the effects of Haptotaxis are now distinctive with a very sharp maximum of the detaching lump of cancer cells seen at  $t = 4$ , which equals the maxima of the remaining tumor cell lump at  $x = 0$ . The substantial increase of Haptotaxis leads to a faster invasion pace of the tumor cells into the tissue, when  $d_c$  is kept konstant. With the creation of the matrix-degrading enzymes while invading the surrounding tissue, a more even distribution of the MDEs is observed as well as faster ECM degradation.

Looking at the right side of the plot 19, the results for increasing  $d_c = 1 \cdot 10^{-3}$  are shown. In total both columns of plots yield the same results, though on the right side, the influence of diffusion is clear to see. Though with a low  $\gamma$  value the red dotted curve depicting the tumor cell density on the right-side plots does not develop a division of tumor cells as well, it invades the tissue considerably faster than the experiemnt with low diffusion values. This change is also clearly visible in the MDE and ECM concentrations. Considering the experiment with high values for both diffusion and Haptotaxis we see that the tumor cells develop the seondary lump of cells detaching from the main lump, yet in this experiment the maximum of it is not as sharp as for the low diffusion and high Haptotaxis experiment.

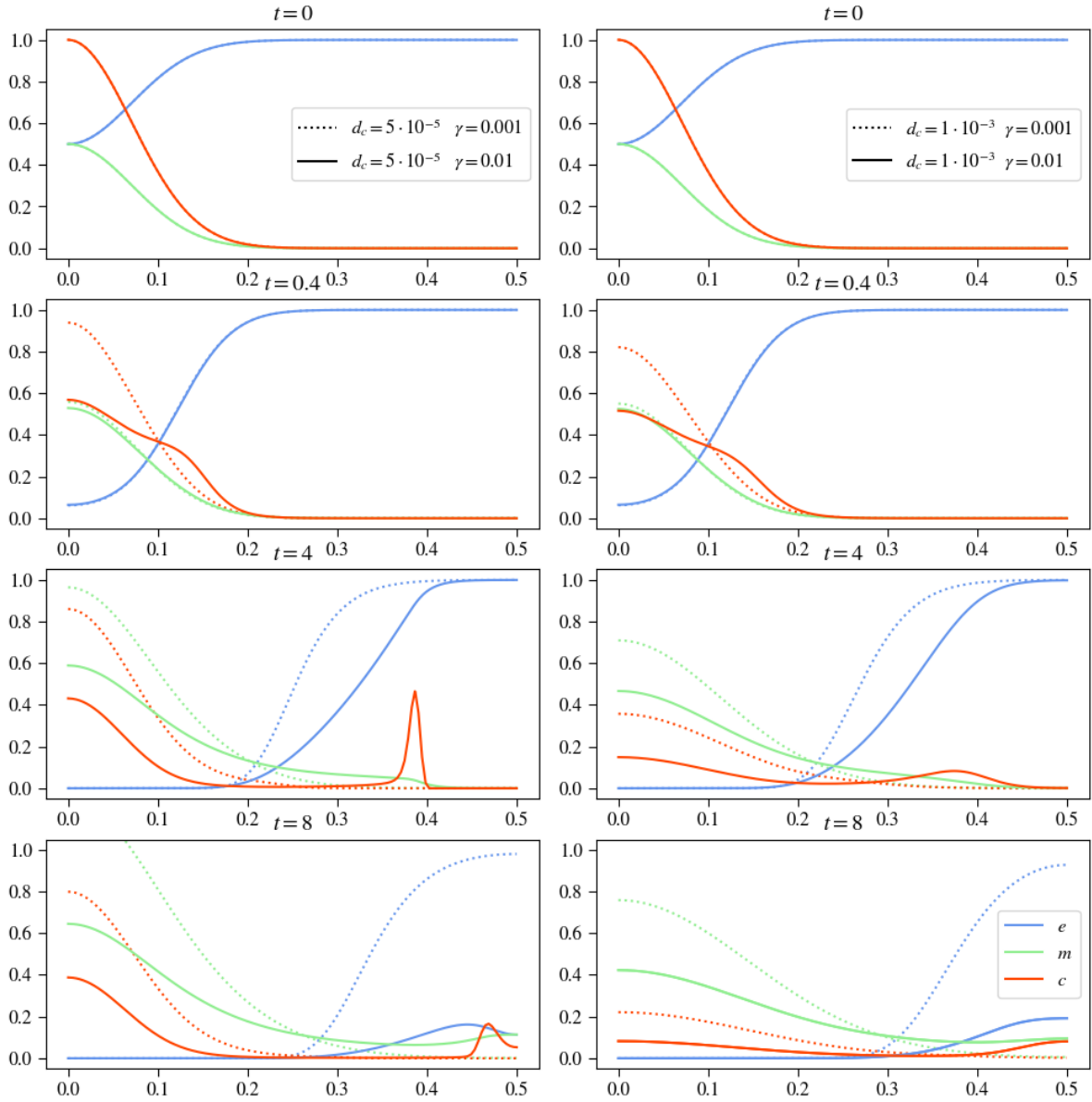
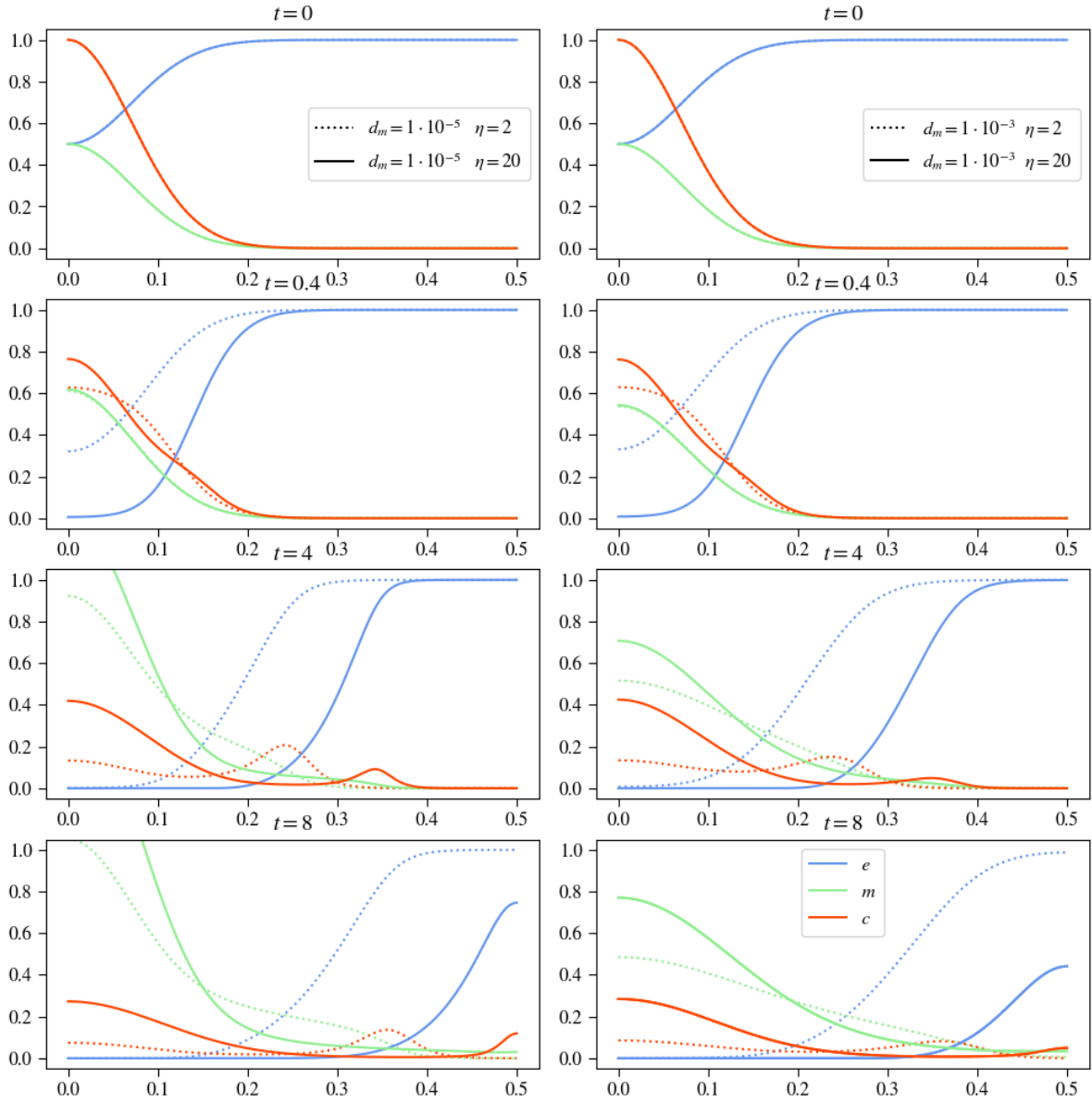


FIGURE 19. Plot results for varying  $d_c, \gamma$ , keeping the other parameters constant

These experiments give an excellent example of the relationship between Haptotaxis and diffusion. With decreasing  $d_c$  but increasing  $\gamma$ , a sharp leading edge develops. The high value for  $\gamma$  was for both cases of  $d_c$  sufficient to form a secondary tumor site invading the tissue separately, though also increasing  $d_c$  showed that this measure decreases the effect of Haptotaxis. Decreasing  $\gamma$  has proven for high and low  $d_c$  values to prevent a secondary lump of cells from developing.

### $\eta - d_m$ Variation

Comparing both columns for varying  $d_m$  in figure 20, though looking at the same  $\eta$  valued experiments, only minor differences are to be seen regarding the shape of the tumor cell

FIGURE 20. Plot results for varying  $\eta, d_m$ , keeping the other parameters constant

density curve and ECM concentration curve. On the left side, the ECM degradation is happening slightly slower, which causes the haptotactic effects on the tumor cells to change, increasing the detaching secondary lump of cells invading the tissue. The curves on the left side regarding tumor cell density and MDE concentration are not as evenly stretched as on the right.

Interestingly, the MDE concentration for lower  $d_m$  values is considerably higher for both experiments varying  $\eta$ , than for the ones with higher  $d_m$  values. Since the tumor cells produce the MDEs, and on the plots on the left side their density is higher in the region near the origin, the exponential production rate can explain this behavior. However it is interesting to see these minimal differences causing drastic changes in the MDE concentration.

These experiments conclude that the diffusive properties of the matrix-degrading enzymes play only a minor role in degrading the extracellular matrix. Tumor cells producing them in their wake play a more crucial role in the degradation process. An intriguing observation in this experiment is that minimal differences in tumor cell density are sufficient to create major differences in the MDE concentration due to their exponential production.

### $\alpha - \beta$ Variation

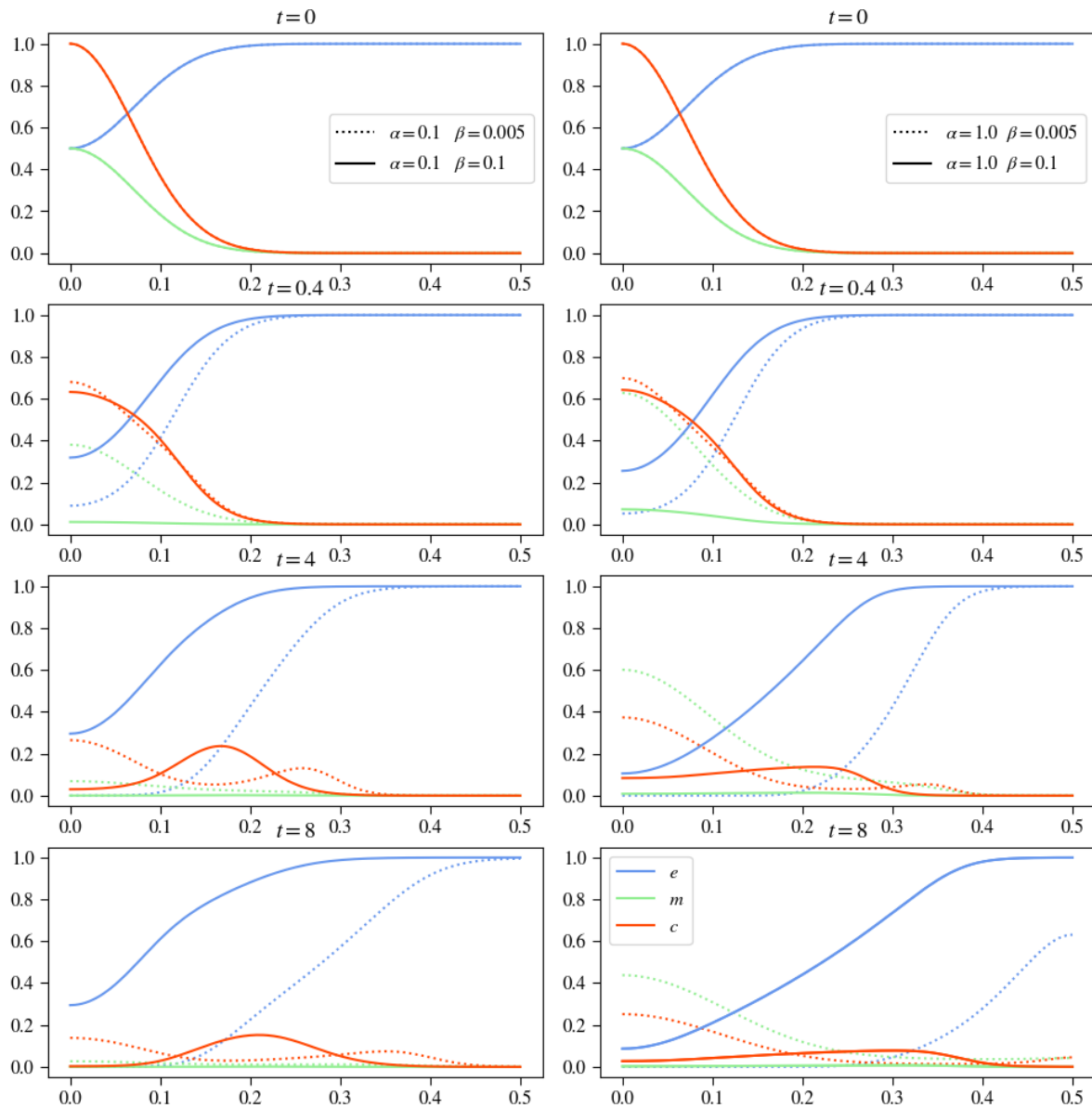


FIGURE 21. Plot results for varying  $\alpha, \beta$ , keeping the other parameters constant

Looking at figure 21 the experimental results varying both  $\alpha$  and  $\beta$  are displayed. For low MDE production and low MDE decay, the curve for the MDEs is still visible at up to  $t = 4$ ; at  $t = 8$ , it is zero. This causes the ECM degrading to happen faster

than for high  $\beta$  values; therefore, the tumor cells develop the two characteristic lumps of cells, with one invading the tissue and the other staying at the origin. The maxima for both lumps are lower than in previous experiments, indicating a more even distribution of the tumor cells between the two lumps. Increasing  $\beta = 0.1$ , the MDE curve appears to be zero after again already  $t = 0.4$  and stays there until the end of this experiment, as was shown in the section varying  $\beta$ . This low concentration of MDEs causes a slower ECM degrading process, leading the tumor cells to develop only one lump, invading the space. For  $\alpha = 0.1$ , both values of  $\beta$  shown to be too high, decaying the matrix-degrading enzymes too fast to keep up with production.

On the other hand, increasing  $\alpha$  to 1.0 and keeping  $\beta = 0.005$ , we see that production outweighs decay. At the end of the experiment at  $t = 8$ , the MDEs still have a considerable concentration left. In this experiment, the ECM degradation was sufficiently fast to make the tumor cells develop two lumps of cells. Increasing both  $\alpha$  and  $\beta$ , the solid line of the right column of figure 21 shows that decay outweighs production again, after  $t = 0.4$  we can only see a small remaining portion of matrix-degrading enzymes at the origin. This again causes slower ECM degradation and develops only one lump of tumor cells due to the strong effects of Haptotaxis, though this singular lump is stretched very flat along the x-axis.

In these experiments we see that varying both  $\alpha$  and  $\beta$  it is possible to find a balance between the two, not letting one of them get the upper hand suppressing important effects.

### $d_m - \alpha - \beta$ Variation

Varying all parameters regarding the equation for the matrix-degrading enzymes required to split the results into two figures, 22 and 23.

Looking at the results for the same  $\alpha$  and  $\beta$  values, the curves describing the tumor cell density share their behavior across varying  $d_m$ . For low  $\beta$  values, the division of tumor cells, detaching from the primary tumor, is observable in every experiment. Considering how  $\alpha$  influences this lump, it is observable that with increasing  $\alpha$ , the lump gets smaller and more of the tumor cells stay near the origin. Taking the experiments with high  $\beta$  values in regard, the curves fail to develop a secondary lump of tumor cells to invade separately in every case of  $d_m$  or  $\alpha$ . As seen in all the experiments varying  $\eta$ , a slowed degradation rate of the extracellular matrix leads to the extended exposition of the tumor cells at the origin to more substantial Haptotaxis effects. This leads to all tumor cells being pulled outward into the tissue, leaving little or no cells near the origin. This results in only one lump of cells to invade the surrounding area.

Taking the curve of the extracellular matrix into account, only minimal deviations when varying  $d_m$  are observable, with no apparent changes in figures 22 and 23 regarding the ECM concentration. That supports our claim from above that the diffusion of the matrix-degrading enzymes plays only a minor role in degrading the ECM, and also for the entire system.

The MDE curve can explain the effects mentioned above on ECM and tumor cell density curves. For every experiment reagrding the high value for  $\beta$  it is observed, that the curve of the MDEs was after already  $t = 0.4$  zero. Increasing the production rate  $\alpha$  was insufficient to counter the matrix-degrading enzymes' fast decay process, resulting

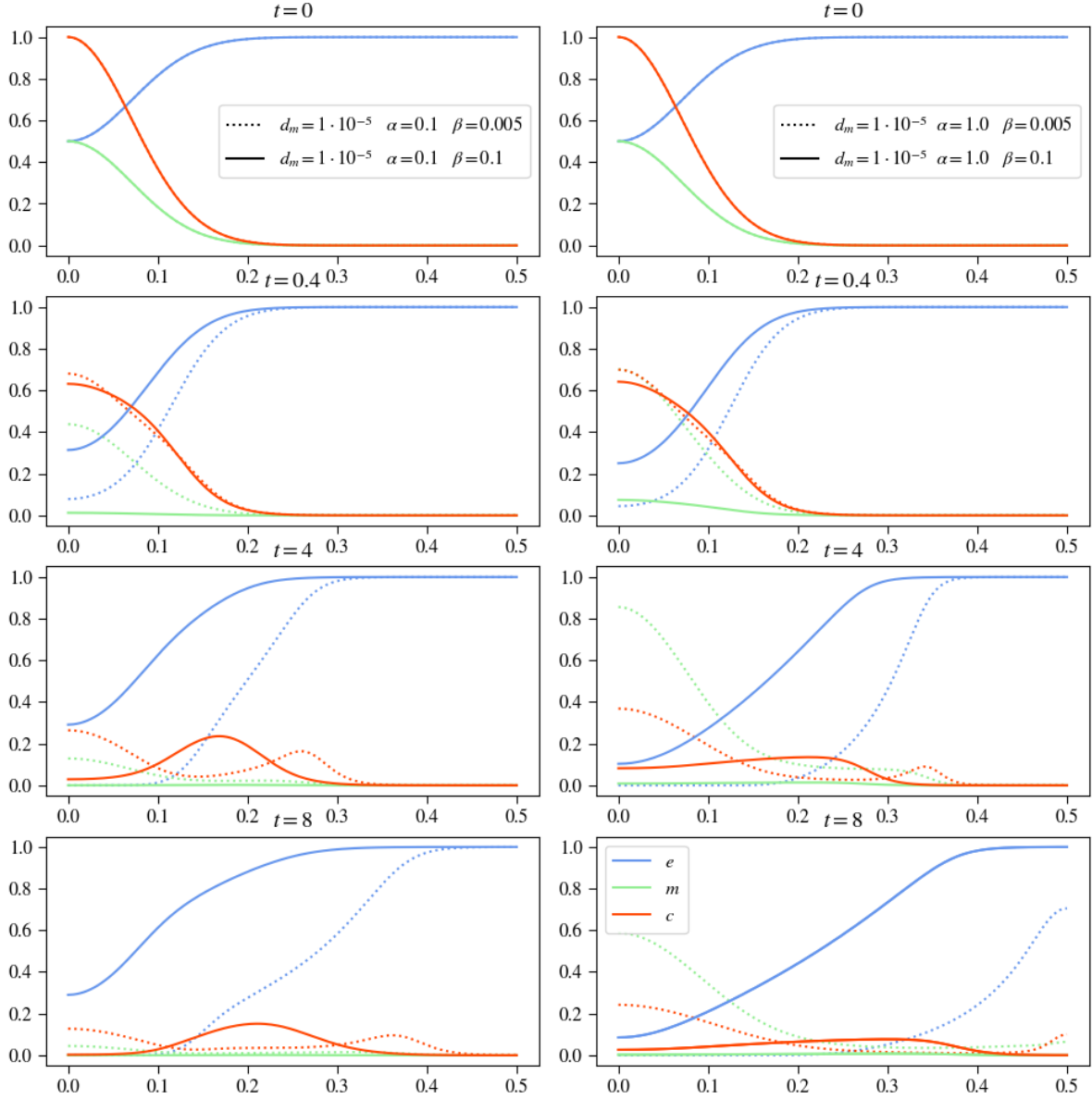
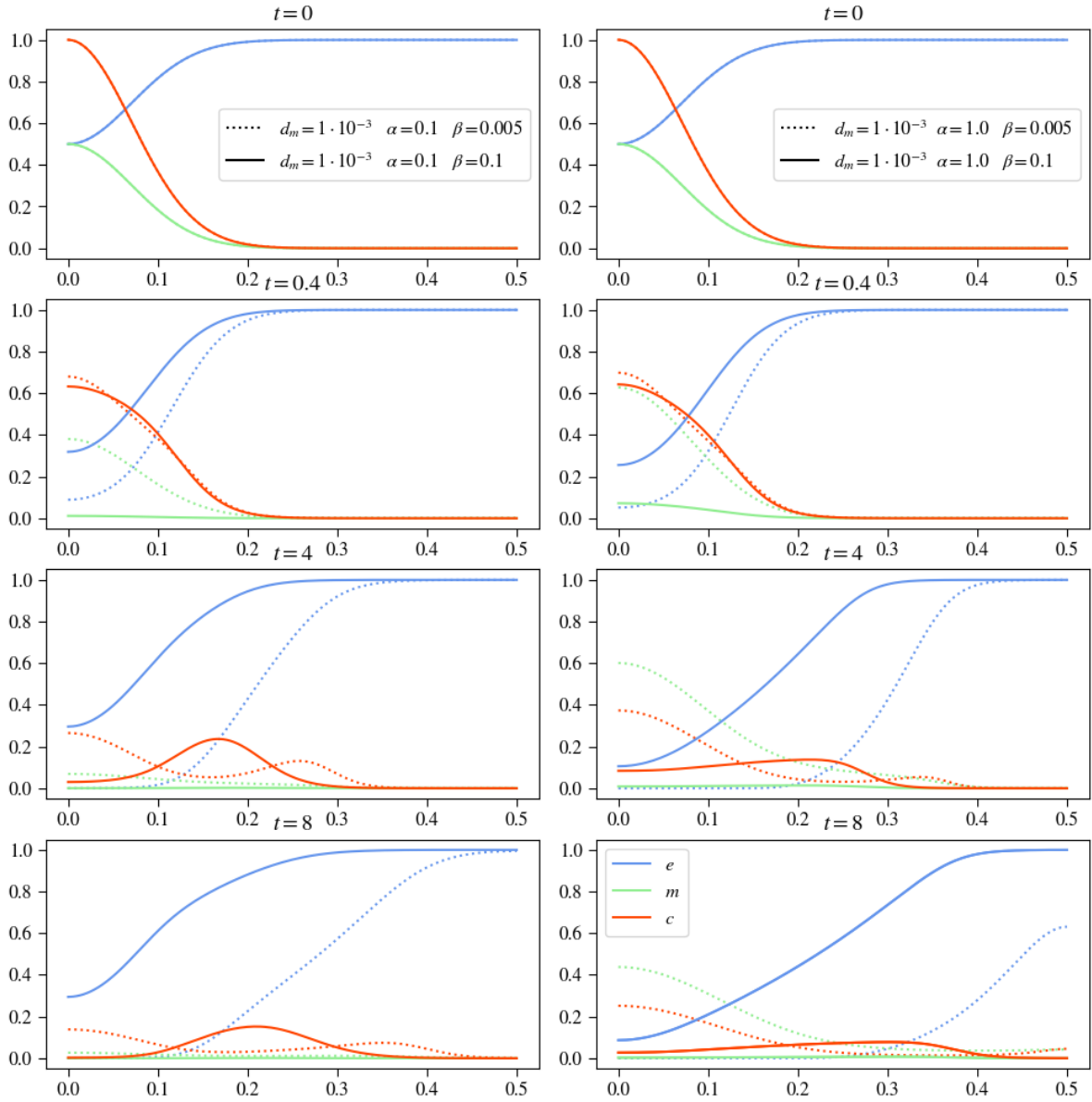


FIGURE 22. Plot results for varying  $d_m, \alpha, \beta$ , keeping the other parameters constant

in the drastically slowed ECM degradation process. That in turn caused the immense effects of Haptotaxis on the tumor cells, explaining why there is no visible change in the experiments varying  $d_m$  and  $\alpha$ . This again underlines the significance of the decay parameter  $\beta$  and setting it not too high distorting the outcomes.

### 4.3 Parameter Analysis with Proliferation and Renewal - Homogenous ECM

This section will examine how introducing tumor cell proliferation and extracellular matrix renewal influences the system. Modeled as logistic growth terms, with a limiting factor of spacial occupation, the parameters  $\mu_1$  for tumor cell proliferation and growth and  $\mu_2$

FIGURE 23. Plot results for varying  $d_m, \alpha, \beta$ , keeping the other parameters constant

for extracellular matrix renewal describe their influences. Instead of treating them as parameters to vary, the entire system is inspected again, since they have the capabilities to change the resulting simulations massively.

Tumor cell proliferation describes the natural ability of cells to proliferate. However, in the case of tumor cells, the production signaling comes from themselves, surpassing the control chain that limits normal cells to proliferate uncontrollably.

The extracellular matrix is a naturally dynamic structure that undergoes continuous degradation and remodeling. It does this in order to secure tissue development, wound repair tasks, regulate cellular functions and many more tasks. In a model describing the ECM, it is crucial to introduce a factor that incorporates these remodeling processes.

As in section 4.2, we use the same initial conditions for all three variables, assuming

we have a homogenous ECM structure. Figure 3 depicts these initial conditions on the three variables  $c, e, m$  at dimensionless time  $t = 0$ .

Figure	Linestyle	$d_c$	$\gamma$	$\mu_1$	$\eta$	$\mu_2$	$d_m$	$\alpha$	$\beta$
24	.....	$5 \cdot 10^{-4}$	0.0055	0	10	0	$1 \cdot 10^{-3}$	0.3564	0
24	—	$5 \cdot 10^{-4}$	0.0055	0.1	10	0.5	$1 \cdot 10^{-3}$	0.3564	0
25	.....	$1 \cdot 10^{-3}$	0.0055	0.1	10	0.5	$1 \cdot 10^{-3}$	0.3564	0
25	—	$1 \cdot 10^{-4}$	0.0055	0.1	10	0.5	$1 \cdot 10^{-3}$	0.3564	0
25	- - -	$5 \cdot 10^{-5}$	0.0055	0.1	10	0.5	$1 \cdot 10^{-3}$	0.3564	0
26	.....	$5 \cdot 10^{-4}$	0.002	0.1	10	0.5	$1 \cdot 10^{-3}$	0.3564	0
26	—	$5 \cdot 10^{-4}$	0.008	0.1	10	0.5	$1 \cdot 10^{-3}$	0.3564	0
26	- - -	$5 \cdot 10^{-4}$	0.01	0.1	10	0.5	$1 \cdot 10^{-3}$	0.3564	0
27	.....	$5 \cdot 10^{-4}$	0.0055	0	10	0.5	$1 \cdot 10^{-3}$	0.3564	0
27	—	$5 \cdot 10^{-4}$	0.0055	0.5	10	0.5	$1 \cdot 10^{-3}$	0.3564	0
27	- - -	$5 \cdot 10^{-4}$	0.0055	1.0	10	0.5	$1 \cdot 10^{-3}$	0.3564	0
28	.....	$5 \cdot 10^{-4}$	0.0055	0.1	2	0.5	$1 \cdot 10^{-3}$	0.3564	0
28	—	$5 \cdot 10^{-4}$	0.0055	0.1	12	0.5	$1 \cdot 10^{-3}$	0.3564	0
28	- - -	$5 \cdot 10^{-4}$	0.0055	0.1	20	0.5	$1 \cdot 10^{-3}$	0.3564	0
29	.....	$5 \cdot 10^{-4}$	0.0055	0.1	10	0.1	$1 \cdot 10^{-3}$	0.3564	0
29	—	$5 \cdot 10^{-4}$	0.0055	0.1	10	0.6	$1 \cdot 10^{-3}$	0.3564	0
29	- - -	$5 \cdot 10^{-4}$	0.0055	0.1	10	1.0	$1 \cdot 10^{-3}$	0.3564	0
30	.....	$5 \cdot 10^{-4}$	0.0055	0.1	10	0.5	$1 \cdot 10^{-3}$	0.3564	0
30	—	$5 \cdot 10^{-4}$	0.0055	0.1	10	0.5	$1 \cdot 10^{-4}$	0.3564	0
30	- - -	$5 \cdot 10^{-4}$	0.0055	0.1	10	0.5	$1 \cdot 10^{-5}$	0.3564	0
31	.....	$5 \cdot 10^{-4}$	0.0055	0.1	10	0.5	$1 \cdot 10^{-3}$	0	0
31	—	$5 \cdot 10^{-4}$	0.0055	0.1	10	0.5	$1 \cdot 10^{-3}$	0.6	0
31	- - -	$5 \cdot 10^{-4}$	0.0055	0.1	10	0.5	$1 \cdot 10^{-3}$	1.0	0
32	.....	$5 \cdot 10^{-4}$	0.0055	0.1	10	0.5	$1 \cdot 10^{-3}$	0.3564	0.1
32	—	$5 \cdot 10^{-4}$	0.0055	0.1	10	0.5	$1 \cdot 10^{-3}$	0.3564	0.01
32	- - -	$5 \cdot 10^{-4}$	0.0055	0.1	10	0.5	$1 \cdot 10^{-3}$	0.3564	0.005
33 - left	.....	$5 \cdot 10^{-4}$	0.0055	0.1	10	0.1	$1 \cdot 10^{-3}$	0.3564	0
33 - left	—	$5 \cdot 10^{-4}$	0.0055	0.1	10	1.0	$1 \cdot 10^{-3}$	0.3564	0
33 - right	.....	$5 \cdot 10^{-4}$	0.0055	1.0	10	0.1	$1 \cdot 10^{-3}$	0.3564	0
33 - right	—	$5 \cdot 10^{-4}$	0.0055	1.0	10	1.0	$1 \cdot 10^{-3}$	0.3564	0
34 - left	.....	$1 \cdot 10^{-5}$	0.001	0.1	10	0.5	$1 \cdot 10^{-3}$	0.3564	0
34 - left	—	$1 \cdot 10^{-5}$	0.001	1.0	10	0.5	$1 \cdot 10^{-3}$	0.3564	0
34 - right	.....	$1 \cdot 10^{-5}$	0.01	0.1	10	0.5	$1 \cdot 10^{-3}$	0.3564	0
34 - right	—	$1 \cdot 10^{-5}$	0.01	1.0	10	0.5	$1 \cdot 10^{-3}$	0.3564	0
35 - left	.....	$1 \cdot 10^{-3}$	0.001	0.1	10	0.5	$1 \cdot 10^{-3}$	0.3564	0
35 - left	—	$1 \cdot 10^{-3}$	0.001	1.0	10	0.5	$1 \cdot 10^{-3}$	0.3564	0
35 - right	.....	$1 \cdot 10^{-3}$	0.01	0.1	10	0.5	$1 \cdot 10^{-3}$	0.3564	0
35 - right	—	$1 \cdot 10^{-3}$	0.01	1.0	10	0.5	$1 \cdot 10^{-3}$	0.3564	0

continued on next page

Figure	Linestyle	$d_c$	$\gamma$	$\mu_1$	$\eta$	$\mu_2$	$d_m$	$\alpha$	$\beta$
36 - left	.....	$5 \cdot 10^{-4}$	0.0055	0.1	2	0.1	$1 \cdot 10^{-3}$	0.3564	0
36 - left	—	$5 \cdot 10^{-4}$	0.0055	0.1	2	1.0	$1 \cdot 10^{-3}$	0.3564	0
36 - right	.....	$5 \cdot 10^{-4}$	0.0055	0.1	20	0.1	$1 \cdot 10^{-3}$	0.3564	0
36 - right	—	$5 \cdot 10^{-4}$	0.0055	0.1	20	1.0	$1 \cdot 10^{-3}$	0.3564	0

TABLE 4. Overview of all experiments conducted for the model with proliferation and renewal producing 2D output

Also like in section 4.2, in table 4 a detailed overview of all the experiments done in this section is displayed for the parameters used to produce the results. All figures describe multiple experiments; the linestyle of the curve in the figure determines which experiment is precisely described by the set of parameters.

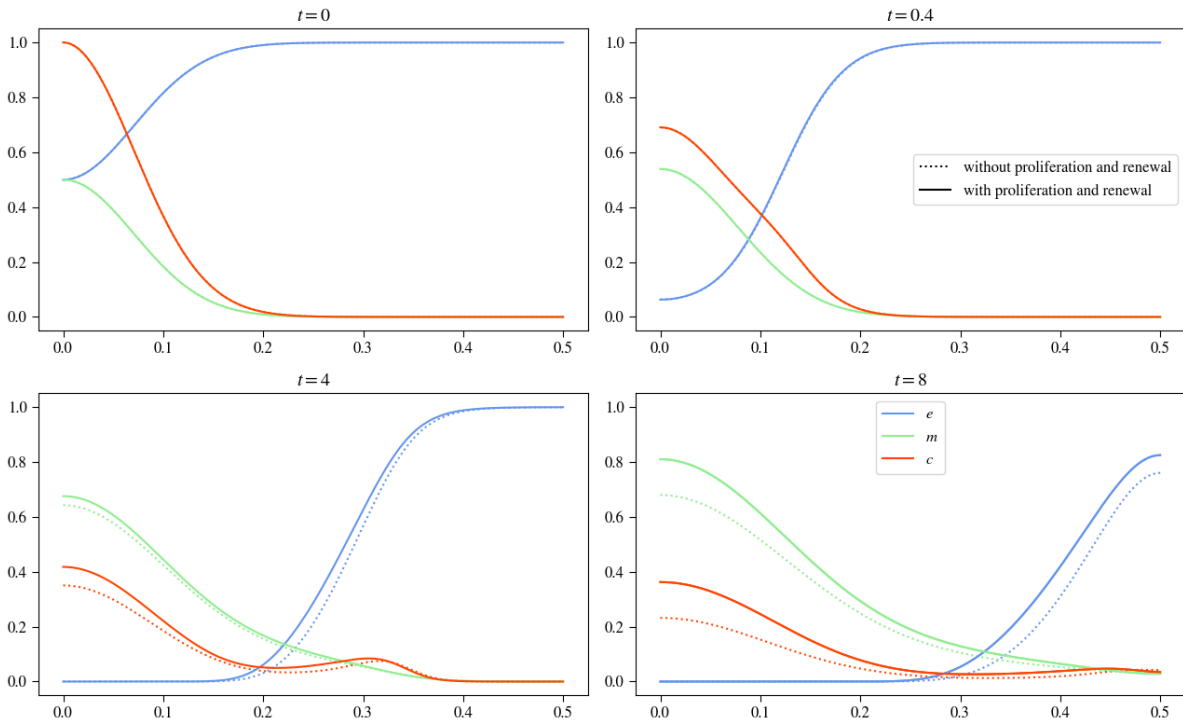


FIGURE 24. Describing the updated basecase, in the image above only the updated basecase is plotted, below it is compared to the initial basecase.

Figure 24 compares how introducing both parameters  $\mu_1 = 0.1$  and  $\mu_2 = 0.5$  affects the system. These estimates are taken from Kolev et al.'s experiments with this model. Like in the Parameter Analysis regarding the system without proliferation and renewal the set of parameters introducing  $\mu_1$  and  $\mu_2$  are used as a foundation to compare the following results against.

Comparing the basecase of the extended model to the basecase of the model without proliferation or renewal, the influences of both  $\mu_1$  and  $\mu_2$  are distinctive. The tumor cell density curve is visibly higher than without proliferation, causing a higher production of

matrix-degrading enzymes. However, this is countered by the renewal factor  $\mu_2$ , causing the ECM concentration to be higher at the end, at  $t = 8$ , than in the initial basecase experiment, yet having both higher density for the tumor cells and the matrix-degrading enzyme concentration.

Regarding the variation of dimensions, these measures can be used to mimic tumor cell density curves better across different dimensions.

For the Parameter Analysis of the model with proliferation and renewal, the focus lies on comparing the extended model's results with those produced by the model without proliferation and renewal. This will underline the influence  $\mu_1$  and  $\mu_2$  have on the system.

### $d_c$ Variation

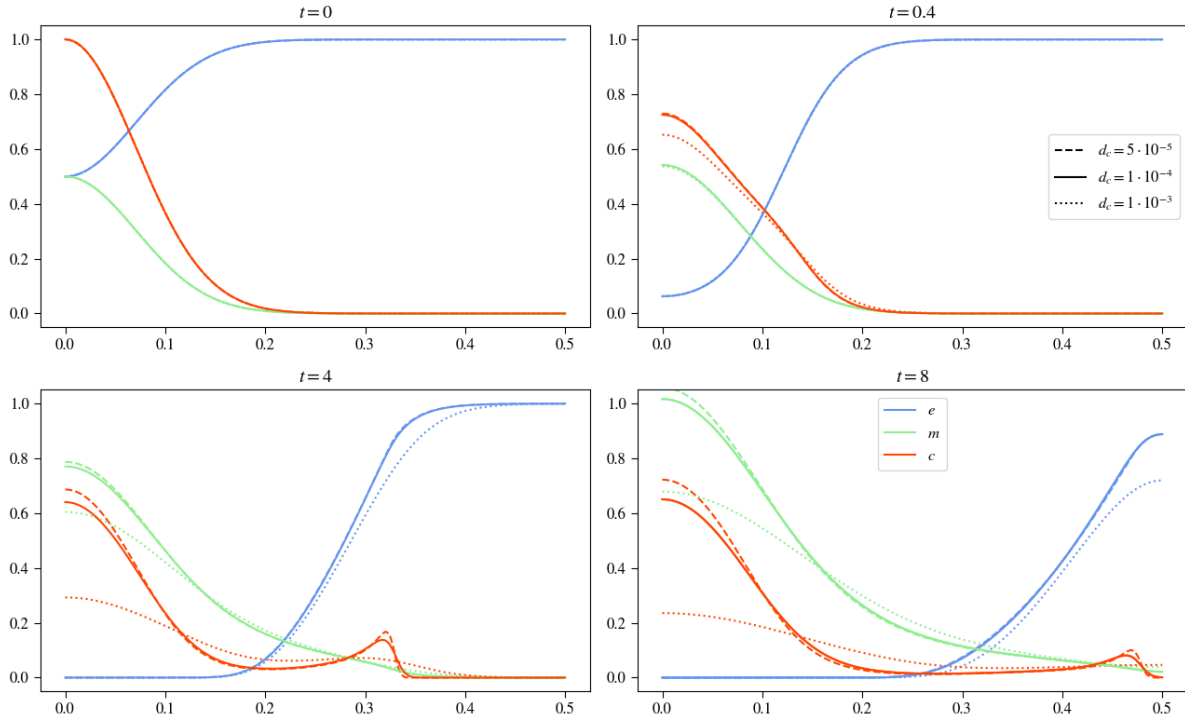


FIGURE 25. Plot results for varying  $d_c$ , keeping the other parameters constant

Varying  $d_c$  with proliferation and renewal terms, the observed effects are the same as without proliferation. Higher values for  $d_c$  cause a more substantial influence of diffusion and a weaker one for Haptotaxis. This leads to a curve with less of secondary lump of tumor cells, but to a more even distribution of them throughout space. The MDE concentration follows this behavior, depending on its production of the tumor cell density distribution in space. The ECM decays faster and the tissue is also faster invaded.

Comparing both models, we see differences regarding the total volume of the tumor cells and on the higher volume of ECM concentration. The increased tumor density results in a MDE production that in the plot of the last point in time exceeds a value of one. Due

to the ECM renewal its' degradation is happening slower and the invasion of the tissue by tumor cells and matrix-degrading enzymes is slowed as well.

### $\gamma$ Variation

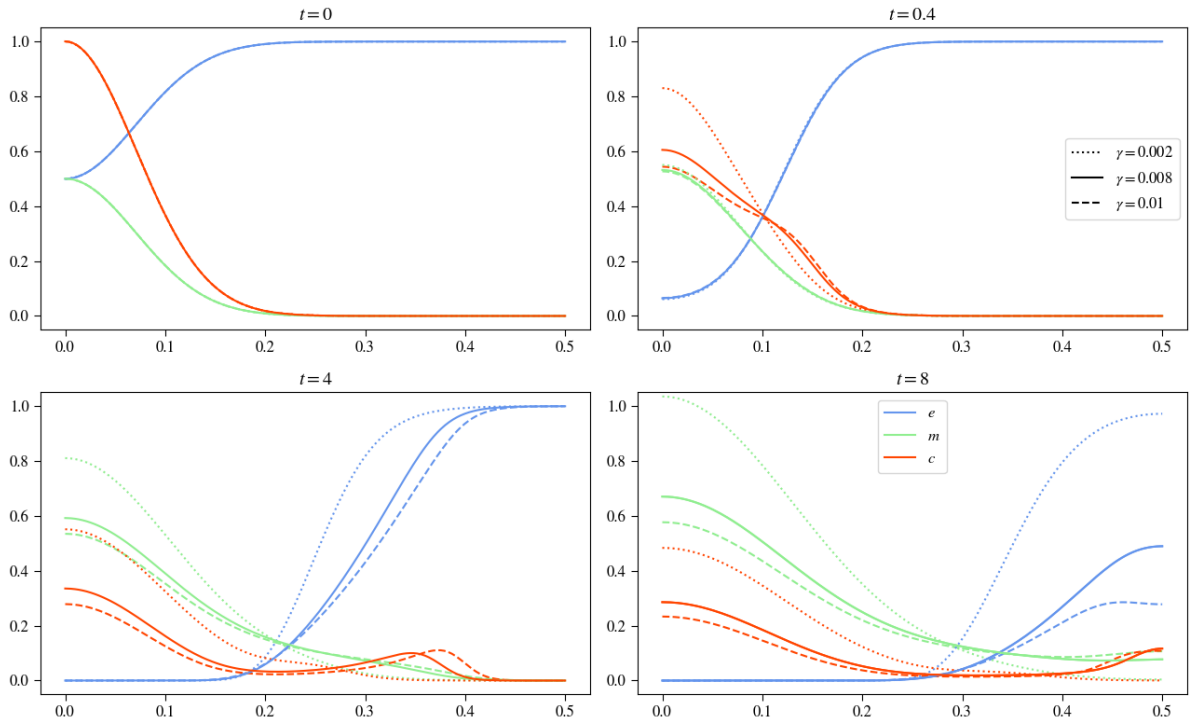


FIGURE 26. Plot results for varying  $\gamma$ , keeping the other parameters constant

Looking at  $\gamma$ , the same effects as the model without proliferation and renewal are observable. Increasing  $\gamma$  means increasing Haptotaxis effects, pulling the tumor cells stronger towards the extracellular matrix molecules. This causes a faster invasion pace, but with a lower density of tumor cells invading the tissue. It also causes the ECM degrading process to happen faster and the MDEs are more evenly distributed through space the higher  $\gamma$  is.

The effects of introducing proliferation and renewal are the same as for varying  $d_c$ . An increase in total tumor cell density and a slowed ECM degradation.

As mentioned above, the same effects come in this experiment, introducing proliferation and renewal, with higher values for tumor cell density, MDE and ECM concentration, especially at the later points in time, clearly depictable. Interestingly, by introducing a renewal factor for the extracellular matrix, the proliferation of the tumor cells causes a faster production of matrix-degrading enzymes, which makes the system produce nearly the same results without proliferation and renewal concerning the ECM concentration. Still, introducing the renewal of the ECM results in slightly higher concentrations overall.

### $\mu_1$ Variation

The parameter  $\mu_1$  describes the proliferation of the tumor cells, using Kolev et al.'s estimate in [13] we assume an even distribution with  $\mu_1 \sim U[0.1, 1.0]$ . Introducing this factor, we can expect a faster production of the matrix-degrading enzymes and a faster degradation of the ECM with an increase in the total amount of tumor cells. Though the effect of the faster ECM degradation might be damped by also introducing a renewal term, we can, especially for higher  $\mu_1$  values, expect to dominate the simulations and accelerate ECM degradation.

Since the basecase, using Kolve et al.'s values, sets the proliferation rate of the tumor cells to  $\mu_1 = 0.1$ ; we consider in the dotted experiment the effects of only introducing the renewal of the ECM.

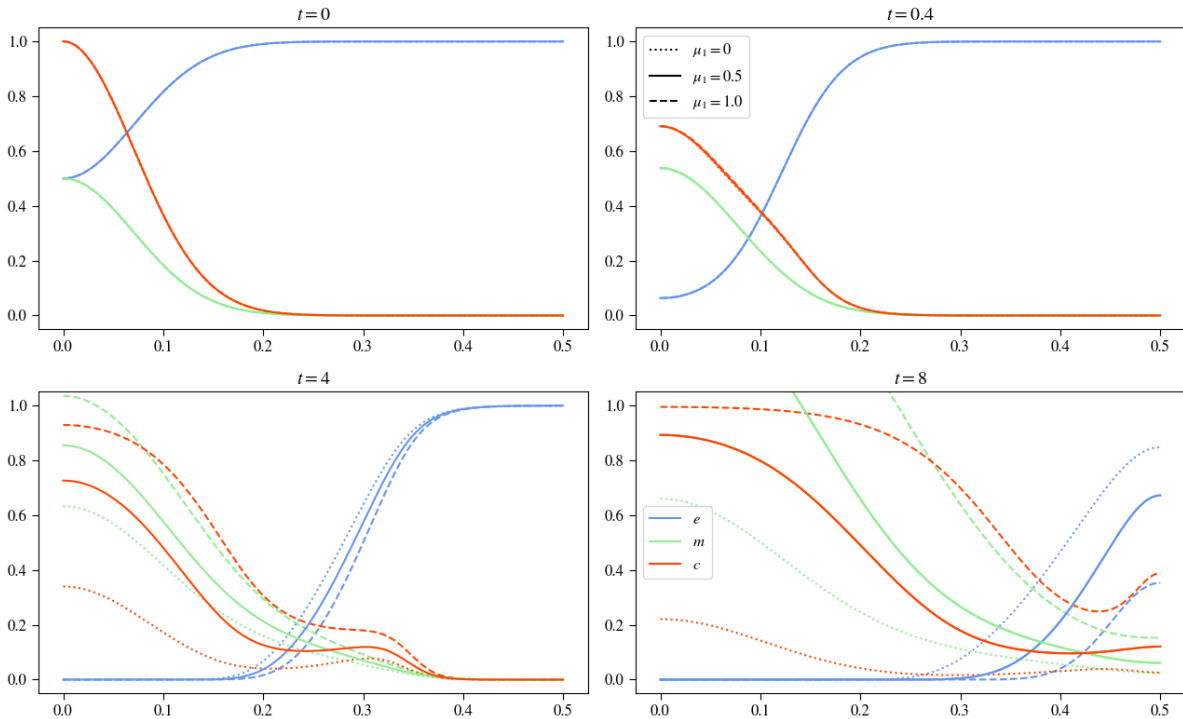


FIGURE 27. Plots show results for varying  $\mu_1$  whilst keeping the other parameters constant.

The effects of  $\mu_1$  take some time to act, as we can see no deviations for all the experiments in figure 27 at  $t = 0.4$ .

At the next point at  $t = 4$ , the differences are striking concerning all variables. With a higher proliferation factor of the tumor cells, the MDE concentration also rises clearly and the ECM degradation is accelerated. However, at this point, the deviations regarding the curve for the ECM concentration are still subtle.

It looks different at the last point in time, at  $t = 8$ . As mentioned above, an increase in total tumor cells drastically increases the MDE concentration and accelerates the ECM degradation.

Introducing  $\mu_1$  means introducing one of the hallmarks of cancer, sustaining prolifer-

ative signaling, which makes the tumor cells themselves responsible for producing them instead of requiring other hormones or enzymes to trigger growth signaling. Setting  $\mu_1 = 0$  could result from a drug working, hindering growth signaling.

### $\eta$ Variation

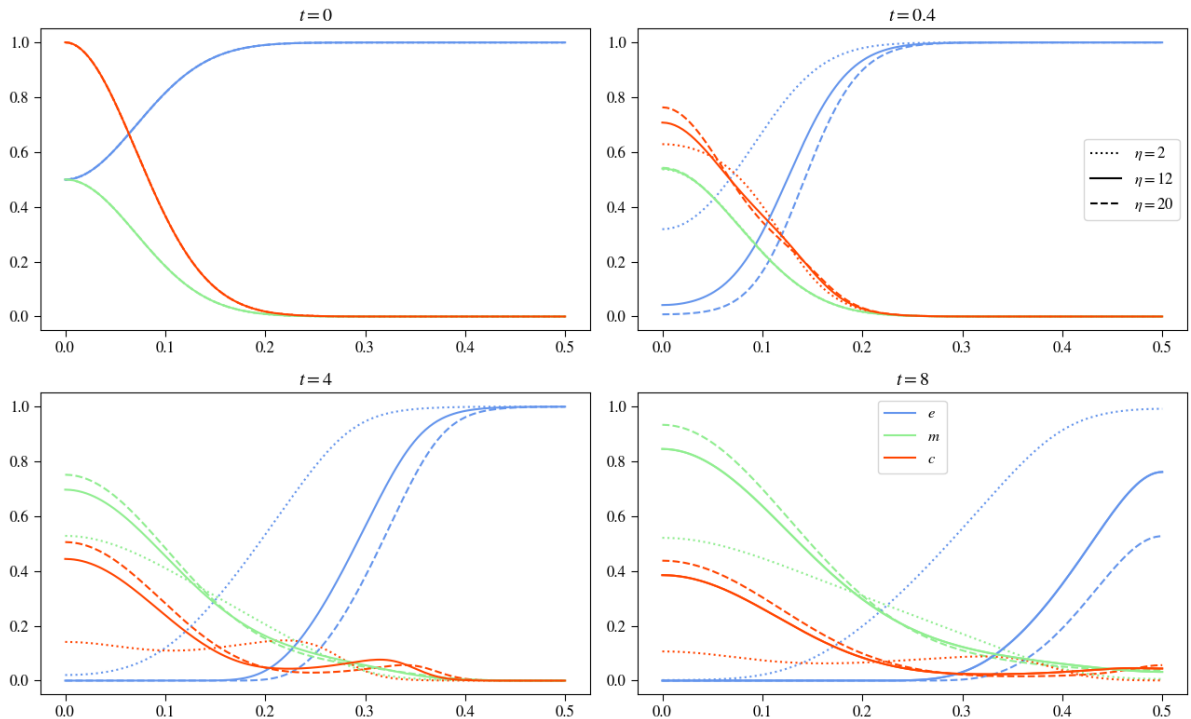


FIGURE 28. Plots show results for varying  $\eta$  whilst keeping the other parameters constant.

We see mostly the same effects as we compare the  $\eta$  variation between with and without proliferation and renewal models. We see little for the solid and dashed curves, though the new model's curves are all slightly raised. Looking at  $\eta = 0$ , we see some interesting deviations. At the time point  $t = 0.4$ , the plots still look somewhat similar, but looking at  $t = 4$ , we see that the curve of the tumor cells has a more even distribution along the x-axis and also its maximum is visibly lower with the value of about 0.2 at  $x = 1.4$  instead of 0.25 at  $x = 1.3$ . This behavior is due to the renewal of the ECM, where without proliferation, this curve stayed constant throughout the experiment. Here, it can increase, which it does, altering the slope of the curve and, therefore, influencing the haptotactic pull for the tumor cells. Additionally, the other two experiments showed a visible increase in the tumor cell density and the matrix-degrading enzyme concentration. However, there is only a slight increase in the ECM concentration; here, we can see no increase in area for the tumor cell density. The renewal of the ECM counters the proliferation of the tumor cells and the slowed ECM degrading process. The ECM has visibly increased at the last two points, with both curves of ECM and tumor cells almost mirroring each other. Summing up the areas of both variables, they occupy the space wholly needed for

the logistic growth terms. This means that proliferation and renewal will play no more critical role in continuing this experiment as they have reached an equilibrium state and cancel each other out.

### $\mu_2$ Variation

The parameter  $\mu_2$  describes the renewal processes of the extracellular matrix molecules. Also, using Kolev et al.'s estimate in [13], we can assume an even distribution with  $\mu_2 \sim U[0.1, 1.0]$ . In natural processes, the renewal of the extracellular matrix is essential to regulate cell differentiation and wound repair, for example [14]. As we see in figure 29,

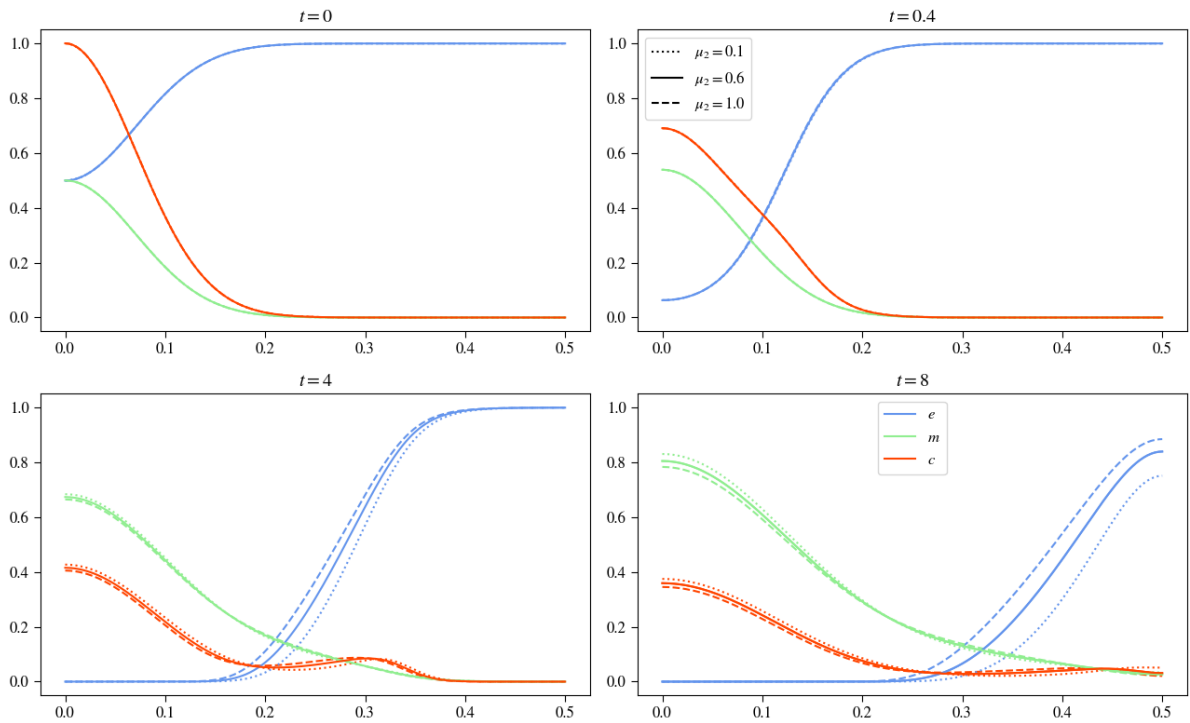


FIGURE 29. Plots show results for varying  $\mu_2$  whilst keeping the other parameters constant.

this renewal process takes some time to show effects. There are no deviations for the experiments after  $t = 0.4$ .

The differences are still subtle when looking at the results later at  $t = 4$ . Increasing  $\mu_2$  slows down the extracellular matrix degradation process and affects the motility of the tumor cells, pulling less of them outwards into the surrounding tissue. The MDE concentration nearly overlays completely, with a minimal higher concentration for the lowest  $\mu_2$  experiment at the origin due to the slightly higher tumor cell density in this area.

The differences at the last point in time at  $t = 8$  are still minor compared to varying the other parameters. As mentioned before, the slowed ECM degradation diminishes haptotactic effects, which leads to slightly less matrix-degrading enzyme concentration at the origin.

Varying the ECM renewal rate at this magnitude shows little influence on the resulting simulations.

At this point, it is important to say that the renewal rates for tissue in the human body strongly vary. Comparing, for example, bone tissue with connective tissue, we see these processes at highly different time scales. Because we did not have experimental data for this parameter, we only investigated Kolev et al.'s estimates, but considering realistic cases, it is important to have better measures for this parameter.

### $d_m$ Variation

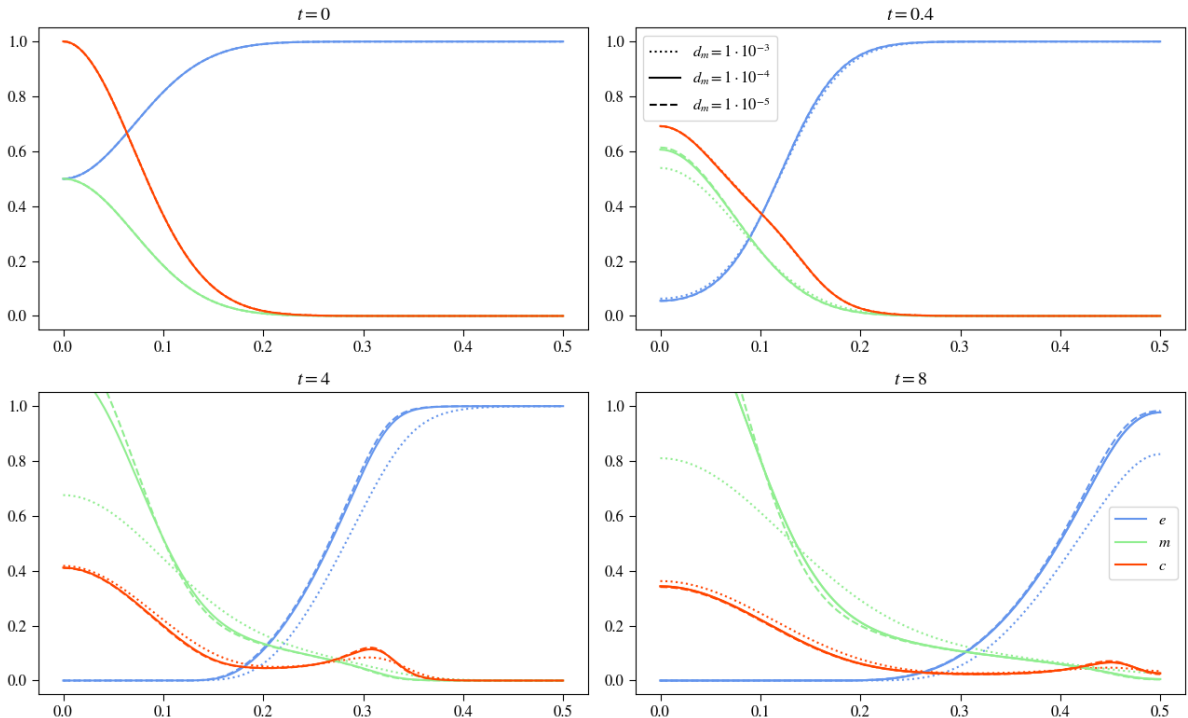


FIGURE 30. Plots show results for varying  $d_m$  whilst keeping the other parameters constant.

Comparing the results varying the diffusion factor of the matrix-degrading enzymes does, as before, yield only minor differences between the initial and updated model. As observed before, the tumor cell density curve and the MDE concentration curves are slightly raised due to the proliferation of the tumor cells. However, the ECM curves for the two lower values of varying  $d_m$  seem to be subject only to minimal change. We can see that it is raised only for very high values of  $d_m$  compared to the model without renewal. The other two curves take off at the same point along the x-axis and finish at the same values for their ECM concentration. Looking at the tumor cell density curves for those  $d_m$  values, we see that towards  $x = 0.5$ , they do not describe an as steep bump as the initial model. This also causes a little less MDE concentration, which is responsible for the seemingly unchanged behavior of the extracellular matrix concentration.

### $\alpha$ Variation

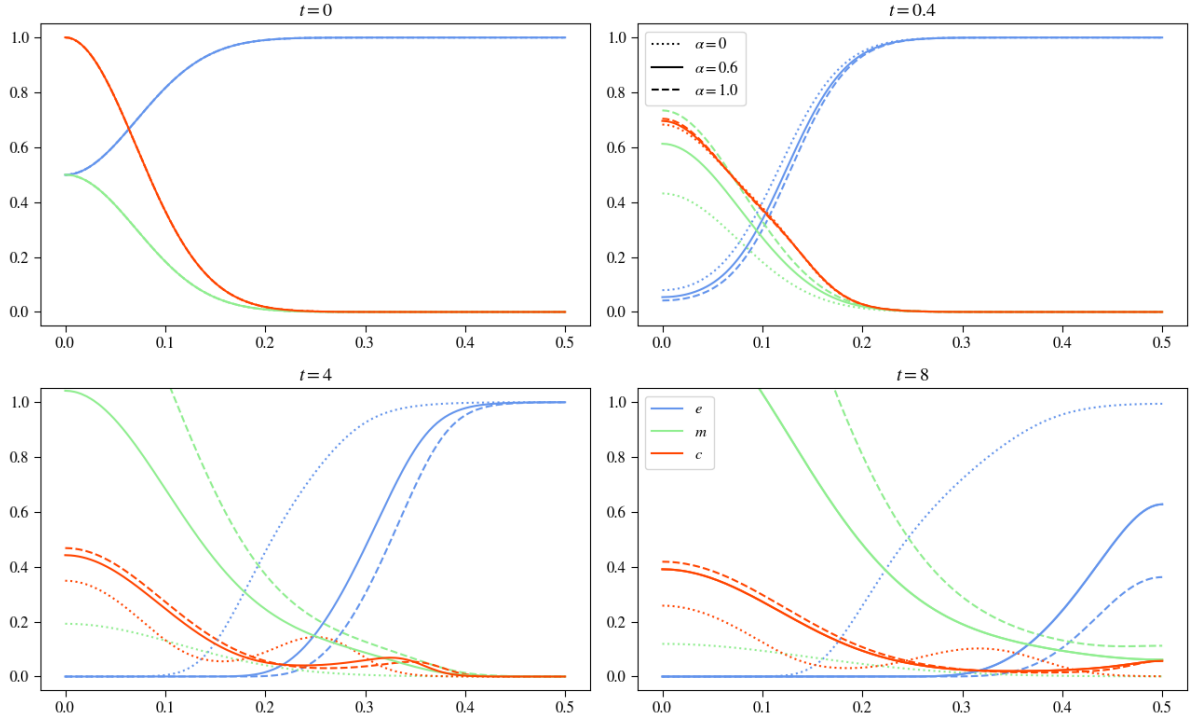


FIGURE 31. Plots show results for varying  $\alpha$  whilst keeping the other parameters constant.

Taking a look at comparing the  $\alpha$ -variation yields more exciting results since  $\mu_1$  acts as a secondary MDE production effect by producing tumor cells, which in turn produce the matrix-degrading enzymes. Though the overall shape and effects to be observed are the same, after  $t = 4$ , the model with proliferation exceeds one at the origin for the MDE concentration for the two higher  $\alpha$  experiments; in contrast, for the model without proliferation, only the one with the highest  $\alpha$  value did so. The tumor cell density curve is slightly raised, which allows the MDE concentration. However, the higher values for the MDEs leave the ECM degrading process untouched, with no visible difference between the initial model and the updated one.

### $\beta$ Variation

Considering  $\beta$ , we can expect that with the introduction of  $\mu_2$ , the ECM degradation will be slowed considerably with rising  $\beta$  since this reduces the MDE concentration and renews the ECM. Looking at the plots, we can see this behavior in the dotted line, which shows the experiment results for the highest  $\beta$  value of 0.1. Though even at the end, it has an overall area that is slightly less than the initial condition, we can see going from timestep  $t = 0.4$  to  $t = 4$  that MDE decay and ECM renewal were sufficiently strong to restore the ECM and going from  $t = 4$  to  $t = 8$  we see this behavior again, renewing the ECM. The other two experiments for  $\beta$  showed no effects as strong as with  $\beta = 0.1$ .

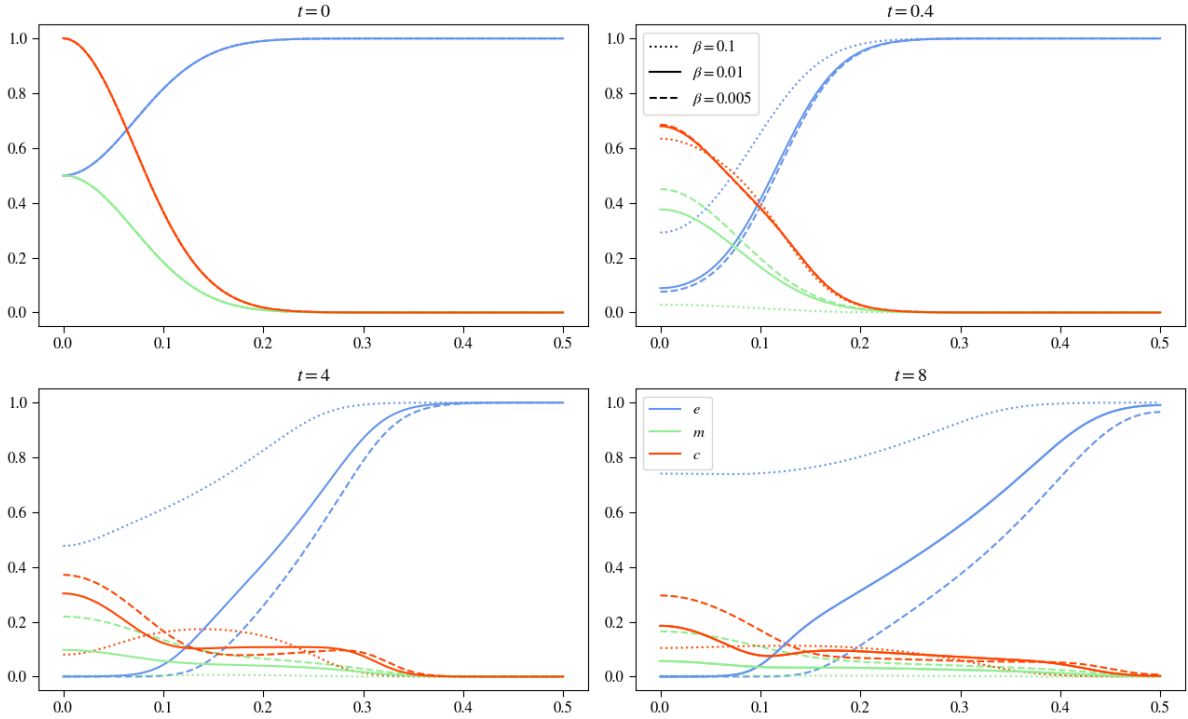


FIGURE 32. Plots show results for varying  $\beta$  whilst keeping the other parameters constant.

However, we can still see the effects of proliferation and renewal especially clear in the solid line,  $\beta = 0.01$ , at the last point in time, where we can observe a visible increase of both ECM and tumor cell density. In this experiment, we see that  $\beta$  is a little too low to counter the effects of ECM degradation; going from  $t = 4$  to  $t = 8$ , we see an apparent decline of ECM concentration, though it is not as striking as for  $\beta = 0.005$ .

## Cross-Variation

### $\mu_1 - \mu_2$ Variation

The effects of observing this cross variation take some time, as did the separate variations of both  $\mu_1$  and  $\mu_2$ . For both  $\mu_1 = \mu_2 = 0.1$ , we see that slower ECM renewal and slower tumor cell proliferation increase the degrading process of the extracellular matrix and, with this, affect the Haptotaxis effect to increase slightly. At the center, a lump remains that has a maximum higher than for the experiment with  $\mu_2 = 1.0$  and the invasion of the tissue has proceeded faster. Increasing  $\mu_2$ , as previously mentioned, results in slower ECM degradation due to the increased renewal term and therefore, the tumor cells are stretched out more evenly along the x-axis. Looking at the results when increasing  $\mu_1$ , we also see the effects only after  $t = 4$ . For  $\mu_2 = 0.1$ , we see that the tumor cell density at  $x = 0$  is slightly more significant and at  $x \approx 2.9$ , the curve for  $\mu_2 = 0.1$  is also slightly larger, being a little below  $\mu_2 = 1.0$  in between  $x \approx 0.2$  and  $x \approx 0.29$ . The curve for the MDEs looks very similar in both cases for  $\mu_2$  due to the very similar tumor cell density curve,  $c$ , though the eECM has visibly faster degraded for  $\mu_2 = 0.1$  due to the slower

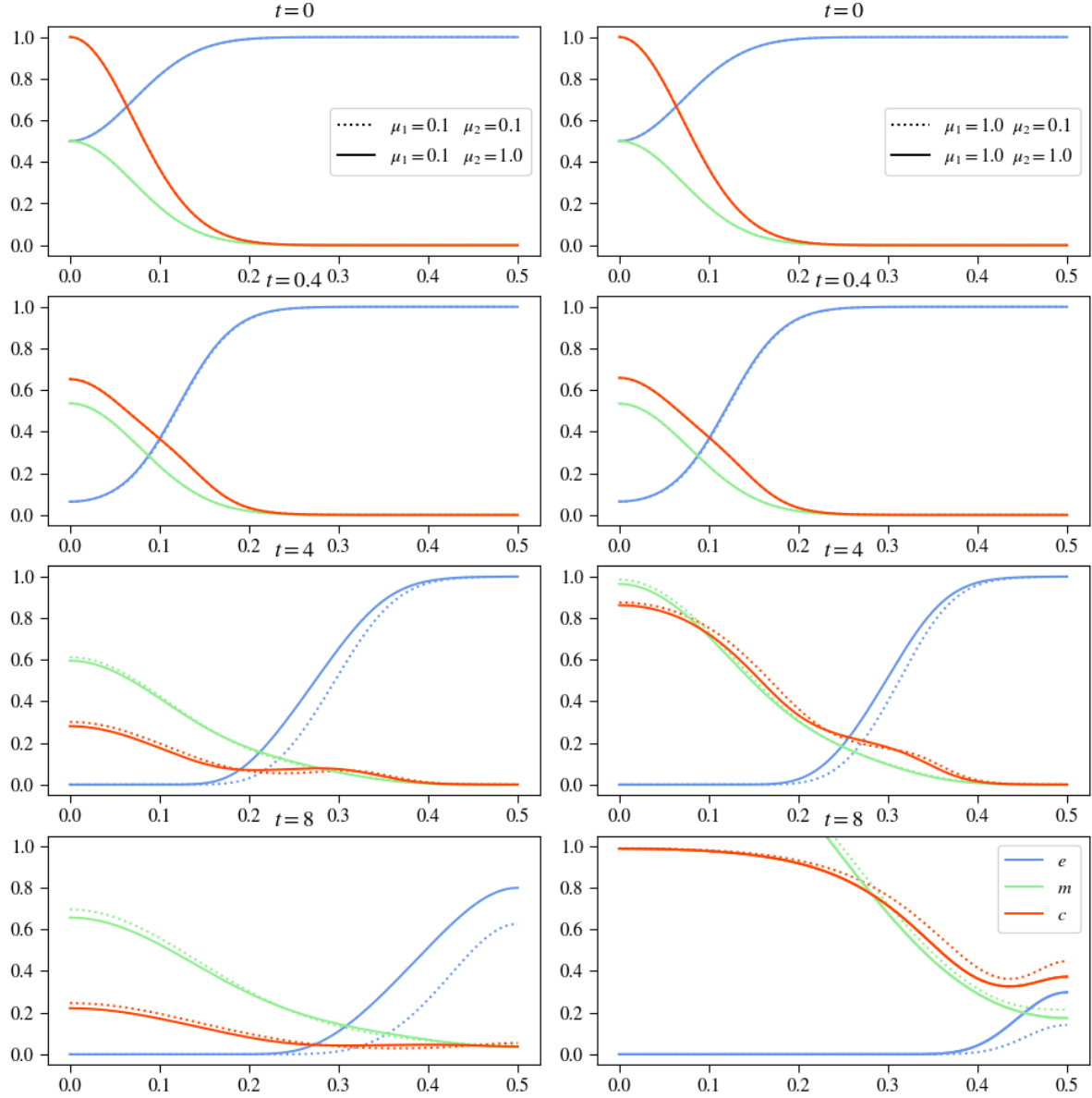


FIGURE 33. Plots show results for varying both  $\mu_1$  and  $\mu_2$  whilst keeping the other parameters constant.

renewal.

### $d_c - \gamma - \mu_1$ Variation

First we are going to take a look at how chaning  $\gamma$  and  $\mu_1$  affects the system whils having lower diffusion values for the tumor cells as the basecase value with  $d_c = 5 \cdot 10^{-5}$ . Figure 34 shows the results of these experiments. Inspecting the dotted curves on the left side column, shows the results for all parameters set to their lower values, we see no division of the tumor cells, indicating that the haptotactic coefficient was set too low. Because of the high concentration of tumor cells near the origin, we see also high values

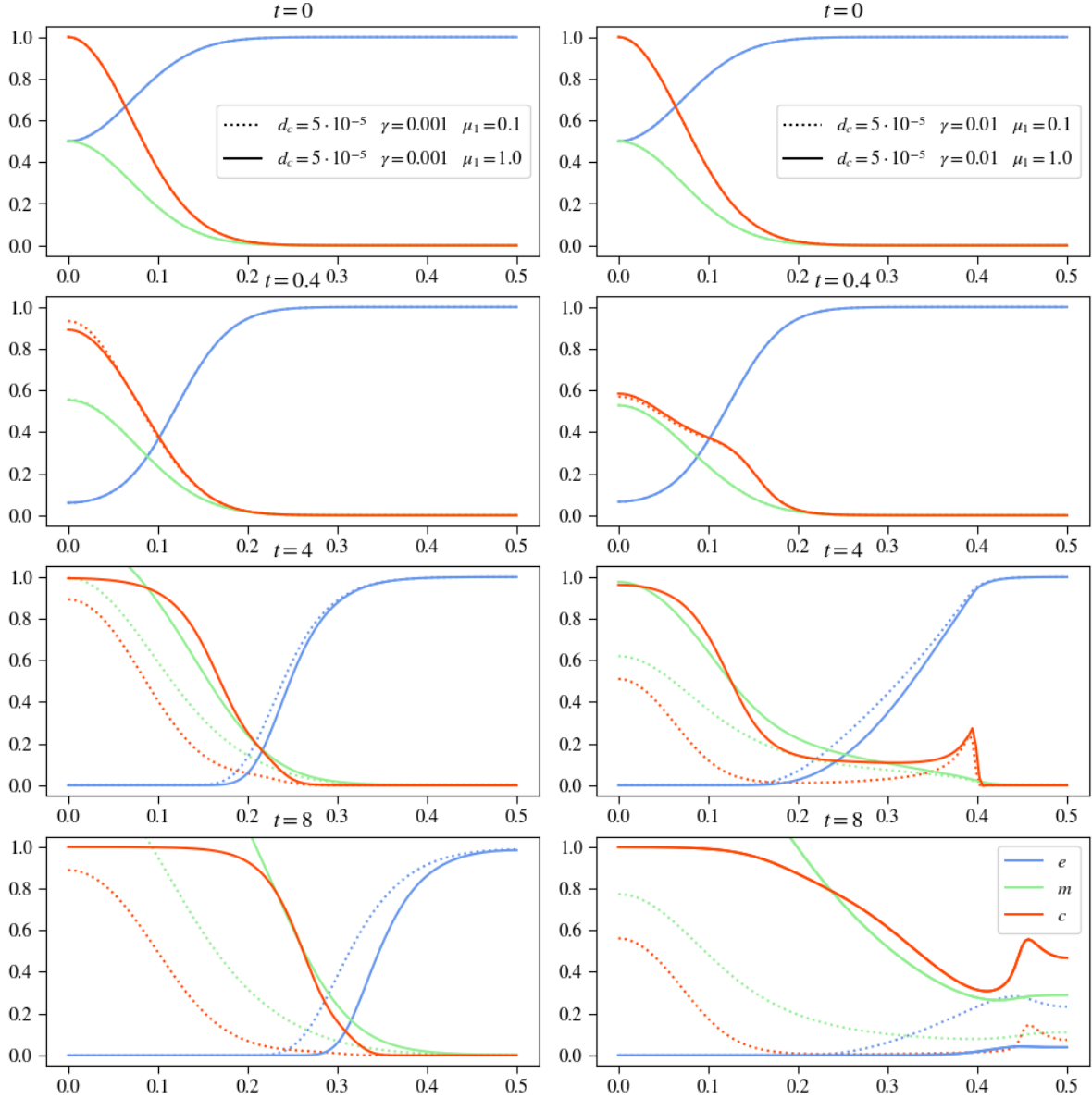


FIGURE 34. Plots show results for varying both  $d_c$ ,  $\gamma$  and  $\mu_1$  whilst keeping the other parameters constant. This plot is the first of two, with the same  $d_c$  value for every plot in this figure.

for the MDE concentration. Due to the decreased motility of the tumor cells we see that the ECM is also slower degraded compared to the other parameters, even when  $\mu_1$  was increased.

The right side of the same figure shows a clear division of tumor cells detaching from the main lump and invading faster. The split off lump of cells even forms for high  $\mu_1$  values a pregnant peak at  $t = 4$ . For both high and low values of  $\mu_1$  we see a considerably faster ECM degradation, though at the last point in time we see that with high proliferation and growth factor on the tumor cells the MDE production is distinctly higher which causes faster ECM degradation.

Taking a look at figure 35, showing results for increased diffusion on the tumor cells,

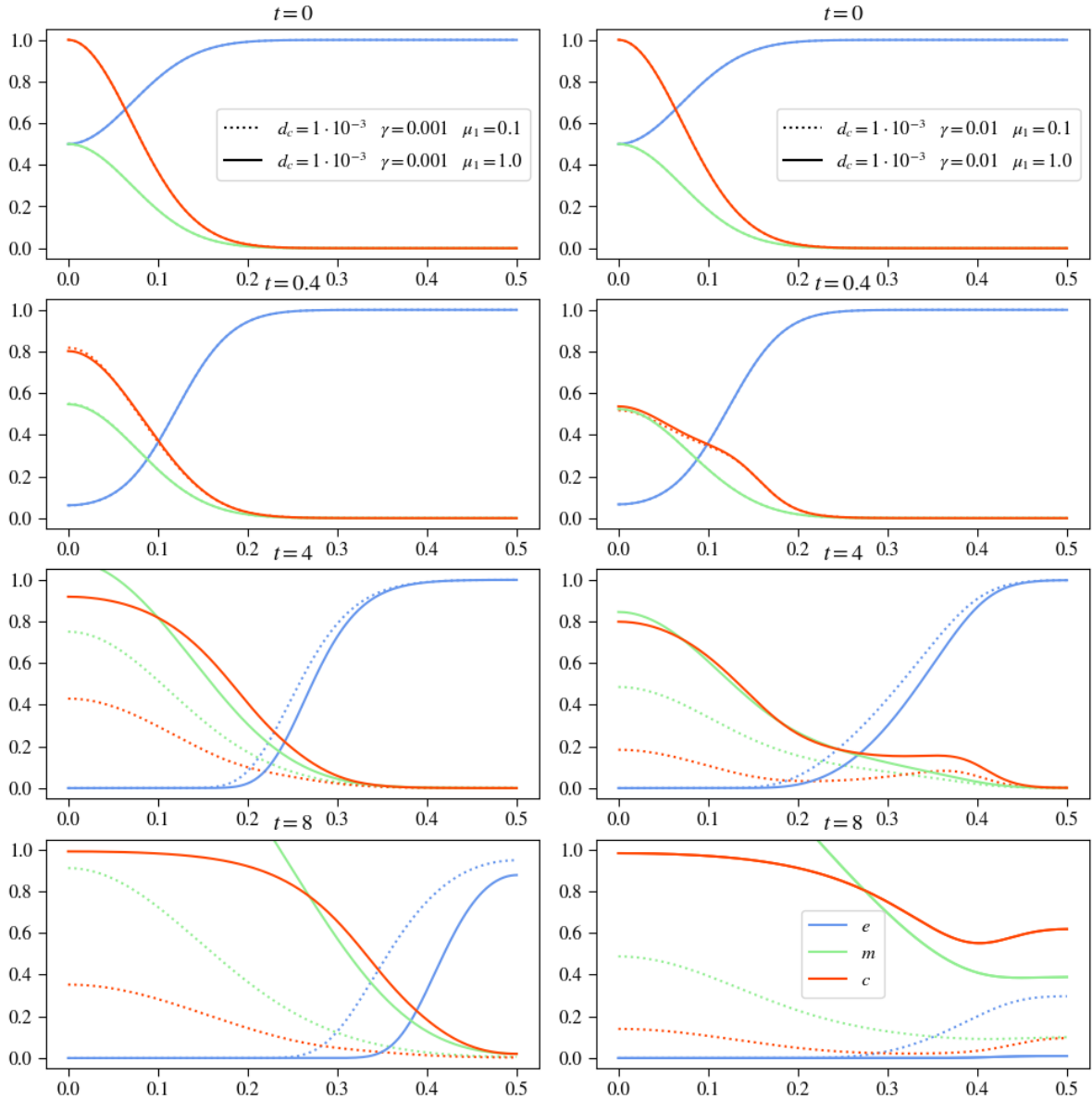


FIGURE 35. Plots show results for varying both  $d_c$ ,  $\gamma$  and  $\mu_1$  whilst keeping the other parameters constant. This plot is the second of two, with the same  $d_c$  value for every plot in this figure.

we see no division on the tumor cell density curve with a low  $\gamma$  value. Regarding the two experiments with low  $\gamma$  and high  $\mu_1$  values we see the effect of diffusion clearly on the tumor cells. Though the red curves look the same in shape the one with the higher diffusion value looks shifted to the right, the same goes for the MDE concentration, resulting in faster ECM degradation. Comparing the results of increasing  $\mu_1$  between diffusion values, we can also observe the effect of diffusion clearly. The curve for the tumor cells is more evenly distributed, which causes the same behavior in the MDE curve and also a lower concentration and density in total in this regard.

The right column of figure 35 shows results for increasing both  $d_c$  and  $\gamma$ . Here we see that the division forming on the tumor cells clearly, though not as pregnant as with low

diffusive values. The fast and even spread of the tumor cells as well as their proliferation term, results in the highest rate of ECM degradation.

This variation is an excellent example of the relationship between Haptotaxis and diffusion. We see with low values on the diffusion coefficient the changes in the haptotactic coefficient more striking, with a pointy peak in the tumor cells curve, but with also high diffusion values the peak is not as pregnant and not as striking.

Another observation is the influence of the logistic growth rate of the tumor cells. In the last experiment we see that with a fast and even spread we get the highest overall density of tumor cells and the fastest ECM degradation.

### $\eta - \mu_2$ Variation

Varying both  $\eta$  and  $\mu_2$ , we can expect apparent changes in the curve describing the ECM concentration. On the left side of figure 36, we see the two experiments for low  $\eta$  values and that increasing  $\mu_1$  has only a little effect. Where we could have expected to see an increase of the ECM, maybe even, we see that the ECM curves for both experiments verify that the renewal factor  $\mu_2$  was too low to counter the ECM degradation, even with a low degradation factor. Still, between  $\mu_2 = 0.1$  and  $\mu_2 = 1.0$ , there are visible differences in the degrading speed of the ECM. We can also observe that with the higher renewal term, the tumor cell density curve receives more of an effect of Haptotaxis, resulting in a more stretched curve with only one long lump of tumor cells, whereas, for the lower renewal factor, we can still clearly see that there is a division that invades the tissue and one that stays at the origin. Concerning the MDE curves, we see little difference for higher  $\mu_2$ , which means more stretched tumor cell density. We can also observe a more stretched MDE curve with a lower maximum at the origin.

Looking at the experiments with raised  $\eta$  to accelerate the ECM degrading process, we can only see pregnant differences in the curve describing the ECM concentration; the other two look across the steps in time to be widely similar. For the ECM curve, we see that the experiment with the lower  $\mu_2$  value results in a faster degradation process.

## 4.4 2D Results with Proliferation and Renewal - Heterogenous ECM

Figure 37 you can see the effects using a heterogenous extracellular matrix structure. The plots show the tumor cell density in the left column, the extracellular matrix concentration in the middle column and the matrix-degrading enzyme concentration on the right. For the parameters, we assumed the basecase studying the model with proliferation.

This experiment describes a more realistic biological scenario, as seen in figure ??, where the tumor cells are located at the basement membrane of neighboring tissue and have degraded this membrane to invade the surrounding tissue and degrade the extracellular matrix.

The first image in the middle column shows the experiment's initial distribution. The extracellular matrix molecule concentration is only on the right side of the plot, which indicates that neighboring tissue has been invaded. In the center of the same image, there

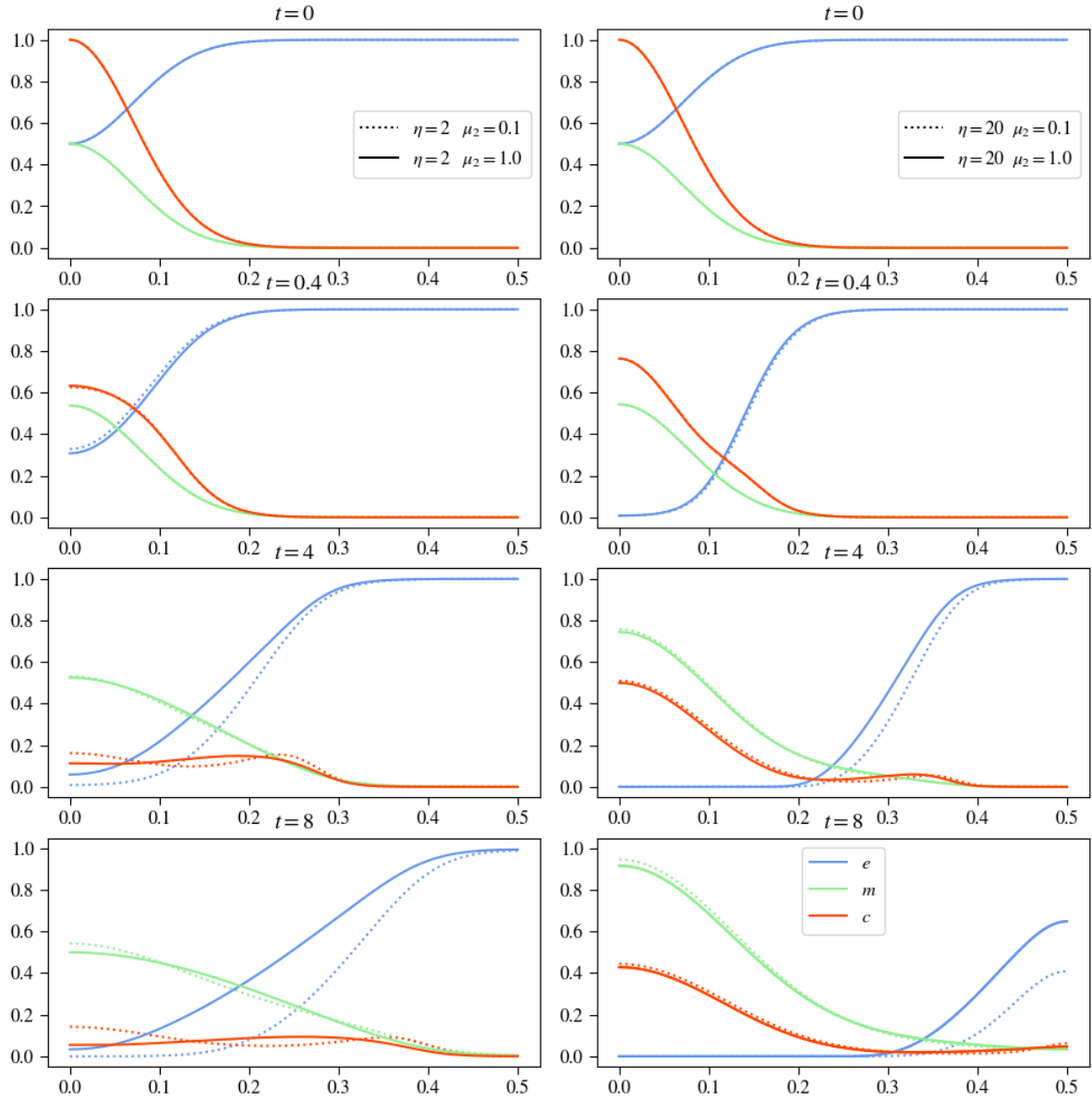


FIGURE 36. Plots show results for varying both  $\eta$  and  $\mu_2$  whilst keeping the other parameters constant.

is a hollow spot where the tumor cells of the initial distribution are located.

After four time steps, the ECM slowly degrades and the tumor cells are pulled further into the neighboring tissue by Haptotaxis caused by the ECM structure. The concentration of the matrix-degrading enzymes shows little difference in their behavior compared to the experiments done with a homogenous ECM. They only depend indirectly on the ECM by being produced where the tumor cells are being pulled by the extracellular matrix concentration.

The next point shows increased ECM degradation, further invading tumor cells into the tissue. The tumor cells behave as a semicircular wave moving into the direction of the ECM; the primary lump remains at the center, with the edge of having containing

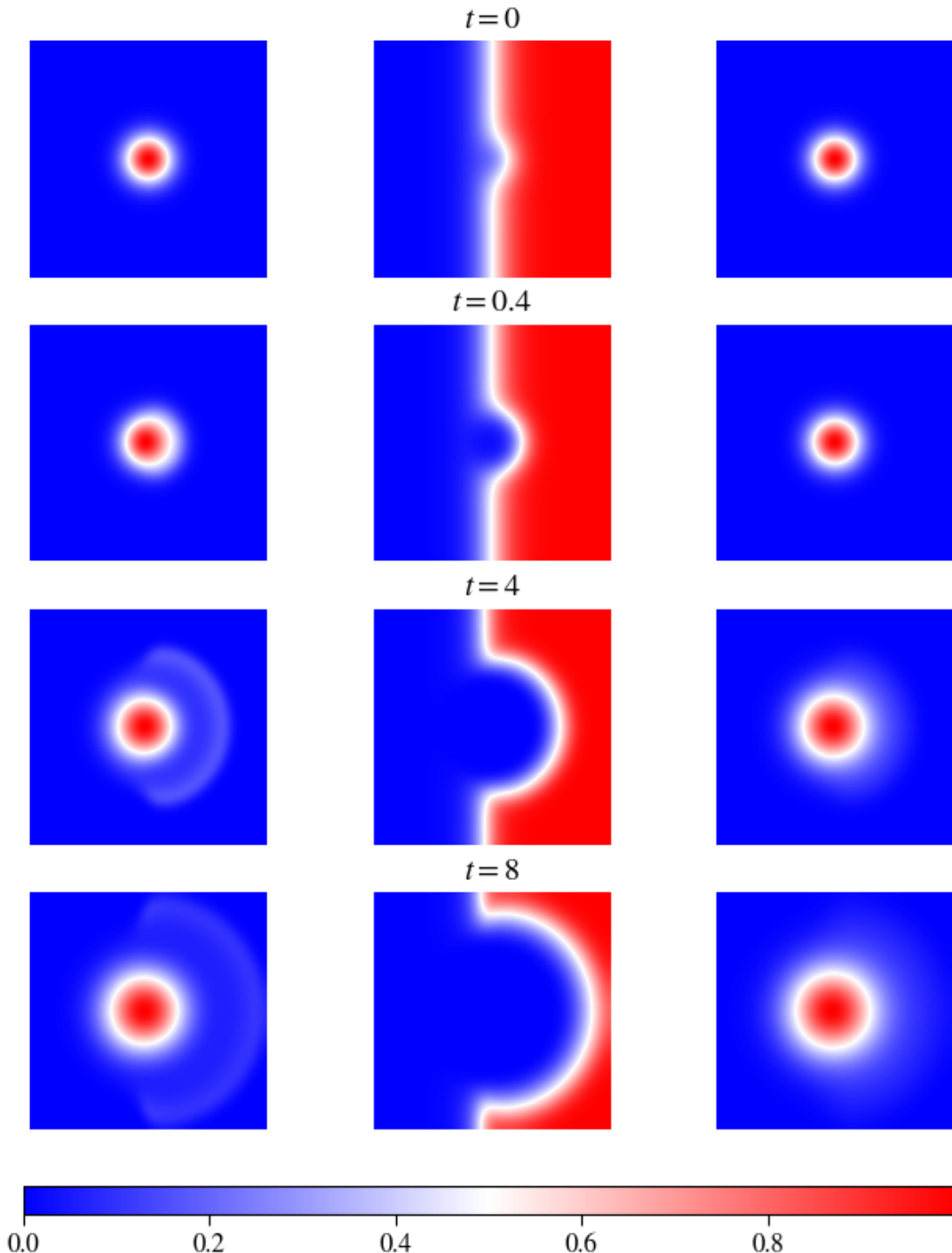


FIGURE 37. 2D Results using a heterogenous ECM with the parameter values:  $d_c = 5 \cdot 10^{-4}$ ,  $\gamma = 0.0055$ ,  $\mu_1 = 0.1$ ,  $\eta = 10$ ,  $\mu_2 = 0.5$ ,  $d_m = 1 \cdot 10^{-3}$ ,  $\alpha = 0.3564$ ,  $\beta = 0$ ; left: tumor cell density, middle: ECM concentration, right: MDE concentration.

a smaller amount of cells moving outwards. The image describing the matrix-degrading enzyme concentration still shows only minor effects; looking closely, we can see that from the center moving to the right, there is a slightly higher concentration than in the other direction.

The last row depicts the experiment after  $t = 8$  timesteps and the above mentioned effects are propagated. The ECM degradation has continued, as has the invasion of the tumor cells. The wave moving in the direction of the remaining extracellular matrix molecules has spread through space, decreasing its strength. The MDEs still show little influence on the heterogeneous ECM structure, with the primary lump staying centered and only making it difficult to recognize more concentration towards the movement of the tumor cells and concentration of the extracellular matrix.

Considering different extracellular matrix molecules and structures or physical influences such as heat or radiation, the ECM structure and the system's behavior can be adjusted to simulate better real-life scenarios of cancer invading tissue.

## 5 Conclusion and Discussion

In this work, we conducted a parameter analysis for a numerical model in tumor development research. The aim was to investigate the impact of varying model parameters, dimensions and the structure of the extracellular matrix on simulation outcomes and provide insights into the model’s behavior under different conditions. This was done to facilitate implementing this model in a real-world biological or medical scenarios, facilitating an entry point for researchers to choose the parameters for their experiments.

The results of our analysis highlight the model’s sensitivity to changes in key parameters, such as the diffusion or Haptotaxis coefficients on the tumor cells, the proliferation and growth rate of the tumor cells, the degradation rate of the extracellular matrix and the production and decay rates for the matrix-degrading enzymes. We observed that small variations in these parameters can lead to significant differences in simulation outcomes, indicating the importance of carefully selecting and calibrating model parameters for accurate representation of biological phenomena.

Furthermore, our study revealed the complex interplay between different parameters during cross-variating them and their effects on tumor invasion and extracellular matrix degradation. For example, it was found that increasing the haptotactic flux coefficient of the tumor cells is the critical component to controlling how many cells of a tumor invade the surrounding tissue and how many stay at the center of the simulation causing drastic changes in the rate at which the extracellular matrix is degraded. Most of the parameters studied increased the invasion pace of the tumor cells and the degradation of the extracellular matrix, when they were increased.

Moreover, the influence of spatial dimensions on simulation outcomes was shown, with simulations in higher dimensions producing qualitatively different results compared to the initial one-dimensional model. This underscores the importance of considering the spatial complexity of biological systems when designing computational models for tumor development.

Additionally, our analysis sheds light on the limitations of the current model and areas for further improvement. The model could be extended in both discrete and continuous ways, for example, by implementing biochemical effects like chemotaxis, which is done in Kolev et al.’s work [13] or implement immune cell interactions or heterogeneity in tumor cell populations, to capture the complexity of the tumor microenvironment better.

In conclusion, our parameter analysis provides valuable insights into the behavior of the investigated numerical model in tumor development research and underscores the importance of parameter selection and model validation in Mathematical Oncology. By refining our understanding of the underlying mechanisms driving tumor progression, such models have the potential to inform therapeutic strategies and improve patient outcomes in the fight against cancer.

## References

1. Anderson, A. Continuous and Discrete Mathematical Models of Tumor-induced Angiogenesis. en. *Bulletin of Mathematical Biology* **60**, 857–899. ISSN: 00928240. <http://link.springer.com/10.1006/bulm.1998.0042> (2023) (Sept. 1998).
2. Anderson, A. R. A., Chaplain, M. A. J., Newman, E. L., Steele, R. J. C. & Thompson, A. M. Mathematical Modelling of Tumour Invasion and Metastasis. en. *Journal of Theoretical Medicine* **2**, 129–154. ISSN: 1027-3662, 1607-8578. <http://www.hindawi.com/journals/cmmm/2000/490902/abs/> (2023) (2000).
3. Bekisz, S. & Geris, L. Cancer modeling: From mechanistic to data-driven approaches, and from fundamental insights to clinical applications. *Journal of Computational Science* **46**. 20 years of computational science, 101198. ISSN: 1877-7503. <https://www.sciencedirect.com/science/article/pii/S1877750320304993> (2020).
4. Hanahan, D. Hallmarks of Cancer: New Dimensions. *Cancer Discovery* **12**, 31–46. ISSN: 2159-8274. eprint: <https://aacrjournals.org/cancerdiscovery/article-pdf/12/1/31/3052722/31.pdf>. <https://doi.org/10.1158/2159-8290.CD-21-1059> (Jan. 2022).
5. Franssen, L. C., Lorenzi, T., Burgess, A. E. F. & Chaplain, M. A. J. A Mathematical Framework for Modelling the Metastatic Spread of Cancer. en. *Bulletin of Mathematical Biology* **81**, 1965–2010. ISSN: 0092-8240, 1522-9602. <http://link.springer.com/10.1007/s11538-019-00597-x> (2023) (June 2019).
6. Yin, A., Moes, D. J. A. R., van Hasselt, J. G. C., Swen, J. J. & Guchelaar, H.-J. A review of mathematical models for tumor dynamics and treatment resistance evolution of solid tumors. en. *CPT Pharmacometrics Syst. Pharmacol.* **8**, 720–737 (Oct. 2019).
7. Chaplain, M., Lolas, G. & ,The SIMBIOS Centre, Division of Mathematics, University of Dundee, Dundee DD1 4HN. Mathematical modelling of cancer invasion of tissue: dynamic heterogeneity. en. *Networks & Heterogeneous Media* **1**, 399–439. ISSN: 1556-181X. <http://aimsciences.org//article/doi/10.3934/nhm.2006.1.399> (2023) (2006).
8. Merino-Casallo, F., Gomez-Benito, M. J., Hervas-Raluy, S. & Garcia-Aznar, J. M. Unravelling cell migration: defining movement from the cell surface. en. *Cell Adh. Migr.* **16**, 25–64 (Dec. 2022).
9. No. 06 (2017): *HiFlow3 – Technical Report on Release 2.0 | Preprint Series of the Engineering Mathematics and Computing Lab* [Online; accessed 30. Apr. 2024]. Apr. 2024. <https://journals.ub.uni-heidelberg.de/index.php/emcl-pp/issue/view/3655>.
10. Kitware, Inc. *ParaView* <https://www.paraview.org/>. Zuletzt abgerufen am [Datum]. 2022.

11. Stéphanou, A., McDougall, S., Anderson, A. & Chaplain, M. Mathematical modelling of the influence of blood rheological properties upon adaptative tumour-induced angiogenesis. *Mathematical and Computer Modelling* **44**. Advances in Business Modeling and Decision Technologies [pp. 1-95], 96–123. ISSN: 0895-7177. <https://www.sciencedirect.com/science/article/pii/S0895717705004565> (2006).
12. Aznavoorian, S., Stracke, M., Krutzsch, H., Schiffmann, E. & Liotta, L. Signal transduction for chemotaxis and haptotaxis by matrix molecules in tumor cells. *The Journal of cell biology* **110**, 1427–38 (May 1990).
13. Kolev, M. & Zubik-Kowal, B. Numerical Solutions for a Model of Tissue Invasion and Migration of Tumour Cells. *Computational and Mathematical Methods in Medicine* **2011**, 452320. ISSN: 1748-670X. <https://doi.org/10.1155/2011/452320> (Dec. 2010).
14. Lu, P., Takai, K., Weaver, V. M. & Werb, Z. Extracellular matrix degradation and remodeling in development and disease. en. *Cold Spring Harb. Perspect. Biol.* **3**, a005058–a005058 (Dec. 2011).